Elastocaloric effect on natural rubber and terpolymer : Temperature variation mechanism, morphology and energy balance during deformation

Yukihiro Yoshida

N°d'ordre NNT : 2016LYSEI070

THESE de DOCTORAT DE L'UNIVERSITE DE LYON
opérée au sein de
l'INSA LYON

Ecole Doctorale ED160
(ELECTRONIQUE, ELECTROTECHNIQUE, AUTOMATIQUE)

Spécialité de doctorat :
Discipline : **Génie Electrique**

Soutenue publiquement le 08/07/2016, par :
Yukihiro YOSHIDA
Amphithéâtre AE2 14h

Effet élastocalorique dans le caoutchouc naturel et le terpolymère : mécanismes responsables de la variation de température et bilan énergétique sous déformation

---

Devant le jury composé de :

DUBUS, Bertrand	Directeur de Recherche	IEMN dept ISEN	Rapporteur
HAJJAJI, Abdelowahed	Professeur HDR	ENSAJ	Rapporteur
MORITA, Takeshi	Associate Professor	UNIVERSITY of TOKYO	Examinateur
POUGET, Joel	Directeur de Recherche	UNIV. PARIS 6	Examinateur
YUSE, Kaori	Maître de Conférences	INSA-LYON	Examinatrice
GUYOMAR, Daniel	Professeur des Universités	INSA-LYON	Directeur de thèse

Département FEDORA – INSA Lyon - Ecoles Doctorales – Quinquennal 2016-2020

SIGLE	ECOLE DOCTORALE	NOM ET COORDONNEES DU RESPONSABLE
CHIMIE	**CHIMIE DE LYON** **http://www.edchimie-lyon.fr** Sec : Renée EL MELHEM Bat Blaise Pascal 3e etage secretariat@edchimie-lyon.fr Insa : R. GOURDON	M. Stéphane DANIELE Institut de Recherches sur la Catalyse et l'Environnement de Lyon IRCELYON-UMR 5256 Équipe CDFA 2 avenue Albert Einstein 69626 Villeurbanne cedex directeur@edchimie-lyon.fr
E.E.A.	**ELECTRONIQUE, ELECTROTECHNIQUE, AUTOMATIQUE** **http://edeea.ec-lyon.fr** Sec : M.C. HAVGOUDOUKIAN Ecole-Doctorale.eea@ec-lyon.fr	M. Gérard SCORLETTI Ecole Centrale de Lyon 36 avenue Guy de Collongue 69134 ECULLY Tél : 04.72.18 60.97 Fax : 04 78 43 37 17 Gerard.scorletti@ec-lyon.fr
E2M2	**EVOLUTION, ECOSYSTEME, MICROBIOLOGIE, MODELISATION** **http://e2m2.universite-lyon.fr** Sec : Safia AIT CHALAL Bat Darwin - UCB Lyon 1 04.72.43.28.91 Insa : H. CHARLES Safia.ait-chalal@univ-lyon1.fr	Mme Gudrun BORNETTE CNRS UMR 5023 LEHNA Université Claude Bernard Lyon 1 Bât Forel 43 bd du 11 novembre 1918 69622 VILLEURBANNE Cédex Tél : 06.07.53.89.13 e2m2@ univ-lyon1.fr
EDISS	**INTERDISCIPLINAIRE SCIENCESSANTE** **http://www.ediss-lyon.fr** Sec : Safia AIT CHALAL Hôpital Louis Pradel - Bron 04 72 68 49 09 Insa : M. LAGARDE Safia.ait-chalal@univ-lyon1.fr	Mme Emmanuelle CANET-SOULAS INSERM U1060, CarMeN lab, Univ. Lyon 1 Bâtiment IMBL 11 avenue Jean Capelle INSA de Lyon 696621 Villeurbanne Tél : 04.72.68.49.09 Fax :04 72 68 49 16 Emmanuelle.canet@univ-lyon1.fr
INFOMATHS	**INFORMATIQUE ET MATHEMATIQUES** **http://infomaths.univ-lyon1.fr** Sec :Renée EL MELHEM Bat Blaise Pascal 3e etage infomaths@univ-lyon1.fr	Mme Sylvie CALABRETTO LIRIS – INSA de Lyon Bat Blaise Pascal 7 avenue Jean Capelle 69622 VILLEURBANNE Cedex Tél : 04.72. 43. 80. 46 Fax 04 72 43 16 87 Sylvie.calabretto@insa-lyon.fr
Matériaux	**MATERIAUX DE LYON** **http://ed34.universite-lyon.fr** Sec : M. LABOUNE PM : 71.70 –Fax : 87.12 Bat. Saint Exupéry Ed.materiaux@insa-lyon.fr	M. Jean-Yves BUFFIERE INSA de Lyon MATEIS Bâtiment Saint Exupéry 7 avenue Jean Capelle 69621 VILLEURBANNE Cedex Tél : 04.72.43 71.70 Fax 04 72 43 85 28 Ed.materiaux@insa-lyon.fr
MEGA	**MECANIQUE, ENERGETIQUE, GENIE CIVIL, ACOUSTIQUE** **http://mega.universite-lyon.fr** Sec : M. LABOUNE PM : 71.70 –Fax : 87.12 Bat. Saint Exupéry mega@insa-lyon.fr	M. Philippe BOISSE INSA de Lyon Laboratoire LAMCOS Bâtiment Jacquard 25 bis avenue Jean Capelle 69621 VILLEURBANNE Cedex Tél : 04.72 .43.71.70 Fax : 04 72 43 72 37 Philippe.boisse@insa-lyon.fr
ScSo	**ScSo*** **http://recherche.univ-lyon2.fr/scso/** Sec : Viviane POLSINELLI Brigitte DUBOIS Insa : J.Y. TOUSSAINT viviane.polsinelli@univ-lyon2.fr	Mme Isabelle VON BUELTZINGLOEWEN Université Lyon 2 86 rue Pasteur 69365 LYON Cedex 07 Tél : 04.78.77.23.86 Fax : 04.37.28.04.48

*ScSo : Histoire, Géographie, Aménagement, Urbanisme, Archéologie, Science politique, Sociologie, Anthropologie

Résumé

Les effets électrocaloriques, qui se traduisent par une variation de température induite par une variation d'entropie ont été étudiés comme alternative aux systèmes de réfrigération utilisant un cycle de compression/détente. Le travail de thèse se focalise sur l'étude de l'effet élastocalorique dans le caoutchouc naturel et le terpolymère (P(VDF-TrFE-CTFE).

En premier lieu, l'effet élastocalorique dans le caoutchouc naturel qui compte parmi les meilleurs candidats, a été évalué pour des cycles de déformation réalisés avec différentes valeurs d'allongement. Une variation de température de 4°C a pu être observée. Il est usuel d'utiliser la relation déformation/contrainte en fonction de la variation de température pour évaluer l'effet élastocalorique. Il a été démontré que cette méthode ne peut pas être utilisée dans le cas du caoutchouc naturel et qu'elle doit être remplacée par la mesure de la variation de l'énergie mécanique en fonction de la température. Et dans ce cas, une variation linéaire entre ces deux dernières grandeurs a été observée. En réalisant un bilan d'énergie pendant l'essai, non seulement, le rendement énergétique a pu être évalué mais il a été aussi possible de prendre en compte l'effet Mullins et la cristallisation induite par la déformation pour le caoutchouc naturel.

Dans un second temps, l'effet élastocalorique a été étudié sur le terpolymère (P(VDF-TrFE-CTFE), ce qui a permis de montrer qu'il était possible d'obtenir une variation de température de 2.1°C sous réserver de pré-déformer le terpolymère à plus de 1050% avant. Par comparaison avec d'autres matériaux présentant une bonne conversion élastocalorique, le fort potentiel de ce matériau a pu être mis en évidence. Enfin, il a été mis en évidence que la plus grande partie de l'énergie mécanique était bien convertie en énergie thermique.

Abstract

Caloric effects (CEs), which are the phenomena that temperature variation is caused by entropy change, have been investigated for the novel system which might be able to replace conventional vapor compression refrigeration system. In the present thesis, the elastocaloric effect (ElCE) of natural rubber (NR) and terpolymer, poly(vinylidene fluoride - trifluoroethylene - chlorotrifluoroethylene) (P(VDF-TrFE-CTFE)), was focused.

First of all, NR, which is an excellent candidate material for ElCE, was evaluated in cyclic deformation with different strain levels. It was found that NR exhibits temperature variation of around 4.0 °C. In general, the relation between stress/strain versus temperature variation is used to evaluate ElCE. The unsuitability of such evaluation method for NR was demonstrated. The evaluation method for ElCE which uses energy balance was then proposed. A linear relation between the temperature variation caused by ElCE and the applied mechanical energy by deformation was experimentally found. This fact verifies the suitability of the proposed method. Using the energy balance, besides, not only the conversion efficiency but also the influences of the Mullins effect and the strain-induced crystallization on the ElCE of NR were discussed.

ElCE of P(VDF-TrFE-CTFE) was also evaluated in order to find out the potential of polymer. It was found that present terpolymer which is not one of the elastomers can also exhibit a large temperature variation, 2.1 °C, caused by ElCE if a large pre-stretch such as more than 1050 % is applied in advance. By comparison with other materials for ElCE, it was demonstrated that P(VDF-TrFE-CTFE) can be a high potential material for ElCE. It was also shown that P(VDF-TrFE-CTFE) converts most of the applied mechanical energy into the heat energy.

Acknowledgements

I would like to express my sincere gratitude my supervisor, Prof. Daniel Guyomer for giving me the opportunity to study in LGEF as a PhD candidate.

I am very grateful to thank Prof. Laurent Lebrun, director of laboratory, for his support and advice on my work. I owe my success to him and will never forget his advice. I would like to thank Dr. Gaël Sebald for his support and advice. Thanks to his support and advice, I was able to progress with my PhD study.

I am especially grateful to Dr. Kaori Yuse. Since her lecture which I attended in Japan when I was master student was quite interesting, I hungered for studying in this laboratory. She has given me kind help and support before start of my PhD study and during it. I can't express how grateful I am.

I also would like to express my gratitude to the committee members: Pr. Bertrand Dubus and Dr. Abdelowahed Hajjaji for reviewing my manuscript and Pr. Joel Pouget and Dr. Takeshi Morita for their comments and suggestions that improved the quality of this work.

I would like to thank Dr. Laurence Seveyrat and Ms. Véronique Perrin for supporting the experimental work. I also would like to thank Mr. Frederic Defromerie for machining the art-like device for my design and experiment, teaching me French and always encouraging me.

I am deeply grateful to Evelyne Dorieux, secretary of laboratory, for her supporting and encouraging. Thanks to her help, I could succeed.

I would like to express my gratitude to all of the members of LGEF and my friends.

In addition, I would like to acknowledge the Japan Student Services Organization (JASSO) for their financial support.

Finally, I want to thank my father, mother, sister and brother-in-law for their understanding, support and encouragement.

Contents

Chapter 3
Elastocaloric effect of natural rubber

Chapter 4
Elastocaloric effect of P(VDF-TrFE-CTFE)

Chapter 5
General conclusions and future works

List of Symbols

A	Area of surface
C	Heat capacity
C_p	Specific heat capacity
C_v	Volumetric heat capacity
E	Electric field
F	Helmholtz free energy
f	Force
H	Magnetic field
h	heat transfer coefficient
l	Length
M	Magnetization
m	Weight
P	Polarization
p	Pressure
Q	Heat energy
$\dot{Q}_c$	Heat dissipation by convection
$\dot{Q}_d$	Total heat dissipation
$\dot{Q}_r$	Heat dissipation by radiation
q_r	Heat flow of reference material
q_s	Heat flow of sample
S	Entropy
S_e	Electronic entropy
S_l	Lattice entropy
S_m	Magnetic entropy
S_T	Entropy of magnetic material
T	Temperature
T_C	Curie temperature
T_s	Surface temperature of sample
T_0	Room temperature
t	Time
U	Internal energy
V	Volumetric heat capacity
W	Mechanical energy

ρ	Density
Σ	Stefan-Boltzmann constant
ε	Engineering strain
ε_{max}	Maximum strain
σ	Engineering stress
η	Conversion efficiency from mechanical energy to heat energy
λ	Elongation
β	Elastocaloric coefficient
γ	Stress elastocaloric coefficient

Chapter 1

General introduction

1.1 Introduction

Cooling technology is used for storage of fresh food, room cooling, manufacturing liquefied gas, etc. The cooling technology is essential for the modern society. The cooling technology has not only advantages but also drawbacks. Conventional cooling system, vapor compression / expansion, is needed to use the high global warming potential refrigerant such as hydrochlorofluorocarbon (HCFCs) and hydrofluorocarbons (HFCs). For protection of the ozone layer and prevention of global warming, the cooling technology which does not use those refrigerants are essential [1-3].

In recent years, caloric effects (CEs) have been investigated as the method which might be able to replace conventional vapor compression refrigeration system [3-7]. CEs are the phenomenon that temperature variation is caused by entropy change. Three types of CEs, magnetocaloric effect (MCE) [4-6], electrocaloric effect (ECE) [7] and elastocaloric effect (ElCE) [8-13], are often discussed as next-generation cooling technology. CE which combined at least two of these CEs is called multicaloric effect. The multicaloric effect has also been studied in recent years, because it is expected to achieve large temperature variation [14-16].

The aim of this chapter is describes the three caloric effect, their advantages and their drawbacks as well as the used materials.

It will also justify the choice we made to study the elastocaloric effect in this thesis.

1.2 Caloric effects

1.2.1 Magnetocaloric effect

The magnetocaloric effect (MCE) is an adiabatic and reversible temperature change based on an entropy change by a magnetic field. MCE occurs in magnetic material and was discovered by Warburg in 1881 [5, 17 and 18].

Entropy of magnetic material (S_T) is expressed with the total of magnetic entropy (S_m), lattice entropy (S_l) and electronic entropy (S_e) as

$$S_T(T, H) = S_m(T, H) + S_l(T) + S_e(T) \qquad (1.1)$$

where T is the temperature and H is the magnetic field. S_m depends on T and H values whereas S_l and S_e only depend on T. As a consequence, S_T both depends on T and H values.

In MCE, S_m is changed by applying a magnetic field. Change in magnetic entropy (ΔS_m) in MCE is expressed as

$$\Delta S_m(T, \Delta H) = \int_{H_0}^{H_1} (\partial M(T,H)/\partial T)_H \, dH \qquad (1.2)$$

The adiabatic temperature variation (ΔT_{ad}) in MCE is expressed as

$$\Delta T_{ad}(T, \Delta H) = -\int_{H_0}^{H_1} \frac{T}{C} \left(\frac{\partial M\ (T,H)}{\partial T}\right)_H dH \qquad (1.3)$$

where M is magnetization and C is heat capacity [19].

Eq. (1.2) and (1.3) show that ΔS_m and ΔT_{ad} depend on T and the variation of H. MCE is high when the magnetization variations versus T are large this is why is better to use magnetic material closed to one of its transition. As M decreased with T, $\frac{\partial M\ (T,H)}{\partial T}$ is negative as well as ΔSm (see Eq.(1.2)). On the contrary, ΔT_{ad} is positive (see Eq.(1.3)). Although the amplitude of ΔT increases with a decrease of C, ΔS is not affected by C values.

Fig 1.1 shows the scheme of MCE [18]. The magnetic moments in the magnetic material are randomly oriented when the magnetic field is null. When the magnetic material enters between the north and the south poles of magnet (a), the magnetic field is applied to the magnetic material and the material is magnetized due to the alignment of the magnetic moments. Since the state of the magnetic moments change from disorder to order, ΔS_m of the magnetic material becomes negative. As previously described, the magnetic material heats up due to MCE when ΔS_m becomes negative (Fig 1.1 (a)). A reverse process is observed when the magnetic field is removed. The magnetic material is removed from the magnet and the material is demagnetized. Since the state of the magnetic moments change from order to disorder, ΔS_m of the magnetic material becomes positive. As a result, the magnetic material cools down due to MCE (Fig 1.1 (b)).

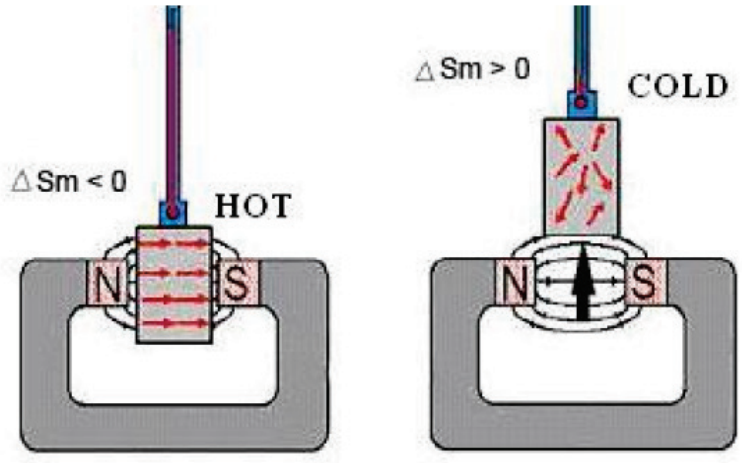

(a) (b)

Fig 1.1 Scheme of MCE (a) magnetization (b) demagnetization [18]

MCE has been investigated as refrigeration in cryogenic range below 1.0 K since 1920s. It is difficult to cool a temperature below 1.0 K with liquid helium which has the largest cooling effect at that time, but a method to cool a temperature below 1.0 K with MCE was reported by Giauque in 1926 [20]. Giauque used gadolinium (Ⅲ) sulfate octahydrate ($Gd_2(SO_4)_3 \cdot 8H_2O$) to obtain a temperature variation in temperature below 1.0 K. Liquid helium were used to cool $Gd_2(SO_4)_3 \cdot 8H_2O$ to a temperature of about 1.5 K and then $Gd_2(SO_4)_3 \cdot 8H_2O$ was cooled until 0.25 K with MCE. The material was ineffective to obtain temperature variation near room temperature.

Since Brown reported magnetic heat pumping near room temperature in 1976 [21], materials for MCE have been studied by many researchers [5, 6]. Brown showed that the gadolinium (Gd) a ferromagnetic material could be used for magnetic refrigeration near room temperature. Thanks to the Curie temperature (T_C) around 294 K, a phase transition occurs near room temperature leading to large variation of M and consequently to a large MCE near room temperature. As an example, a ΔT_{ad} value of 20K was observed for a ΔH of 10 T. In order to increase MCE effect, Gd alloy have been prepared using lanthanide metal but only a shift of the Tc has been observed.

Although the Gd based alloys show benefits for magnetocaloric effect, Gd is very expensive and Gd and its alloys are easily oxidized. Research works have been devoted to the replacement of Gd. In addition to their low oxidation, large magnetic entropy change was found in the perovskite manganese oxides, explaining why $LaCaMnO_3$ has been studied [22, 23]. But La is still a rare-earth metal so to reduce the cost other systems have been investigated including NiMnGa without finding any large MCE effect.

In refrigeration system using MCE, the needed cooling effect cannot be achieved with a single cycle. In addition, a heat transferred is required between the cold magnetic material and the system that needs to be cooled. As a refrigeration system which can store the cooling effect, active magnetic regenerator (AMR) was presented by Steyert and Barclay in 1978 and 1982 [24-26]. AMR is generally composed of porous bed of magnetic material which exhibits MCE, magnet to create the magnetic field, heat exchanger, heat exchange fluid and displacer. The schematic cycles of AMR are shown in Fig 1.2 [18]. In Fig 1.2, temperatures of magnetic material and of the fluid are shown in the insert. The solid line indicates the temperature of the bed of magnetic material and the dash line indicates the temperature of the fluid. The processes of AMR are as follows:

(a) The external magnets move and the magnetic material exposed to the magnetic field became magnetized. The magnetic entropy of the magnetic material decreases and

the temperature of the material increases due to MCE, as reported at the beginning of the chapter.

(b) The heat exchange fluid flows from the cold external heat exchanger (CHEX) to the hot external heat exchanger (HHEX) through the hot magnetic material in order to remove the heat from the material. The heat collected by the fluid is dissipated by the HHEX. The magnetic field is kept constant during this process.

(c) The external magnets are removed and the applied magnetic field to the material decreases. As the magnetic entropy of the material increases, the temperature of the material decreases due to MCE.

(d) The fluid flows from HHEX to CHEX through the cold material. The fluid is cooled by the cold material and then absorbs heat from CHEX. As a result, CHEX obtains the cooling effect from the fluid.

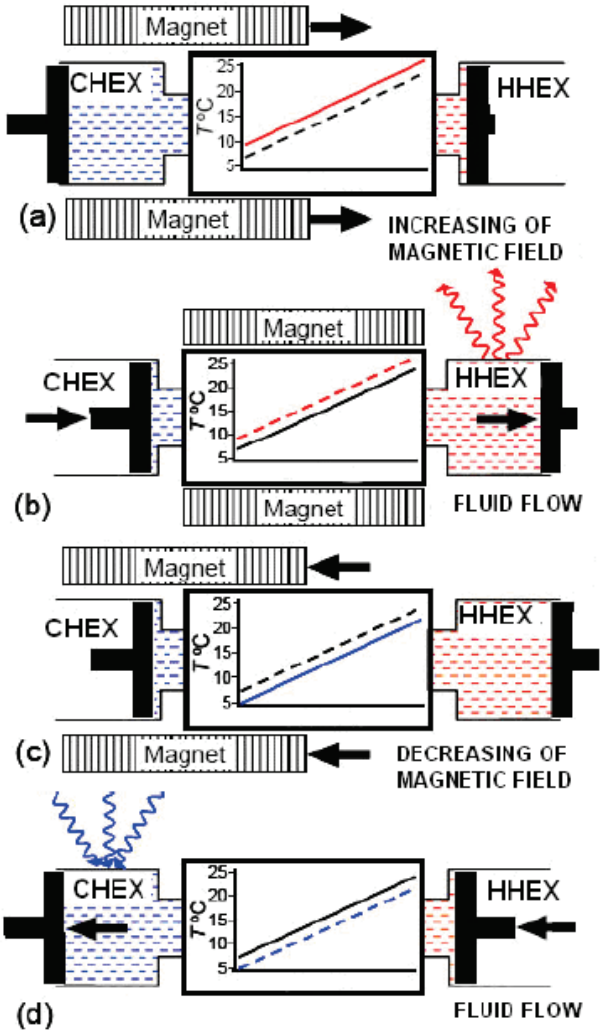

Fig 1.2 Schematic cycles of AMR [18]

The CHEX described Fig 1.2 can be used to pump heat from a hot source and consequently to cool it. Fig 1.3 describes the scheme of a reciprocating AMR [27]. With the pneumatic drive, the magnetic refrigerant beds move vertically through the superconducting magnet and are alternatively magnetized and demagnetized. With the help of pump, a fluid circulates only when the beds are immobilized. Heat from the bed inside the superconducting magnet ($\Delta S_m < 0$, $\Delta T > 0$) is exchanged with fluid and then dissipated by the HHEX. The bed outside magnet ($\Delta S_m > 0$, $\Delta T < 0$) cools the fluid and the CHEX. The heat from environment can be absorbed by the CHEX.

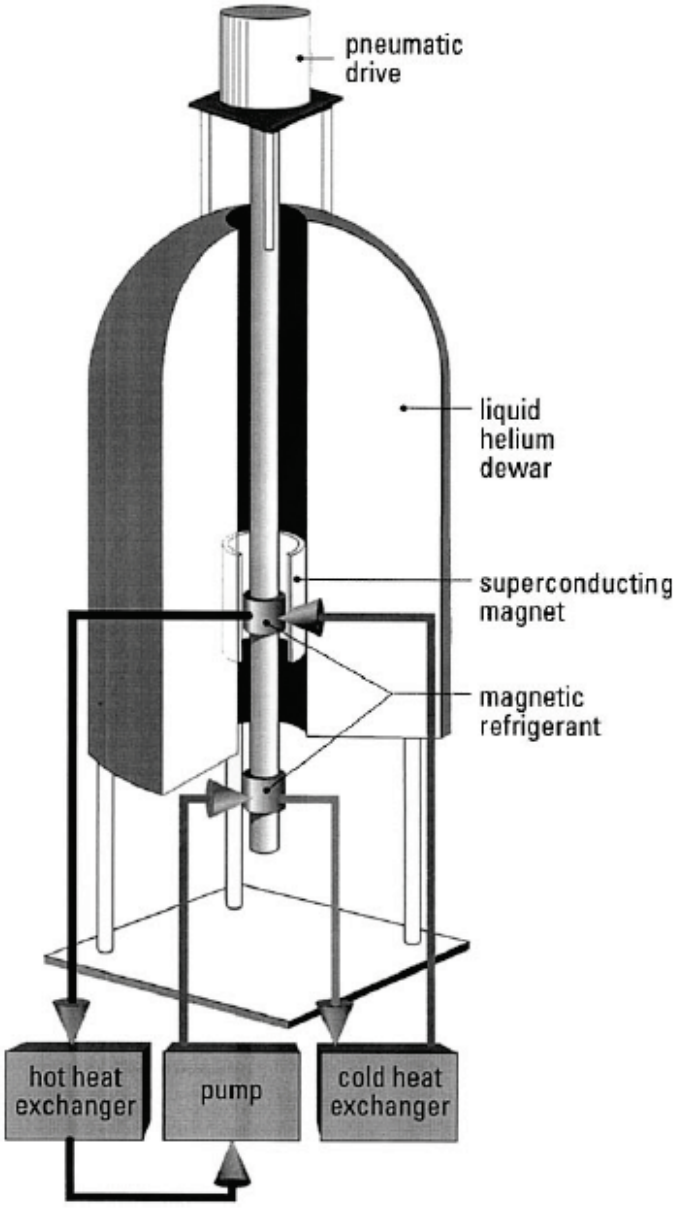

Fig 1.3 Scheme of reciprocating AMR [27, 28]

In 1997, Zimm et al reported that a temperature span (T_{HHEX} - T_{CHEX}) of 23 °C, can be obtained by applying a magnetic field of 5 T to Gd spheres at room temperature with this type of reciprocating AMR [27].

Although the reciprocating AMR shows large temperature span, the reciprocating AMR has drawbacks. The first concerns the operating frequency of the reciprocating AMR which is only 0.16 Hz because the fluid flow must be stopped when the beds move. As the cycle frequency is low, a large temperature variation must be obtained at each cycle. For that there is need of a large magnetic field variation which can only be obtained by using a superconducting magnet. Consequently, the second drawbacks are the use of a superconducting magnet, niobium-titanium (NbTi), to apply this large magnetic field, which requires liquid helium to maintain the temperature below the critical temperature of the superconducting magnet 10 K. The power for cooling the superconducting magnet is incomparably larger than this one obtained from reciprocating AMR. In order to overcome this limitation and to allow the use of regular magnets, the frequency of the cycles must be increased to compensate the decrease of the MCE induced temperature span. Fig 1.4 presents the scheme of a rotary AMR refrigerator using a permanent magnet [28].

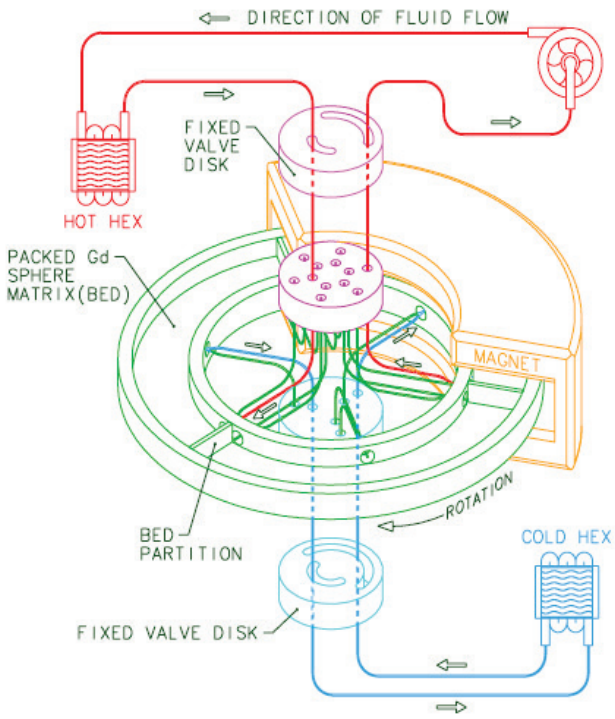

Fig 1.4 Scheme of rotary AMR [28]

In the rotary AMR, the magnetic material beds are rotated through permanent magnets. The cooling system uses the same strategy than this one of the reciprocating AMR (fluid circulation using a pump). The fluid is alternatively heated and cooled by the beds, which are inside and outside the magnet respectively. In comparison with the first system, the frequency is 25 higher.

Ongoing efforts are put on the development of materials which exhibit higher MCE.

1.2.2 Electrocaloric effect

The electrocaloric effect (ECE) which occurs in polar material is an adiabatic and reversible temperature change based on an entropy change by an electric field. By replacing the magnetization (M) by the polarization (P) and the magnetic field (H) by the electrical field (E), change in entropy in ECE is expressed as

$$\Delta S(T, \Delta E) = \int_{E_1}^{E_2} (\partial P / \partial T)_E dE \qquad (1.4)$$

The adiabatic temperature variation (ΔT_{ad}) in ECE is expressed as

$$\Delta T_{ad}(T, \Delta E) = -\frac{1}{\rho} \int_{E_1}^{E_2} \frac{T}{C_p} (\partial P / \partial T)_E dE \qquad (1.5)$$

where T is the temperature, ρ is the density and C_p is the specific heat capacity. Consequently, the mechanism of ECE is similar to this one observed of MCE: large variation of P versus T are necessary to obtain large ΔT_{ad}, this is why it is also better to use the material closed to one of its phase transition.

The Schematic ECE is shown in Fig 1.5 [7]. The processes of ECE are as follows:

(1) When the electric field is applied to the polar material, the material is polarized due to the alignment of the dipoles. Since the state of the dipoles change from disorder to order, ΔS of the polar material becomes negative. As a result, the polar material heats up due to ECE.

(2) The heat of the polar material is dissipated outside. During this stage, the electric field is kept constant in order not to change the entropy and the dipoles of the material are kept oriented.

(3) When the electric field is removed from the polar material, the material is depolarized. Since the state of dipoles change from order to disorder, ΔS of the polar material becomes positive. As a result, the polar material cools down due to ECE.

(4) The polar material absorbs external heat. During this stage, the electric field is null and the dipoles of the material are randomly oriented.

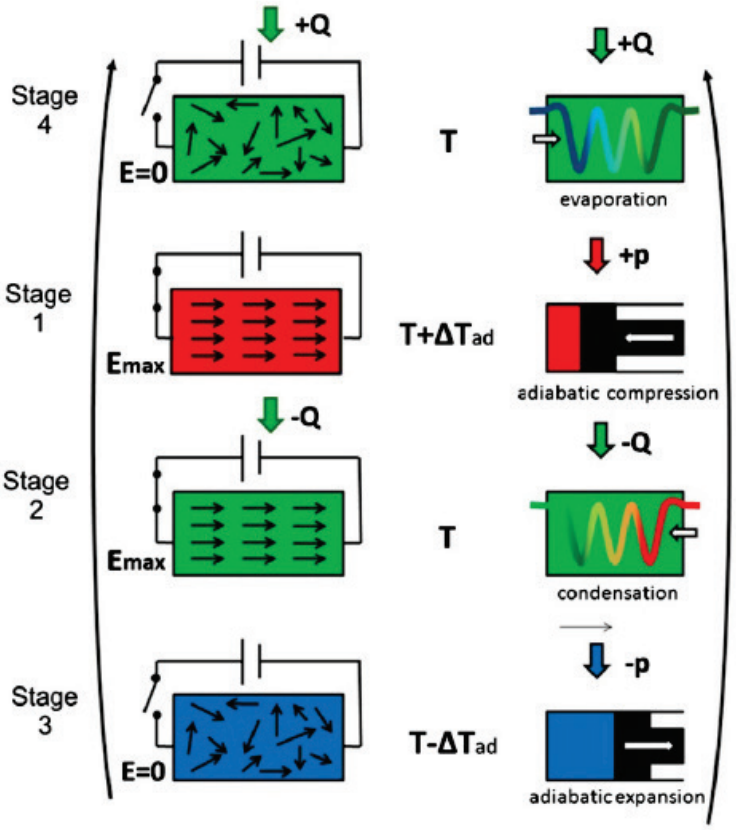

Fig 1.5 Scheme of ECE [7]

Compared with MCE, the advantage of ECE is that it is much easier to generate a high electric field than to generate a high magnetic field. It is expected that cooling system with ECE operates at lower cost than that with MCE. However, some issues need to be overcome.

The polar material has a very low electric conductivity, so that it behaves as insulating material. An increase in the electric conductivity causes leakage current under applying an electric field. The Joule heat is generated by the leakage current [7, 29]. As a result, the polar material continues to heat up during applying an electric field. When a large Joule heat occurs, the cooling effect due to ECE is hardly obtained.

The polar material has a very low electric conductivity, so that it behaves as insulating material. An increase in the electric conductivity causes leakage current under applying an electric field. The Joule heat is generated by the leakage current [29].

The alignment of the dipoles within the material generally requires a high applied electrical field, increasing the risk of the sample breakdown [30, 31]. Breakdown mechanisms depend on the sample thickness. Bulk and thick materials generally contain a large number of micrometric defects within their structure in comparison with

thin films. As a consequence, the breakdown mechanism of thin films is the electron avalanche whereas this one of bulk and thick materials is the electromechanical breakdown for which the micro defects are the origin of the fracture [32-34]. The mechanical breakdown generally occurs for a smaller electrical field than this one required for inducing electron avalanches. Consequently, thin film can withstand a higher electric field than bulk and think material. For example, thin film of $Pb(Mg_{1/3}Nb_{2/3})O_3$-$PbTiO_3$ (PMN-PT) 93/7 with a thickness of 210 nm only exhibits the ΔT of 9 °C under a 72 MV/m electric field at 25 °C whereas bulk material of PMN-PT 92/8 exhibits the ΔT of 1.35 °C under a 1.5 MV/m electric field at 23 °C [35, 36]. If a large ΔT can be obtained by ECE, by using thin films, due to the low volume V of the sample, only small heat variations (ΔQ) is observed ($\Delta Q = C_v V \Delta T$), where C_v is the volumetric heat capacity [7].

Alternative solutions consist of using bulk ceramic and thick polymer film near a phase transition in order to increase ΔT and to keep ΔQ as high as possible. Since ferroelectrics exhibit a large ΔP near the Curie temperature (T_C), a large ΔT can be obtained near T_C by ECE of ferroelectrics. Especially, ceramics containing lead (Pb) exhibit a quite large ΔP near T_C because the permittivity of ceramics containing Pb is a quite large near T_C. Thus, ceramics containing Pb exhibit a large ΔT near T_C. As an example, a ΔT value of 2.7 K was observed with PMN-PT 72/28 when ΔE of 1.2 MV/m is applied at 130 °C. Consequently, research for ECE has focused on ferroelectrics, especially ceramics containing Pb, in order to obtain a large ΔT.

In material selection, it is affected by social trends as well as by performance of material. Ceramics and single crystal with Pb have been widely used for ECE because they exhibit a large ΔT due to ECE as described previously. However, Pb is a poisonous material. The trend of research is changing to use Pb-free compounds in recent years in order to give consideration to the effect on humans. Not only ceramics and single crystal but also ferroelectric polymeric materials such as PVDF-based polymers are used in research for ECE to replace Pb [7].

Neese et al. reported ECE of P(VDF-TrFE) in 2008 [37]. PVDF-based polymers exhibit a large ΔT with thicker film than in ceramics. Ceramics require thickness of several hundred nanometers to exhibit ΔT of more than 5 °C but PVDF-based polymers exhibit ΔT of more than 5 °C even though the thickness is several micrometers. Moreover, PVDF-based polymers improved the temperature range of ECE. In order to achieve a large $|\Delta T|$ of more than 10 °C, some ceramics require temperature condition of more than 140 °C but PVDF-based polymers require temperature condition of less than 100 °C [31, 35, 37-45]. PVDF-based polymers have been investigated as materials

for ECE since Neese et al reported ECE of P(VDF-TrFE) [46-51].

However, ΔQ of materials due to ECE is smaller than that one obtained by MCE and the temperature range for obtaining a large ΔQ is still high. The improvement of the material is the priority issue for early realization of commercial refrigerator using ECE.

1.2.3 Elastocaloric effect

The elastocaloric effect (ElCE) is an adiabatic and reversible temperature variation based on a strain induced entropy variation. Similar to MCE and ECE, the entropy change (ΔS) in ElCE is expressed as

$$\Delta S(T, \Delta l) = -\int_{l_0}^{l_1} (\partial F/\partial T)_l dl \qquad (1.6)$$

The adiabatic temperature variation (ΔT_{ad}) in ElCE is expressed as

$$\Delta T_{ad}(T, \Delta l) = \int_{l_0}^{l_1} \frac{T}{C} (\partial F/\partial T)_l dl \qquad (1.7)$$

where T is the temperature, l is the displacement, F is force and C is the heat capacity. Consequently, the mechanism of ElCE is similar to this one observed of MCE and ECE: large variation of l and F versus T are necessary to obtain a large ΔT_{ad}. For ElCE, a material which shows entropic elasticity is used. The material contributes an applied force to an entropy change. Shape memory alloy (SMA) and polymer especially rubber show the entropic elasticity [8, 52-54].

The schematic ElCE is shown in Fig 1.6 [8]. Processes of ElCE with the material which shows entropic elasticity are explained as follows:

(a) Molecular chains of the material exhibiting entropic elasticity are disordered when the displacement is null.

(b) When the strain is applied to the material, the molecular chains of the material become aligned. Since the state of the molecular chains changes from disorder to order, ΔS of the material becomes negative. As a result, the material heats up due to ElCE.

(c) When the strain is released and the material returns to its original shape, the molecular chains of the material are randomly oriented. Since the state of the molecular chains changes from order to disorder, ΔS of the material becomes positive. As a result, the material cools down due to ElCE.

(d) The material absorbs the external heat and then the temperature of the material returns to room temperature.

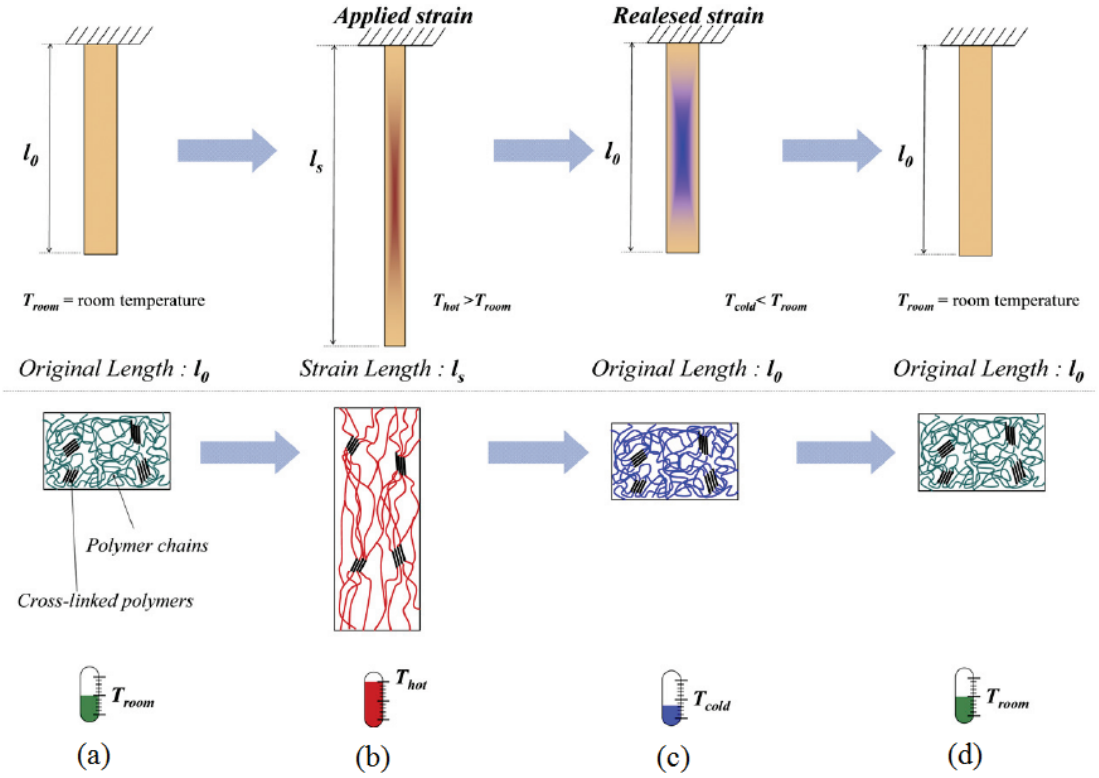

Fig 1.6 Scheme of elastocaloric effect [8]

ElCE has the advantages over MCE and ECE : the used materials (Shape Memory Alloy (SMA) and elastomer) are non-rare earth metals and consequently less expensive and non-toxic. Thick samples can also be used and large temperature variation can be achieved around the room temperature. The issues that need to be overcome are the heat dissipation during deformation and the generation of heat due to internal friction, a permanent strain by deformation and a reduction in elasticity by fatigue.

Figure 1.7 depicts the temperature variation (ΔT) versus time for a 20 µm NiTi film, at different strain rates, during a loading and an unloading cycle of same duration [10]. The maximal ΔT value decrease when the strain rates decrease whereas the ΔT peak width increases. This is the effect of the heat dissipation. As a consequence, in order to obtain a large ΔT, the material has to be stretched in an adiabatic process, which implies to build an experimental bench able to stretch the materials to be tested at high strain rates.

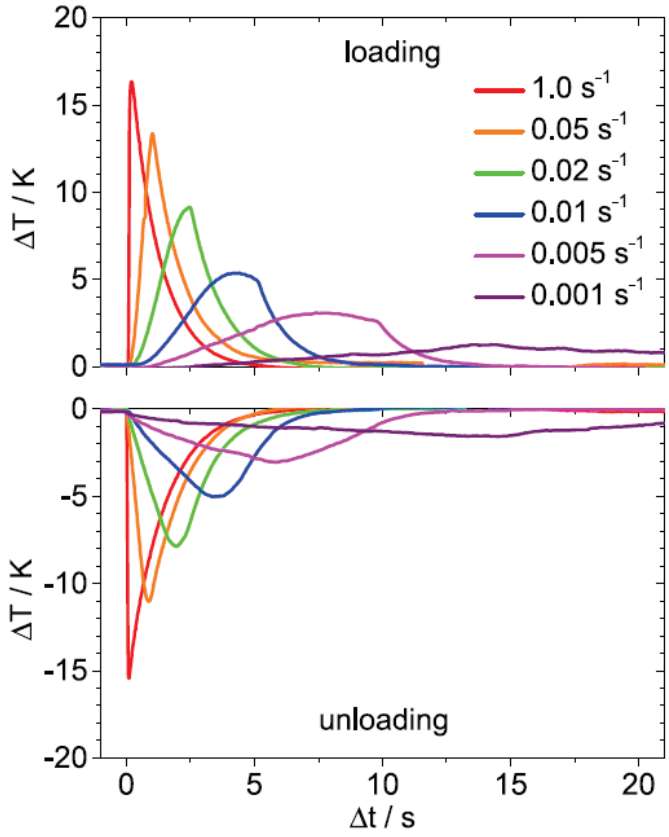

Fig 1.7 Relationships between time and ΔT of NiTi during loading and unloading of different strain rates [10]

However, the material heats up beyond the original performance value of ΔT due to ElCE when the deformation speed is too fast. Figure 1.8 shows ΔT at loading cycle versus the stretching time for natural rubber (NR) and natural rubber filled with carbon black (CB) [55]. The maximum ΔT value linearly decreases when the stretching time is increased. A slope variation is observed for the stretching time of 0.2 s. CB filled NR exhibit a higher ΔT for stretching times lower than 0.2s. No significant difference between NR and CB filled NR is observed for the highest stretching times.

This is the effect of internal friction. ΔT at unloading may also be affected by the effect. ElCE at unloading is endothermic reaction but internal friction at both loading and unloading is exothermic reaction. Since internal friction reduces ΔT in unloading process, the cooling effect decreases when the deformation speed is too fast. As a result, ΔT at unloading becomes lower than an expectation value. In order to confirm the presence or absence of the effect of internal friction, it is needed to compare ΔT at loading and unloading. If ΔT at loading is quite larger than ΔT at unloadting, this suggests that ΔT is affected by the internal friction.

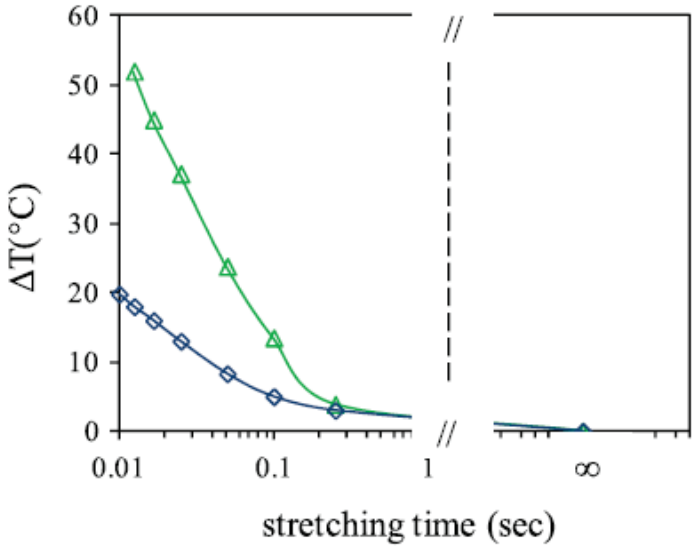

Fig 1.8 ΔT of NR without CB (diamond symbols) and NR with CB (triangle symbols) at loading cycle versus the stretching time [55]

When a material is stretched with a large displacement, permanent strain occurs and length of the material increases. After that, an applied force to the material decreases even if the material is stretched with the same displacement. Since ΔT decreases with a decrease in an applied force when the displacement is constant, permanent strain leads to a reduction in ΔT [46]. A reduction in elasticity by fatigue also causes a reduction in force even if the displacement is constant and the permanent strain does not occur. Thus, the reduction in elasticity by fatigue also leads to a reduction in ΔT. For the cooling system with ElCE, the material is stretched repeatedly. When the cyclic deformation controlled by displacement is conducted, the material is strongly affected by both permanent strain and fatigue. Amount of ΔT decreases gradually when stretching material is repeated. In order to reduce the effects of permanent strain and fatigue to ΔT, SMA and elastomer are used for ElCE because they are excellent in fatigue resistance and hyperelastic materials.

Table 1 shows examples of characteristics of SMA and elastomer in ElCE. ΔT of more than 2.0 °C can be obtained near room temperature by ECE, and NiTi especially exhibit a large ΔT (ΔT >15.0 °C). SMA exhibit a large ΔT with strain of several percent but stress exceeds 100 MPa. On the other hand, natural rubber (NR) exhibits ΔT of 2 °C and −6 °C with strain of 500 %. In order to exhibit a large ΔT, NR requires approximately 100 times larger strain than SMA. NR needs a large space for deforming but SMA does not need such a large space. If we focus on stress, NR has an advantage. NR generally receives a stress 15 MPa or less when strain of 500 % is applied. Thus, SMA requires

100 or more times larger stress than NR. NR exhibits a large ΔT with a small stress.

Shape memory alloys (SMAs) have been investigated as materials for ElCE because SMAs are excellent in fatigue, hyperelastic materials and do not need to apply a large deformation as previously described. Moreover, SMAs are non-toxicity and easy to obtain in comparison to material for MCE [9, 10, 13, 56-62]. On the other hand, polymers also exhibit an entropy change by deformation but they generate permanent strain and are affected by fatigue easily except for elastomer. Elastomer is excellent in fatigue but requires a large displacement to obtain a large ΔT. Since it is needed a long time to apply a large displacement, the heat dissipation occurs and it is difficult to obtain a large ΔT. Consequently, research papers about ElCE of polymers including elastomer are relatively less than those of SMAs.

There is other issue in ElCE. Previous research has evaluated the materials for ElCE with relationship between ΔT and stress, or ΔT and strain. Since ElCE depends on force and displacement, it is possible to evaluate the materials with the relationships when the materials are linear elastic material. However, it is improper to focus only on stress or strain when non-linear elastic material such as rubber is used. Stress-strain (S-S) curve of linear elastic material is proportional but that of nonlinear elastic material is not proportional. If S-S curve shows logarithmic or exponential curve, ΔT becomes large even though stress or strain variation is quite small. In these cases, it is difficult to evaluate the performance of material with only stress or strain. In order to evaluate and compare the performance of materials for ElCE, an effective index for that is needed.

Table 1.1 Characteristics of materials for elastocaloric effect

Material	Thickness (mm)	Stress (MPa)	Strain (%)	T (°C)	ΔT (°C)		ref.
					stretching	contracting	
NR	0.05	-	500	24	2	-6	[8]
Fe-31.2Pd	11.6	200	-	27	2.5	-2.5	[9]
$Ni_{45}Mn_{36.4}In_{13.6}Co_5$	5.5	150	5	23	4	-4	[13]
NiTi	0.025	500	5	room temperature	17	-16	[10]
NiTi	3.0	700	8	22	25.5	-17	[59]

1.3 Work mechanism of elastocaloric effect

As described in the previous section, the temperature variation (ΔT) in elastocaloric material is caused by the entropy change due to the deformation. The mechanism of

ElCE is presented in details in this section. The entropy change and the temperature variation due to stretching are modeled with the help of the constitutive laws of thermodynamics.

The entropy change due to deformation can be explained by the first and second laws of thermodynamics [63-65]. The first and the second law of thermodynamics are expressed as:

$$dU = dQ + dW \quad (1.8)$$

$$TdS = dQ \quad (1.9)$$

where dU is the variation of the internal energy, dQ is the heat energy received from external sources, dW is the mechanical energy received from external sources, T is the temperature and dS the entropy change. When the external force f is applied to material causing the displacement dl, dW is given by

$$dW = fdl - pdV \quad (1.10)$$

where p is the pressure and dV is the variation of volume. By assuming that dV due to deformation is quite small, pdV is neglected in the equation (1.10).

Eq. (1.8), (1.9) and (1.10) give:

$$dU = TdS + fdl \quad (1.11)$$

Under a constant temperature condition, the external force f is expressed as:

$$f = (\partial U / \partial l)_T - T(\partial S / \partial l)_T \quad (1.12)$$

Eq. (1.12) shows that the external force is divided into the force contributing to the internal energy and the force contributing to the entropy change.

Here, the Helmholtz free energy F is defined as:

$$F = U - TS \quad (1.13)$$

We use the differential form of Eq. (1.13) to get the energy variation as:

$$dF = dU - TdS - SdT \quad (1.14)$$

(1.11) and (1.14) give:

$$dF = fdl - SdT \quad (1.15)$$

The Maxwell relation of the cross derivative gives:

$$-(\partial f / \partial T)_l = (\partial S / \partial l)_T \quad (1.16)$$

Finally, Eq. (1.12) can be written:

$$f = (\partial U / \partial l)_T + T(\partial f / \partial T)_l \quad (1.17)$$

According to Eq. (1.17), it is possible to measure the force contributing to the internal energy and the force contributing to the entropy change by applying temperature change under constant length.

In case of material which shows energetic elasticity such as spring, percentage of the force contributing to internal energy is quite high. In case of material which shows

entropic elasticity such as rubber, on the other hand, percentage of the force contributing to entropy change is quite high. Fig 1.9 shows the distribution of force in natural rubber [64-65]. It is seen that most of the external force contributes to the entropy change when strain exceeds 100 %. According to a study published by R. L. Anthony [65], the force contributing to the entropy change has a high proportion, more than 90 %, of the external force. However, the force contributing to the internal energy has a high proportion of the external force in regions of small strains [64].

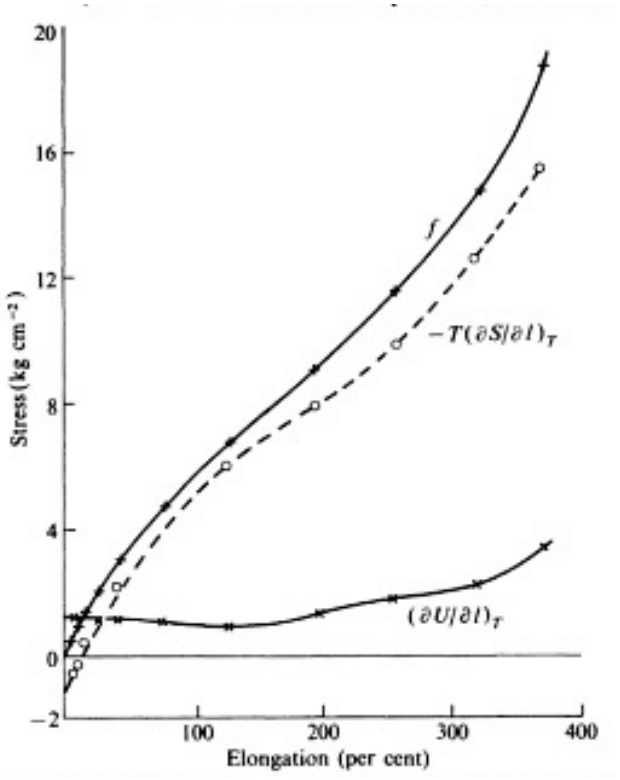

Fig 1.9 Distribution of force in rubber [64]

Temperature variation in ElCE is derived from entropy change. Entropy change under constant pressure is expressed as

$$dS = (\partial S/\partial T)_l \, dT + (\partial S/\partial l)_T \, dl \quad (1.18)$$

Eq(1.18) can be rewritten using thermal capacity $C = T(\partial S/\partial T)_l$ as

$$dS = (C/T) \, dT + (\partial S/\partial l)_T \, dl \quad (1.19)$$

In deformation under adiabatic process, there is no heat exchange between material and the environment ($dQ = 0$ and from Eq. (1.9), $dS = 0$). Thus, $0 = (C/T)dt + (\partial S/\partial l)_T \, dl$:

$$\Delta T_{ad}(T,\ \Delta l) = -\ T/C\ \ \int(\partial S/\partial l)_T\, dl \qquad (1.20)$$

Eq. (1.16) and (1.20) give:

$$\Delta T_{ad}(T,\ \Delta l) = T/C\ \ \int(\partial f/\partial T)_l\, dl \qquad (1.21)$$

Since the entropy change depends on the displacement and becomes large when the force variation versus T is large, ΔT_{ad} in ElCE increases with the increase in the displacement and becomes large when the force variation versus T is large.

Ideal material exhibiting entropic elasticity does not change its internal energy during stretching. Putting $dU = 0$ in Eq. (1.8) we obtain

$$dW = -dQ \qquad (1.22)$$

The ideal rubber completely converts the mechanical energy received from external sources to the heat energy because the external force completely contributes to the entropy change. Since the mechanical energy is completely converted to the heat energy, the ideal rubber is an extremely efficient material for ElCE.

1.4 Elastomer

Elastomers are polymers which consist of relatively long molecular chains having a high degree of flexibility and mobility. Elastomers have low modulus and their fracture strain is quite large because of the flexibility and mobility of molecular chains. Rubber, a famous example of elastomers, can be stretched up to several times its original length. Stretched elastomer returns to original length due to Brownian motion when the stress is removed. As a result, elastomers show entropic elasticity [66-68]. As a typical example of elastomer, characteristics of rubbers are described blow.

1.4.1 Rubber

Rubber is obtained by purifying latex from the Hevea Brasiliensis, commonly called rubber tree. The rubber obtained from the rubber tree is natural rubber (NR). NR is a elastomer which is composed of cis-polyisoprene ($(C_5H_8)_n$) [63, 64]. This purified NR (unvulcanized NR) is elastic body and has been used as gum eraser. Rubber can be obtained not only from the rubber tree but also by chemical synthesis. The rubber obtained by this method is called synthetic rubber. Polyisoprene (isoprene rubber, IR) obtained by chemical polymerization of isoprene has the same molecular formula as natural rubber but their structural formulas are different. Fig 1.10 (a), (b) and (c) shows structural formula of isoprene, cis-polyisoprene and trans-polyisoprene, respectively [69]. The structural formula of most natural rubbers is consisted of 100 % of cis-type but that of IR is not consisted of 100 % of cis-type because it is extremely difficult to produce 100 % cis-type artificially. Thus, molecular structure of natural rubber exhibits so high

stereoregularity that it cannot be attained by chemical polymerization. Although the difference in the structure does not affect significantly the behavior of molecular orientation and the crystal fraction at high strain due to deformation, the decrease in the stereoregularity becomes a factor of delaying the progress of the crystallization due to deformation at not high strain region [70].

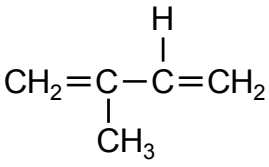

(a) isoprene

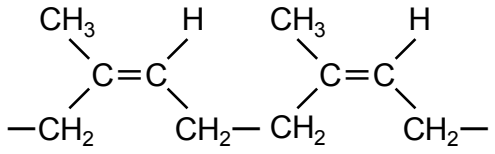

(b) cis-polyisoprene

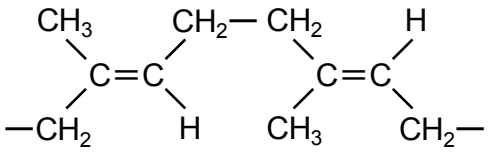

(c) trans-polyisoprene

Fig 1.10 Structural formula of isoprene, cis and trans type of polyisoprene [69]

In 1839, vulcanization method was discovered by Chales Goodyear [63, 64]. As the discovery of vulcanization method, applications of rubber have changed dramatically. Rubber is used as tire, vibration proof material, etc. at the present time. The vulcanization method discovered by Chales Goodyear is a chemical reaction with sulfur. At present, vulcanization method with peroxide is also well known [71].

Vulcanization is one of cross-linking reactions to change chemical and physical properties. Vulcanized rubber expresses unique and famous characteristic. The general vulcanization process is that vulcanizing agent, vulcanization accelerator, activator and degradation preventing agent are added to unvulcanized rubber and then the mixture is heated for a certain period of time. Vulcanizing agent links with molecular chains of rubber as shown in Fig 1.11 and vulcanized rubber forms the three-dimensional network structure [72]. As a result, vulcanized rubber can be stretched several times larger than original length with small stress and then rubber returns to original length when the stress is removed. The cross-link density increases with an increase in amount of vulcanizing agent and the modulus increases with an increase in the cross-link density. However, excessive vulcanization causes degradation in physical properties due to losing mobility of molecular [73, 74]. Vulcanization using sulfur can be conducted to

rubbers having double bond in molecule (unsaturated rubber) such as NR, IR but cannot be conducted to rubbers not having double bond in molecule (saturated rubber) such as ethylene-propylene copolymer (EPM) and silicone rubber (Q). Although the physical property of the unsaturated rubber can be improved by the vulcanization, the unsaturated rubber is easily affected by heat and chemical reaction. On the other hand, the saturated rubber is hardly affected by heat, chemical reaction and oil. However, a large strain cannot be applied to the saturated rubber with some exceptions because mobility and flexibility of molecules in the saturated rubber is low [66]. The steric hindrance also causes the decrease in them. The mobility and the flexibility are based on the rotation of molecular chains [63, 67]. Since the rotation is restricted by steric hindrance between neighboring atoms or side-groups, the effect of steric hindrance becomes large when large side-groups such as methyl and aryl substituent exist on the molecular chains [75]. Thus, a rubber such as butyl rubber (IIR) exhibits low mobility and flexibility due to the steric hindrance [76, 77].

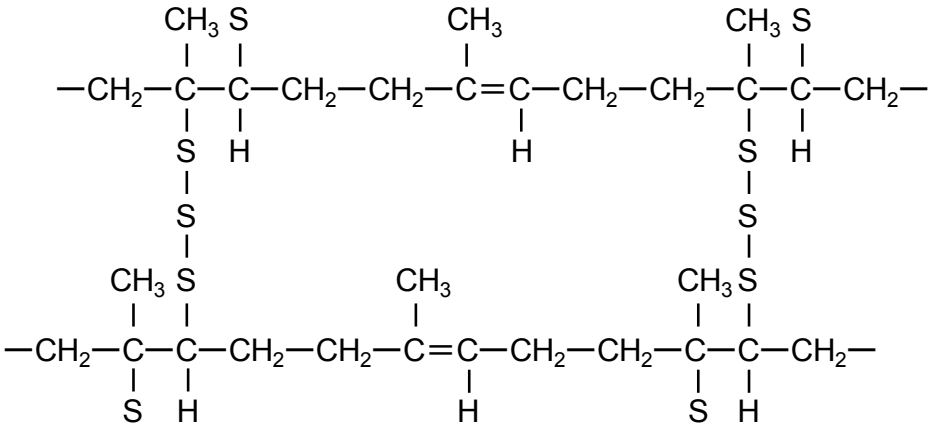

Fig 1.11 Example of structural formula of vulcanized natural rubber (NR) [72]

Adding fillers such as carbon black (CB) to rubber is a method for strengthening rubber [73, 78]. Fukahori proposed a hypothesis which explains mechanism of reinforcement of rubber by using CB in 2004 [79]. According to Fukahori's hypothesis, two polymer phases which rubber and CB are mixed are formed around CB as shown in Fig 1.12 [79]. The inner polymer layer is glassy hard (GH) layer and the outer polymer layer is sticky hard (SH) layer. Since GH layer is strongly adhered to the surface of CB, the mobility of GH layer is strictly constrained. GH layer does not affect the reinforcement of rubber but SH layer affects that. Although SH layer is loosely bound phase, SH layer becomes hard under large extension because of oriented molecular of

SH layer. As a result, strength of rubber increases. Since modulus, strength and fatigue resistance of rubber are improved by adding fillers, fillers are often added to a rubber especially for industrial use. The reinforcement effects of fillers depend on kind of filler and rubber.

As previously described, rubber can be stretched several times larger than original length with small stress and then rubber returns to original length when the stress is removed. Other famous physical characteristic is that stress-strain (S-S) curve of rubber clearly shows non-linear. Since elasticity of rubber depends on strain rate, Hook's law that the applied force to material is directly proportional to the displacement cannot apply to rubber. Strain-induced crystallization (SIC) and Mullins effect can be given as the reasons which rubber shows distinctive S-S curve. SIC and Mullins effect are described below.

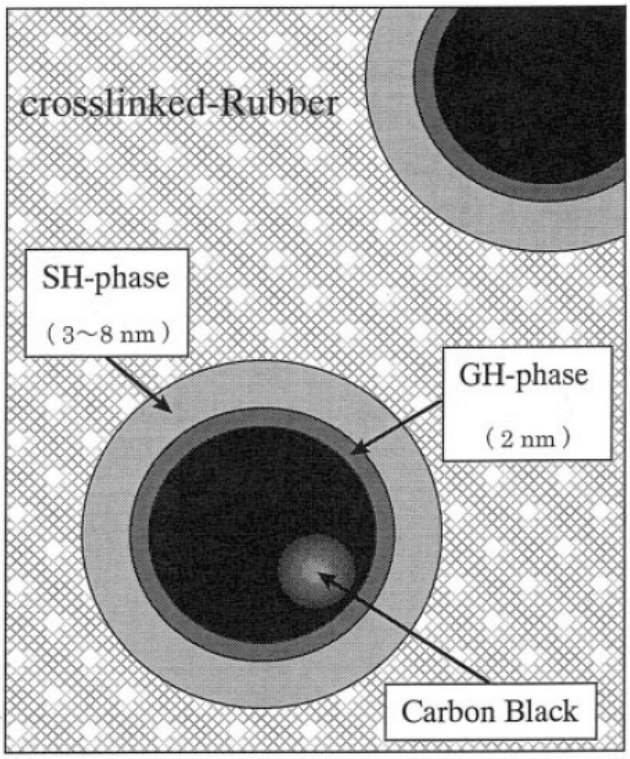

Fig 1.12 A double-layer interface model consisting of a GH layer and a SH layer [79]

1.4.2 Crystallization

Some elastomers such as NR, IR and polychloroprene (CR) exhibit crystalline due to a decrease in temperature and a large strain [63, 64, 73 and 74]. When the elastomer crystallizes, elastic modulus of the elastomer increases. The stress of the elastomer increases drastically during stretching due to the increase in elastic modulus. Thus, S-S

curve of the rubber become non-linear. Crystallization caused by a decrease in temperature is temperature-induced crystallization (TIC) and that caused by a large strain is SIC [80~95]. For TIC, the temperature and the duration are important factors. When the elastomer is kept at a temperature of less than 0 °C for several hours, TIC is observed [93, 96]. In TIC, molecular chains crystallize in the randomly oriented state because strain is not applied to elastomer. As a result, crystallization is oriented randomly. On the other hand, SIC is considered as behavior which a part of fully stretched molecular chains act as nucleus of crystallites (see Fig 1.13 [81]). Molecular chains are oriented randomly before stretching (Fig 1.13 (a)). The molecular chains are oriented gradually in the direction of extension due to stretching. Since these are differences in the length of molecular chains, long chains are still randomly oriented but short chains are fully stretched when the extension exceeds threshold (Fig 1.13 (b)). The movement of the fully stretched chains is restricted. As a result, the fully stretched molecular chains behave as nucleus of crystallites (Fig 1.13 (c)). Crystallinity is increased by extension when the extension exceeds threshold and then decreased by contracting because fully stretched molecular chains return to random state. A strain which crystals melt completely is smaller than the threshold strain of crystallization. Besides, it is reported that the crystallinity increases due to maintaining the crystallized state [91]. Since elastic modulus of the elastomer increases due to fully stretched molecular chains in the crystallized state, stress increases drastically in the crystallized state. Consequently, stress-strain curve of the elastomer shows non-linear.

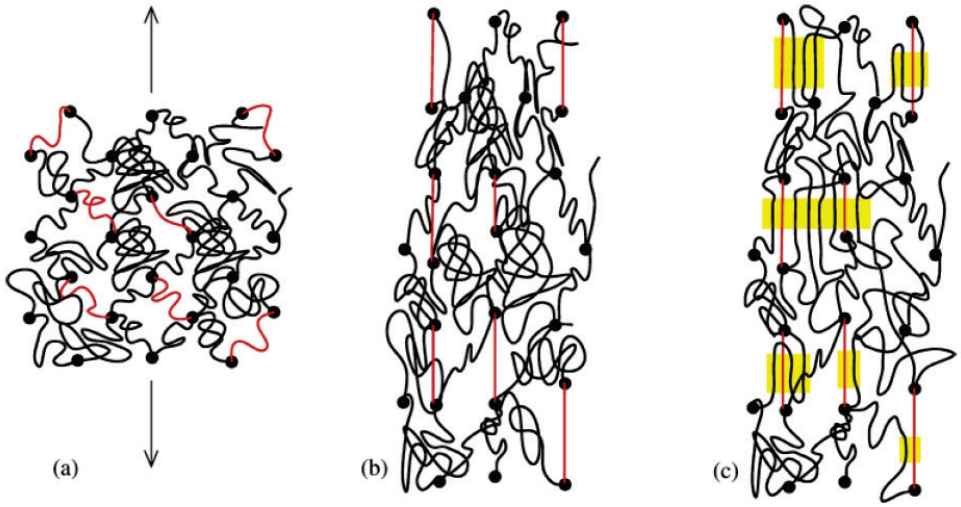

Fig 1.13 Model of nucleation and crystallization in NR; (a) Before deformation (short chains are drawn as red lines) (b) After deformation (c) Fully stretched chains act as nucleus of crystallites (yellow parts) [81]

In SIC research, Wide angle X-ray diffraction (WAXD) and small angle X-ray scattering (SAXS) measurements have been conducted in order to evaluate crystallinity and orientation of molecular chain during deformation. Since the performance of testing devises has been improved, the research technique has been developed over the past dozen years. Evaluation of SIC in real time with synchrotron X-ray, rapid-response CCD camera and small size tension testing machine is an example. Thanks to real time evaluation, observation of SIC during deformation became available.

Fig 1.14 shows stress-strain curve and selected WAXD patterns of NR during stretching and contracting at 0 °C [70]. NR-S means NR vulcanized by sulfur. In the deformation test, the stretching speed was 10 mm/min. In stretching process, the WAXD pattern at strain of 1.0 (strain of 100 %) shows only circle shape which indicates the isotropic amorphous. Thus, no crystallinity is observed at strain of 1.0. Oriented crystalline pattern begins to appear at a strain around 2.0 and crystallinity increases with an increase in strain. Fig 1.14 clearly shows that stress increases drastically after the increase in crystallinity. On the other hand, crystallinity during contracting is much more apparent than that during stretching at the same strain even though the stress during contracting is much smaller than the during stretching. No crystallinity is

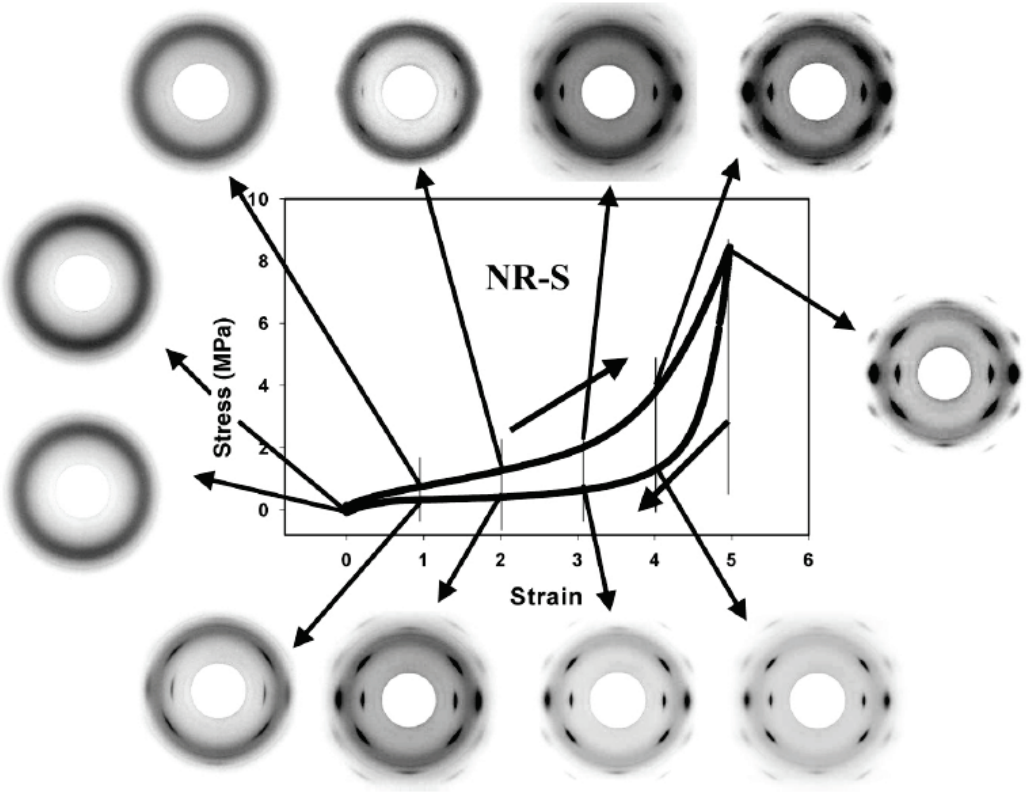

Fig 1.14 Stress-strain curve and selected WAXD patterns during extension and contraction [70]

observed at strain of 1.0 during stretching but crystallinity is clearly seen at strain of 1.0 during contracting. When the strain returns to zero, the crystallinity disappears completely.

Toki reported that the strain-induced crystalline network is reoriented during the first extension and contraction cycle and then the network structure becomes stable. Toki showed that different processes of SIC during the first and the second extension and contraction cycle with propylene based ethylene-propylene copolymer (EPM) [82]. The total crystal fraction, oriented crystal fraction and unoriented crystal fraction during the first cycle is shown in Fig 1.15 (a) and those during the second cycle is shown in Fig 1.15 (b). In the first cycle, strain was applied to EPM from strain of 0 to 5 and then removed from EPM from strain of 5.0 to 1.7. At strain 1.7, stress returned to 0 because of permanent strain. The second cycle started from strain of 1.7 and strain was applied until 5.0. All crystal was unoriented at strain zero before expansion. During expansion in the first cycle, the oriented crystal fraction was almost 0 % until strain 0.7 and then increased with an increase in strain. The oriented crystal fraction exceeded 20 % at strain 5.0. During contracting, the oriented crystal fraction decreased with a decrease in strain but the amount of the fraction was larger than that during extension. After contracting, the oriented crystal fraction was about 15 % at strain 1.7 even though the fraction was less than 10 % at strain 1.7 during expansion. On the other hand, the unoriented crystal fraction decreased during expansion. The fraction decreased from 14 % to 4 % with an increase in strain from 0 to 1.9 and then decreased slightly when strain was applied from 1.9 to 5.0. During contracting, the fraction increased very slightly with a decrease in strain. In total crystal fraction, the fraction decreased with an increase in strain as well as the unoriented crystal until strain 0.7. Since the oriented crystal fraction increased when strain exceeded 0.7 and the effect of increase

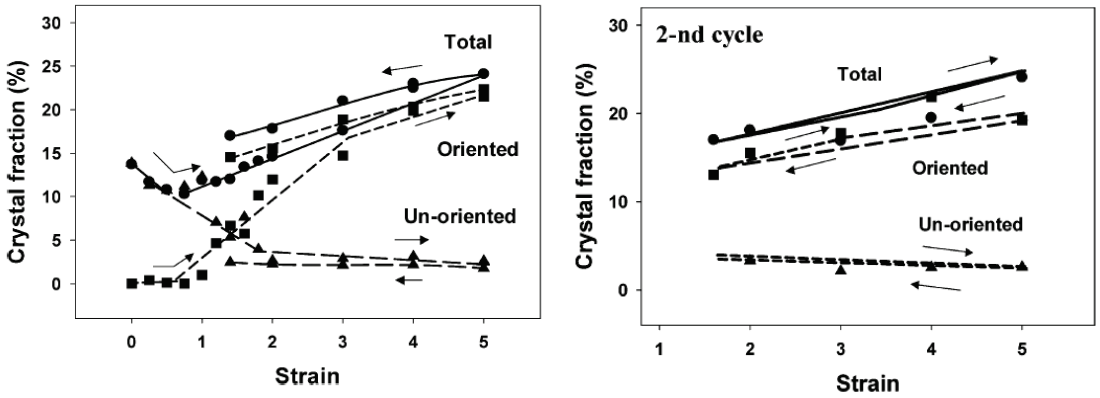

Fig 1.15 Crystal fraction during extension and contraction
(a) First cycle, (b) Second cycle [82]

rate of the oriented crystal fraction was larger than the effect of decrease rate of the unoriented crystal fraction, the total crystal fraction increased gradually with an increase in strain when strain exceeded 0.7 and increased up to 25 % at strain 5.0. During contraction, the total crystal fraction decreased gradually with a decrease in strain and became about 17 % at strain 1.7. The oriented crystal fraction and the total crystal fraction were increased and the unoriented crystal fraction was decreased by the first cycle. Moreover, it was observed that the processes of crystallizations during expansion are not opposite to those during contraction in the first cycle. In other word, SIC in the first cycle is irreversible process. On the other hand, process of crystallization during the second cycle is different from that of the first cycle as shown in Fig 1.15(b). It was seen that both the total crystal fraction and the oriented crystal fraction increased with an increase in strain and decreased with a decrease in strain. Those crystal fractions during contraction were almost the same as those during expansion. The unoriented crystal fraction decreased with an increase in strain and increased with a decrease in strain. The tendency of the unoriented crystal fraction is different from the total and the oriented crystal fraction but the unoriented crystal fraction during contraction is almost the same as that during expansion. As a result, it was found that the SIC in the second cycle is different from that of the first cycle, and reversible process. Since the network structure of strain-induced crystalline was reoriented during the first extension and contraction cycle and the network structure became stable after the first cycle, the process of SIC in the second cycle became reversible.

As described previously, stress increases drastically due to fully stretched molecular chains when the elastomer is stretched enough to be crystallized. As a result, the work received from external source (W) of the elastomer increases drastically. Since the entropy change in ElCE is significantly affected by W, it is inferred that the increase in the stress leads to the increase in the amount of temperature variation by ElCE.

SIC is irreversible process in the first cycle but the process becomes stable after the first cycle. As a result, the effect of SIC on the S-S curve does not change greatly from the second cycle. Since the effect of SIC on mechanical property does not change greatly, it is inferred that the effect of SIC on temperature variation by ElCE does not change greatly after the first cycle.

1.4.3 Mullins effect

Elastomer is remarkably softened by the first extension. The remarkable softening caused by extension occurs by the first extension but does not occur from the second

extension. Thus, S-S curve of the first extension shows different tendency from that of after the first extension. The softening has been intensively investigated by Leonard Mullins and the mechanical behavior is called Mullins effect [97~99]. In evaluating the mechanical property of elastomer, it is necessary to consider Mullins effect.

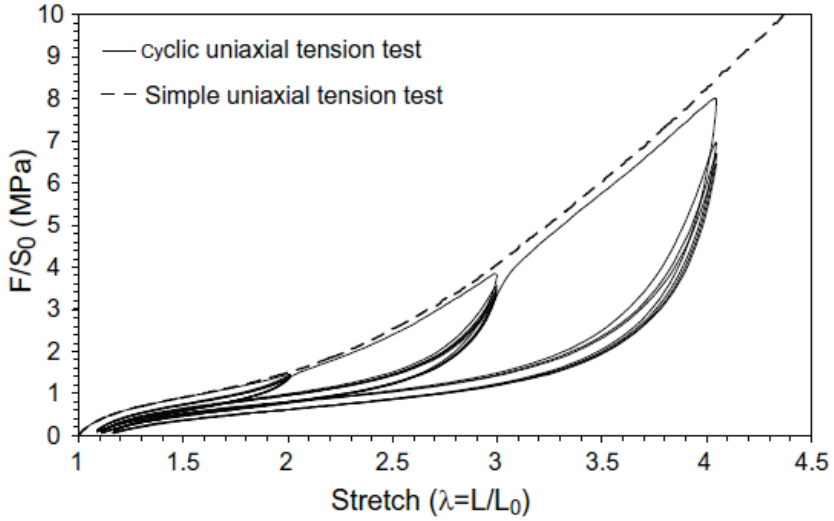

Fig 1.16 Stress-strain curve during cyclic deformation with increasing maximum strain every 5 cycles [98]

As an example of Mullins effect, S-S curve of styrene-butadiene rubber (SBR) during cyclic deformation with increasing maximum strain every 5 cycles is shown in Fig 1.16 [98]. The initial lengths of samples are express as “stretch” of 1.0 in Fig 1.16, “stretch” becomes 4.0 when strain of 300 % is applied. The results of cyclic deformation and unused sample are depicted in the solid line and the dash line, respectively. The effect of softening on S-S curve depends on the maximum strain applied previously. Since the largest softening effect occurs due to the first cycle, there is a large difference between S-S curve of the first cycle and after the first cycles when the same strain is applied. Compared with the first cycle, stress at the maximum strain of after the first cycles is lower and stress before reach the maximum strain is considerably lower. After the first cycle, the stress at the maximum strain decreases slightly with an increase in number of cycles and stress before reach the maximum strain is hardly changed with an increase in number of cycles. This result indicates that rubber is considerably affected by the Mullins effect in the first cycle and then affected by fatigue rather than the Mullins effect after the first cycle. When the extension exceeds the maximum strain applied previously, S-S curve shows similar curve of unused material. The effect of softening on S-S curve appears clearly in extension but does not appear in contracting.

It is well known that the recovery from the softening caused by the Mullins effect occurs due to exposing at a high temperature for long time [100]. Mullins measured the stress at a strain of 200 % of NR stretched up to strain of 420 % and compared it with that of unused NR. The stress at a strain of 200 % recovered to less than 20 % at room temperature but it recovered to 80 % due to heating at 100 °C for two days. Julie Diani reported the recovery with SBR [98]. Fig 1.17 shows the comparison of S-S curve between unused SBR and SBR conducted recovery process. The recovery process was conducted at 80 °C in vacuum and samples were stretched up to strain of 200 % before the recovery process. Although the effect of recovery was incompletely obtained when the recovery process was conducted for 3 hours, S-S curve showed almost the same shape as unused sample after the recovery process of 17 hours. The recovery from the softening occurs under room temperature but the effect of the recovery is quite small. In order to obtain a large effect of the recovery, it is necessary to expose the material to high temperature for long time.

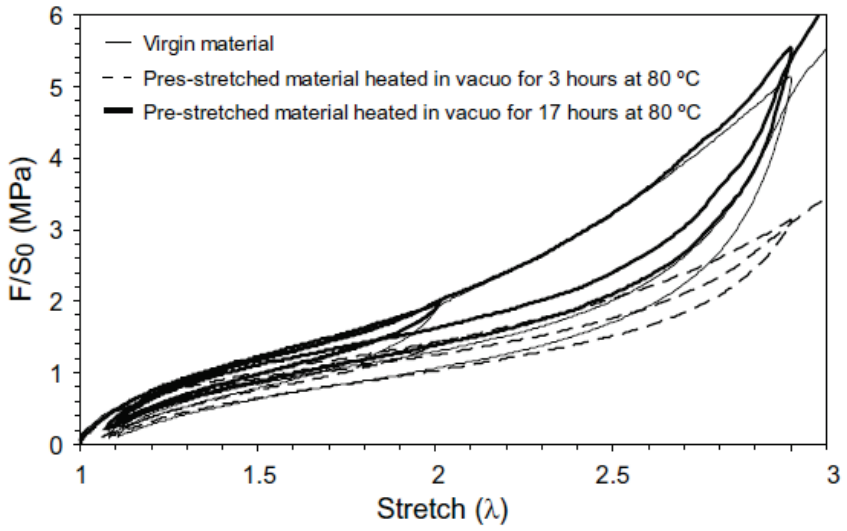

Fig 1.17 Recovery of pre-stretch softening by in vacuo heating [98]

In order to understand the Mullins effect, several physical interpretations have been proposed as shown in Fig 1.18 [98]. Blanchard and Parkinson made a hypothesis that the Mullins effect is caused by bond ruptures [101]. The softening occurs because the weak bonds are ruptured by applied strain in the hypothesis. However, it is difficult to explain the recovery from Mullins effect with the hypothesis. Especially, the small recovery at room temperature cannot be explained.

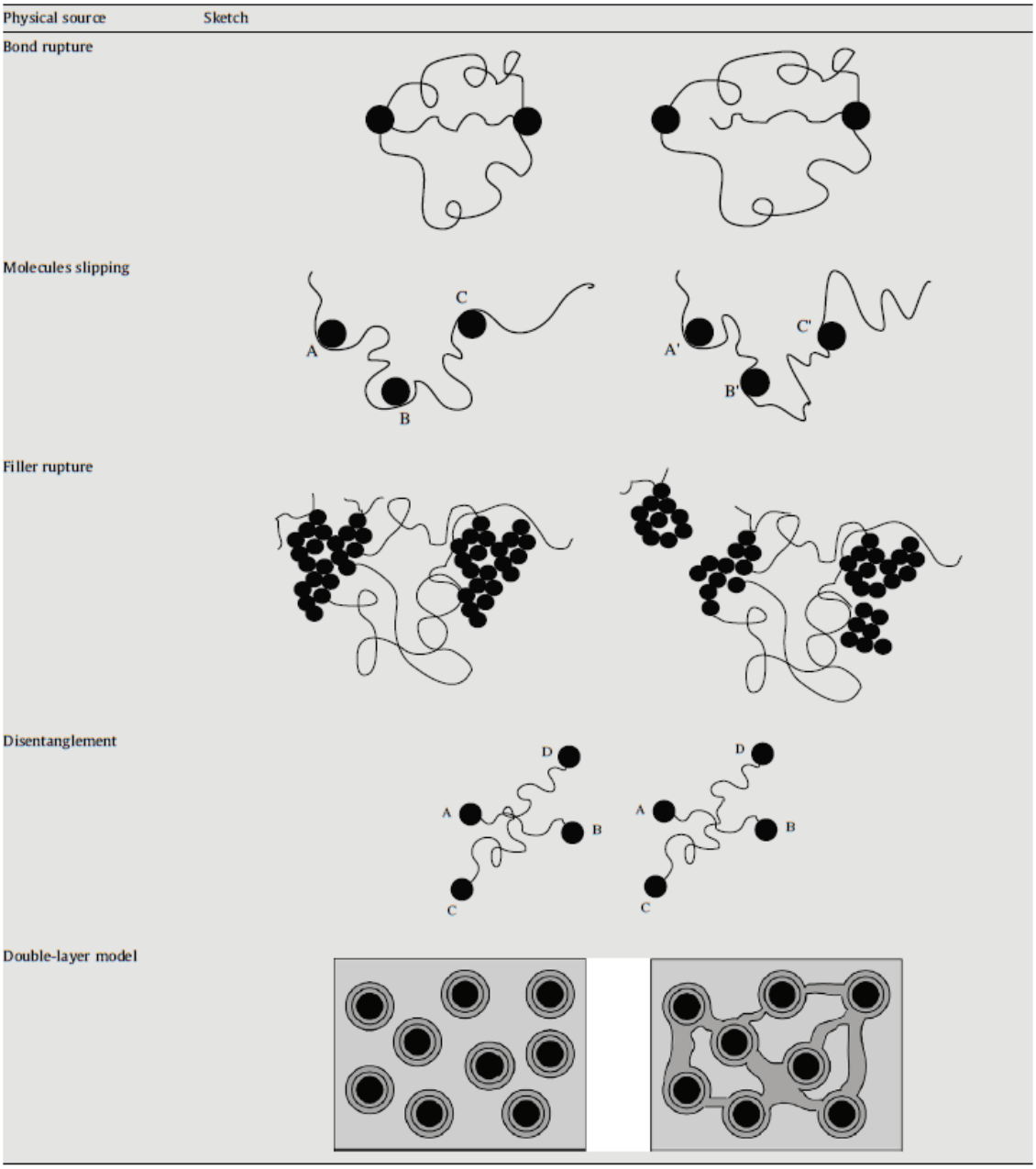

Fig 1.18 Physical explanations of the Mullins effect [98]

Houwink made a hypothesis that molecules slip over the surface of fillers during the first cycle and then new bonds are instantaneously created along molecular chains [102]. Since molecules cannot slip when there is no filler, this hypothesis cannot fit unfilled rubbers.

Kraus explained that the Mullins effect is caused by rupture of fillers structure in filled rubber [103]. However, the rupture of fillers structure is almost irreversible. The recovery cannot be explained with this hypothesis. Moreover, this hypothesis also

cannot fit unfilled rubbers because the rupture of fillers structure does not occur in unfilled rubbers.

Hanson explained that untying the entanglement of molecular chains causes the Mullins effect [104]. A large stress is needed to apply to rubber in order to remove the entanglement. Since a required stress for stretching rubber decreases after untying the entanglement, the Mullins effect occurs. In this theory, thermal motions of molecular chains during the recovery process produce new entanglements. As a result, the recovery occurs due to the thermal motions. The principal deficiency with this theory is that this theory has not been examined the effects of chain slack.

Fukahori proposed a hypothesis that rubber consists of two layers [105]. The inner layer is the glassy hard (GH) and the outer layer is sticky hard (SH). Fukahori explained that the SH layers orient and extend during the first extension and then create a super-network structure by connecting with other SH layers. The super-network structure relaxes due to contraction. Consequently, stress during extension shows small value until the super-network extended. However, this hypothesis cannot explain the softening of unfilled rubbers.

Researchers have proposed the hypothesis of Mullins effect but principle still has not been completely clarified.

As described previously, the stress before reach the maximum strain ever applied of elastomer decreases drastically due to the Mullins effect. As a result, the work received from external source (W) of the materials decreases drastically. Since the entropy change in ElCE is significantly affected by W, it is inferred that the decrease in the stress leads to the decrease in the amount of temperature variation due to ElCE. Thus, it is necessary to evaluate the performance with cyclic deformation or in stable state when ElCE of elastomer is evaluated in order not to be affected by the Mullins effect.

The effects of the Mullins effect and the crystallization on ElCE have not been investigated in detail. The S-S curve of softened material due to the Mullins effect shows that stress just before reach the maximum strain ever applied increases sharply. Similarly, it is seen that stress increases sharply when rubber is crystallized. Both the Mullins effect and the crystallization become factors which the S-S curve shows non-linear but mechanisms are not same. There is a possibility that these effects on ElCE are different due to difference in mechanisms even if it is difficult to distinguish whether which of these two has the greater effect only from mechanical property.

1.5 Objective of the work written in the present thesis

In the present chapter, three caloric effects and their advantages and drawbacks were described. These caloric effects are expected as future cooling technologies. In a comparison of these caloric effects, elastocaloric effect (ElCE) is found to be the most suitable candidate because of safety, low cost and exhibiting a large variation of heat energy.

As we can see from Eq. (1.8), the heat energy, released from material, increases with an increase in the mechanical energy applied to material when the internal energy has very small variation. Researches about ElCE of elastomers have, however, just been activated in recent years. It is much more difficult to find these works than ones of Shape Memory Alloys (SMAs). Elastomers, especially natural rubber (NR), are softer than SMAs so that a larger strain can be applied. Since they show entropic elasticity and can be applied a large mechanical energy with a small stress due to applying a large strain, elastomers would exhibit a large ΔT with a small stress. Mechanical property of NR is strongly affected by the Mullins effect and the strain-induced crystallization (SIC). Although it can be estimated that they affect ElCE of NR, those influences have not become clear yet.

In the present work, ElCE using NR is first of all investigated and the above mentioned influences on the ElCE of NR are evaluated in Chapter 3. Showing inconvenience of traditional ElCE evaluation method, a novel method is proposed, using energy balance. In order to find out the potential of ElCE with non- elastomeric polymer, terpolymer, poly(vinylidene fluoride-trifluoroethylene-chlorotrifluoroethylene) (P(VDF-TrFE-CTFE)), is also investigated in Chapter 4. The conclusions are already in details in these two Chapters, 3 and 4, because the work is enough independent. Chapter 5 is devoted, however, to give a clear conclusion of the whole thesis.

Chapter 2

Material, experimental set up and preparation

2.1 Introduction

The temperature variation in elastocaloric effect (ElCE) occurs due to the entropy change caused by mechanical deformation. A large temperature variation can be obtained when a large stress or a large strain is applied to the material. Elastomers can be used for ElCE because their entropy varies due to the mechanical deformation. Among elastomers, natural rubber (NR) is an excellent candidate for the material for ElCE. The reasons are because NR has a high fatigue resistance and can be stretched several times larger than its original length. Thus, NR was chosen in the present thesis. In order to improve the strength of NR, carbon black (CB) filled NR was used.

In ElCE, the temperature variation is affected by not only the stress and the strain but also the deformation speed. The heat dissipation occurs during the deformation when the deformation speed is slow ($< 0.2\ s^{-1}$) [10]. In order not to be affected by the heat dissipation, it is needed to deform the material at a high speed. However, the internal friction occurs inside the material when the deformation is quite large and quite fast. The heat caused by the internal friction increases the temperature of the material [55]. In case that the heat caused by internal friction is quite large, amount of the temperature variation of ElCE during extension is increased by the heat and ElCE during contraction is relatively decreased. In other words, the heating effect is increased and the cooling effect is decreased because of the internal friction. Thus, the proper deformation speed for which the heat dissipation and the internal friction do not occur must be chosen to obtain a large temperature variation, especially during contraction.

This chapter presents the fabrication method of the material and the experimental set ups. Besides, the thermal and the mechanical properties of the material and the validity of the experimental set ups are evaluated.

2.2 Material and properties characterization

2.2.1 Natural rubber (NR)

As previously described, polymers can contribute applied force to entropy change. To develop the elastocaloric effect, polymers need to be cyclically deformed leading to fatigue. However, they generate residual strain due to the deformation and are affected by fatigue easily except for elastomer [64, 65]. In addition, a large steric hindrance due to the side chains and the neighboring atoms causes small flexibility and mobility of molecular chain. Low flexibility and mobility prevent the applying a large strain to the material [63, 67]. Thanks to its special property that it returns to original length when the applied stress is removed, to its high resistance to fatigue and to its relatively small

steric hindrance, NR was chosen as material for ElCE. A typical industrial rubber contains CB to improve the strength and the fatigue resistance. This is why CB filled NR was used for this thesis work.

CB filled NR sheet with a hardness of Shore 53A was purchased from Tohto Rubber Industry Co., Ltd (Japan). Carbon black masterbatch (CMB) is made by mixing and decentralizing CB and additives into raw material rubber. Compound is prepared by mixing CMB (100 phr (part per hundred rubber by weight)), sulfur (1.00 phr) and Nokusera-CZ (Ouchi Shinko Chemical Industrial Co., Ltd., Japan) (0.75 phr) which is a vulcanization accelerator. Afterward, vulcanized rubber sheet is obtained by hot pressing at 160 °C during 6min.

It is speculated that an increase in hardness of rubber leads to an increase in the rate of force contributing to internal energy. On the other hand, it is speculated that soft rubber results in a decrease in temperature variation because small stress results in small entropy change. Therefore, shore 53A is selected as a proper hardness.

2.2.2 Volumetric specific heat

The volumetric specific heat C_v is required to calculate the thermal energy from temperature variation. In order to calculate the volumetric specific heat of materials, the specific heat and the density of materials were measured.

The specific heat was measured by differential scanning calorimetry (DSC) with DSC 131 evo (SETARAM Instrumentation, France) and thermal analysis software CALISTO (SETARAM Instrumentation, France). The heating rate was 10 °C /min. The crucible is made of aluminum. Alumina was used as reference material. The specific heat of alumina is 0.80 J/g °C.

The weight of NR was 17.0 mg and the temperature range of the experiment was set from -20 to 60 °C.

The specific heat of sample is given by:

$$C_p = \frac{q_s}{q_r}\ \frac{m_s}{m_r}\ C_p' \quad (2.1)$$

where C_p is the specific heat of sample, C_p' is the specific heat of reference material, q_r is the difference of heat flow between an empty crucible and a crucible containing reference material, q_s is the difference of heat flow between an empty crucible and a crucible containing sample, m_r is the weight of reference material, and m_s is the weight of sample.

The result of DSC measurement of NR is shown in Fig 2.1. With this result, the specific heat of NR is achieved.

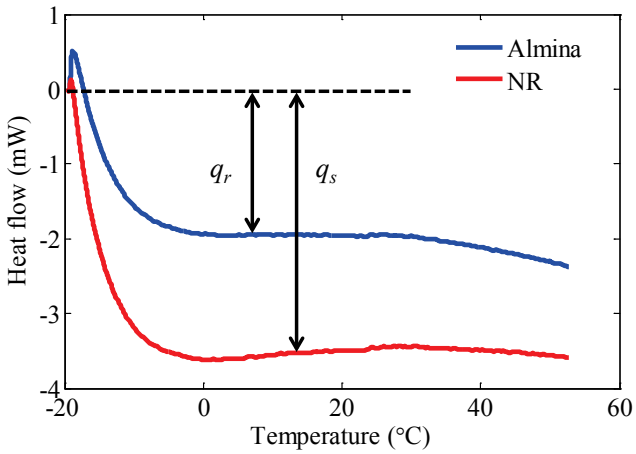

Fig 2.1 Example of result of DSC

The density was measured with the pycnometer. In this method, the density of sample is measured by comparing the weights of distilled water and sample when the volume of sample equal to that of distilled water. To measure the density with pycnometer, four different weights need to be measured as shown in Fig 2.2. First, the weight of the dried empty pycnometer (m_a) is measured. Second, the sample is put in the empty pycnometer and then the weight of filled pycnometer (m_b) is measured. Next, distilled water is poured into the pycnometer up to reference line and then the weight of pycnometer containing sample and distilled water (m_c) is measured. Afterward, the sample is removed and the pycnometer is filled up to the reference line with only distilled water. The weight of pycnometer filled with only distilled water (m_d) is measured. The density of sample (ρ_s) is expressed as:

$$\rho_s = \frac{m_b - m_a}{m_d - m_a - (m_c - m_b)} \rho_w \qquad (2.2)$$

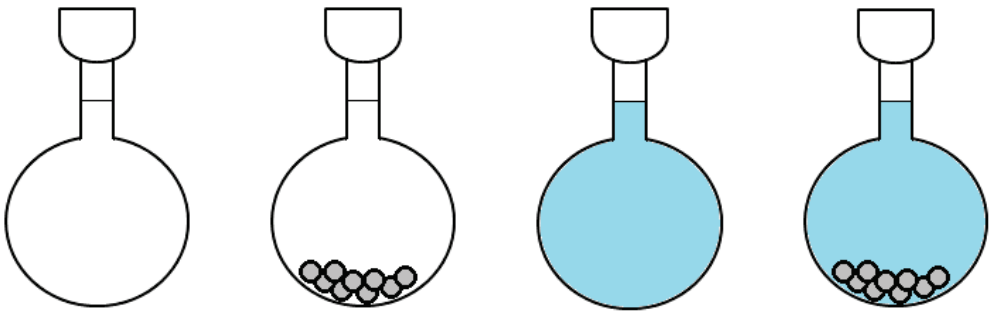

(a) (b) (c) (d)

Fig 2.2 Four different weights to measure the density (a) Empty pycnometer (m_a), (b) Pycnometer + sample (m_b), (c) Pycnometer + distilled water (m_c), (d) Pycnometer + distilled water + sample (m_d)

where ρ_w is the density of distilled water.

As a result, the density of NR was found to be equal to 1390 kg/m^3.

2.2.3 Temperature calibration

In order to accurately observe the temperature variation caused by ElCE, temperature calibration of the thermal camera was conducted. A sample which was cut to 60 mm of length and 20 mm of width from the sheet (thickness 850 μm) was fixed in a thermostatic chamber. A temperature of the sample was measured by a thermal camera (NEC G-120, NEC, Japan) at a set temperature. Six levels of set temperatures were chosen, 0, 10, 20, 30, 40 and 50 °C. In order to measure the steady state temperature, the sample has been kept at the set temperature during 10 minutes. By comparison between a set temperature and a measured temperature, its correction factor is calculated.

2.2.4 Heat dissipation

In case that the material is out of contact with others, the thermal energy transport between the material and the ambient air is based on the convective heat transfer and the radiative heat transfer as follow;

$$\dot{Q}_d = \dot{Q}_r + \dot{Q}_c \qquad (2.3)$$

where $\dot{Q}_d$ is the total heat dissipation, $\dot{Q}_r$ is the heat dissipation by radiation and $\dot{Q}_c$ is the heat dissipation by convection.

$\dot{Q}_r$ and $\dot{Q}_c$ are expressed as:

$$\dot{Q}_r = Ae\Sigma(T_s^4 - T_0^4) \qquad (2.4)$$

$$\dot{Q}_c = Ah(T_s - T_0) \qquad (2.5)$$

where A is the exchange surface, e is the emissivity of the sample, Σ is the Stefan-Boltzmann constant (5.67×10^{-8} W/m^2 °C^4), T_s is the surface temperature of the sample (degree in Kelvin), T_0 is the room temperature (degree in Kelvin) and h W/m^2 °C is the heat transfer coefficient. e is the characteristic value of the material [66], which was taken equal to 0.90 for NR, according to manual of thermal camera. h depends on the flow of ambient environment.

2.3 Experimental device with RSDG2

Fig 2.3 illustrates a diagram of the experimental setup for characterizing the mechanical property and the ElCE produced by NR. The sample was fixed on the testing device by clamping. A single axis robot (RSDG212, MISUMI Corporation, Japan) uniaxially stretches the sample while generated force is recorded by a force sensor

(XFTC300-200N, Measurement Specialities, France). The displacement of the single axis robot is measured by using a vibrometer controller (OFV-5000, Polytec, Germany). The temperature change, generated by the strain-induced entropy, is measured using a thermal camera (NEC G-120, NEC, Japan). This thermal camera can record thermal images of the sample at 10 Hz. The accuracy of the temperature measurement with this thermal camera is ± 0.1 °C. A light sensor (BPW 34 B, Osram Opto Semiconductors GmbH, Germany) is put on monitor of the thermal camera to record light signals of monitor. Displacement, force, and information captured by light sensor are displayed on an oscilloscope (DSO 7034A, Agilent, USA). Since the thermal camera cannot connect directly to the oscilloscope, the time line of the thermal images recorded by it cannot be correlated accurately with the time lines of displacement and force. By connecting the thermal camera to the oscilloscope indirectly by using the light sensor,it is possible to correlate accurately the time lines among displacement, force and temperature change.

Space between clamps, i.e. the length of a sample, was set at 20.0 mm. The samples which were cut to 20 mm of width from the sheet (thickness 850 μm) were fixed with the clamps.

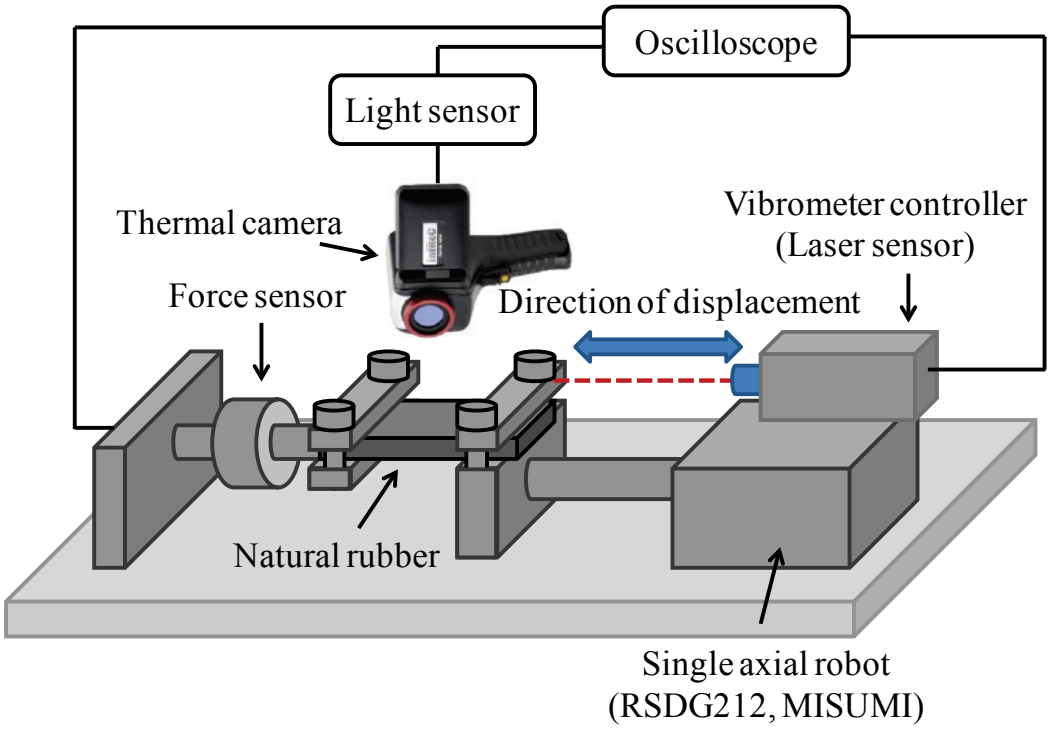

Fig.2.3 Scheme of experimental device with RSDG2

2.4 Results

2.4.1 Volumetric specific heat capacity

The specific heat C_p of NR is measured with of the help of DSC measurement and is shown in Fig 2.4. C_p of NR reaches a maximum value at 0 °C and then decreases gradually when the temperature is increased. C_p of 1.212 J/g °C is obtained around 20 °C. Since the density of NR is 1390 kg/m^3, the volumetric specific heat capacity C_v around 20 °C is 1684 kJ/m^3 °C.

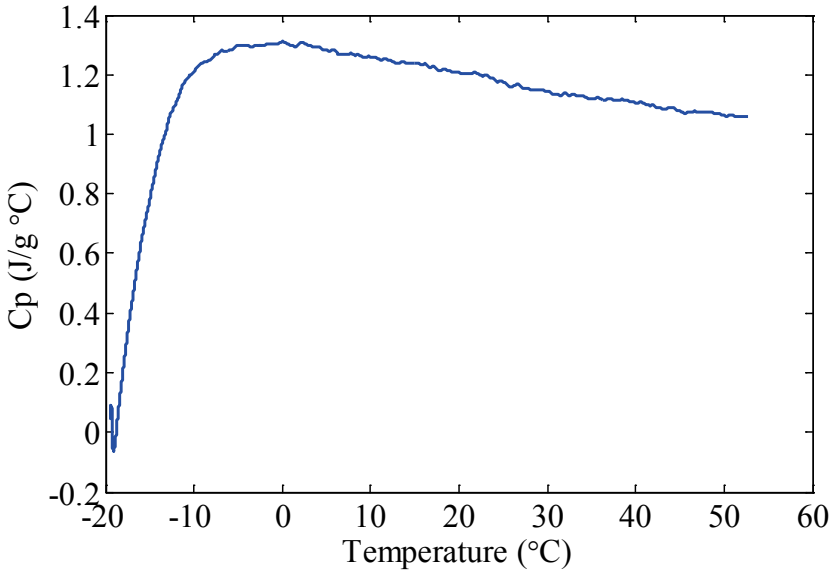

Fig 2.4 C_p of NR as a function of temperature

2.4.2 Temperature calibration

Fig 2.5 shows the relationship between a given set temperature (x) of the thermostatic chamber and the measured temperature (y) by the thermal camera. A linear relation is observed. For the following, the calibrated temperature will be presented when the temperature of sample is presented.

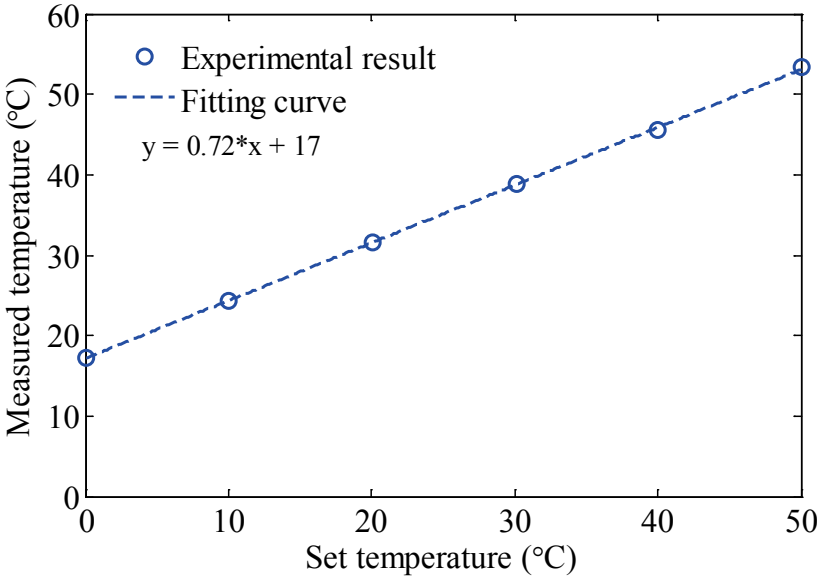

Fig 2.5 Measured temperatures as a function of set temperature

2.4.3 Fracture strain

The stress-strain (S-S) curves of the sample with deformation speed of 2.0 mm/s is shown in Fig 2.6. The stress and the strain were calculated with sample size before deformation, so that they are the engineering stress and the engineering strain. The stress increases approximately linearly with an increase in the strain until up to 688 % and then the sample rupture at the strain. Since it was confirmed the fracture strain of the sample, ElCE of the sample will be evaluated with a strain below the value.

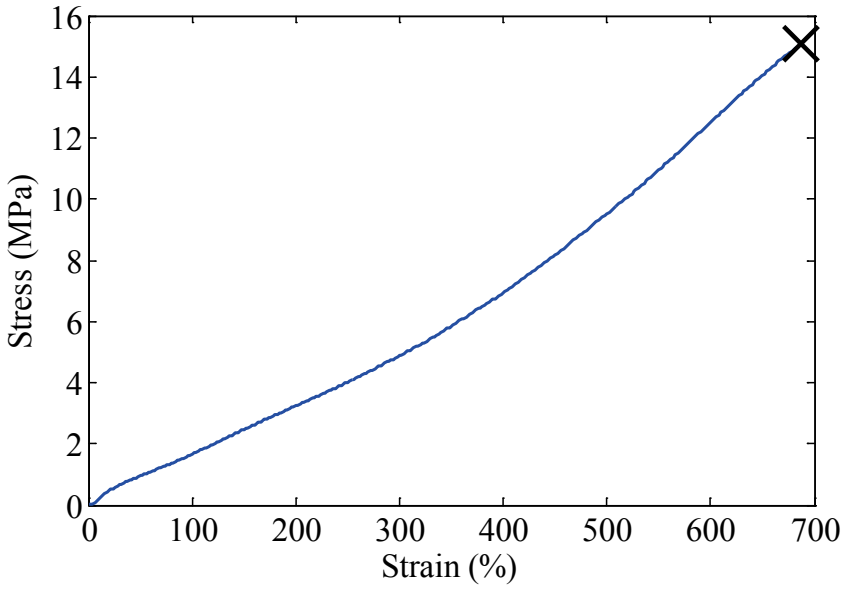

Fig 2.6 S-S curve of CB filled NR with deformation speed of 2.0 mm/s

2.5 Results and discussion

2.5.1 Deformation speed of the experimental device

The proper deformation speed which the heat dissipation and the internal friction do not occur must be chosen to obtain a large temperature variation. Fig 2.7 shows time versus displacement of the experimental device when the maximum deformation speed is selected. Although the maximum speed is indicated as 320 mm/s in the manual, it takes 0.5 s to move 80 mm. It should be noted that the acceleration of the experimental device is not large (1.13 m/s^2). Consequently, the experimental device cannot move at its maximum speed when the deformation is 80 mm. However, the device moves 80 mm at elongation rate of 1.0 s^{-1}. It was reported that a sample is deformed in an adiabatic process when the elongation rate is higher than 0.2 s^{-1}. Since the experimental device can deforms a sample with elongation rate of higher than 0.2 s^{-1}, it was confirmed that the experimental device can deform a sample in an adiabatic process.

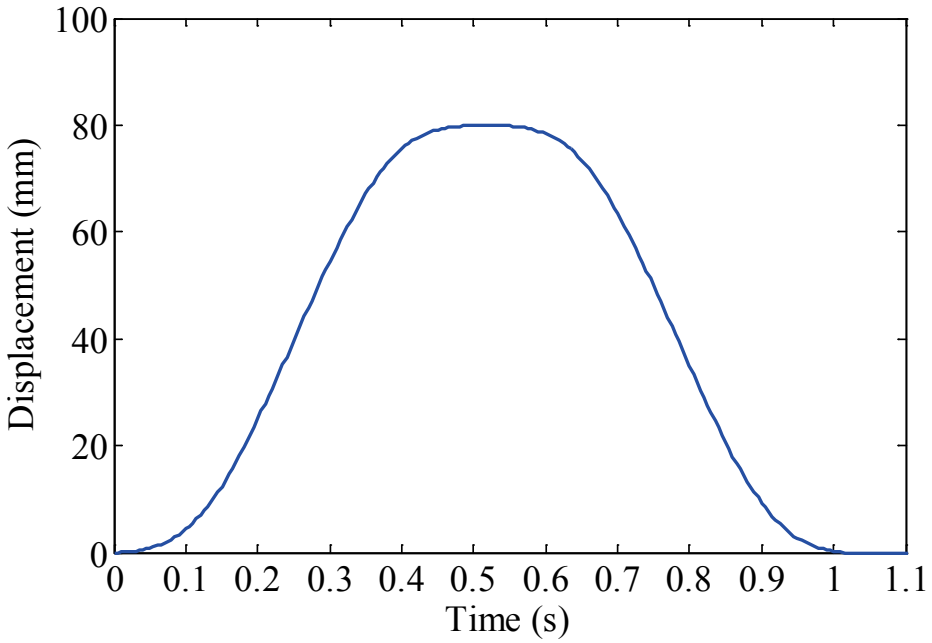

Fig 2.7 Time versus displacement of the experimental device when the displacement of 80 mm is applied with the maximum deformation speed

2.5.2 Mechanical property

S-S curves on cyclic deformation test were observed in order to confirm the mechanical property of the sample. In the experiment, the strains of 100 %, 200 % 400 % and 600 % were applied to the samples with the deformation speed of 2.0 mm/s. After reach the maximum strain, the strain was returned to zero with the same

deformation speed. Each strain was applied three times continuously.

Fig 2.8 shows S-S curves when the strains of 100 % (blue line) and 200 % (red line) are applied. In the first cycle of both case, the stress increases nonlinearly with an increase in the strain before the strain exceeds approximately 50 % and then increases linearly with an increase in the strain when the strain exceeds approximately 50 %. In contraction process, the stress largely decreases just after the start of contraction and then decreases linearly gradually with a decrease in the strain until the strain of approximately 50 %. Afterword, it decreases largely with a decrease in the strain. Moreover, it was indicated that the hysteresis loop of the maximum strain of 100 % is relatively small whereas that of the maximum strain of 200 % is quite large.

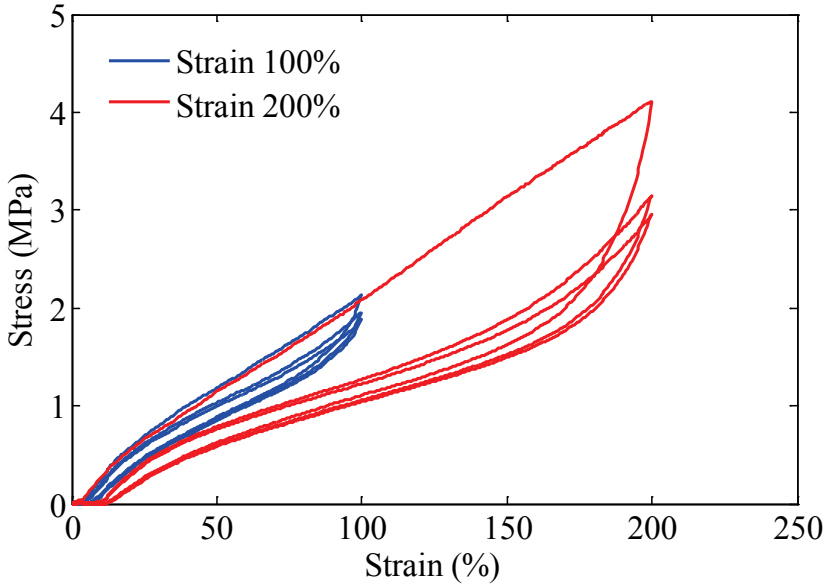

Fig 2.8 S-S curves of CB filled NR when the maximum strains of 100 % and 200 % are applied three times with deformation speed of 2.0 mm/s

After the first cycle, it is clearly seen that the S-S curve depends on the maximum strains ever applied. In case of the maximum strain of 100 %, the stresses during extension and at the maximum strain of the second cycle are slight lower than those of the first cycle. On the other hand, those of the second cycle largely decrease when the maximum strain of 200 % is applied. As a result, it was found that the sample is hardly affected by the Mullins effect when the maximum strain of 100 % is applied whereas it is affected by the Mullins effect when the maximum strain of 200 % is applied. It was not shown a large difference between the second and the third cycle in both maximum strains.

Fig 2.9 shows S-S curves when the strains of 200 % (blue), 400 % (red line) and 600 %

(green line) are applied. The results when the maximum strain of 400 % and 600 % is applied are similar to it of the maximum strain of 200 %. The stresses during extension and at the maximum strain of the second cycle are quite lower than those of the first cycle. Besides, it can be seen that the hysteresis loop of the first cycle is quite large and that after the first cycle becomes small. As a result, the influence of the Mullins effect was confirmed when the maximum strain of more than 200 % is applied to the sample. Although it is generally said that the stress increases drastically when SIC occurs as described previously in the Chapter 1 [70, 73], the S-S curve of the sample shows the same tendency due to the Mullins effect when the maximum strain of more than 200 % is applied. Thus, it was concluded that the influence of the SIC cannot be recognized only from these results.

It is clearly seen that the stresses after the first cycle start to increase not from strain of 0 % when the maximum strains of 400 % and 600 % are applied. This indicates that a residual strain is generated by a large strain. The values of the residual strains are approximately 10 % of the maximum strains. Since there is no difference of the values of it between the second and the third cycle in both maximum strain, it was found that the main factor of the residual strain as well as the Mullins effect is the maximum strain ever applied.

With the experimental results in section 2.3.4 and this section, the test condition of ElCE of the sample will be chosen in Chapter 3.

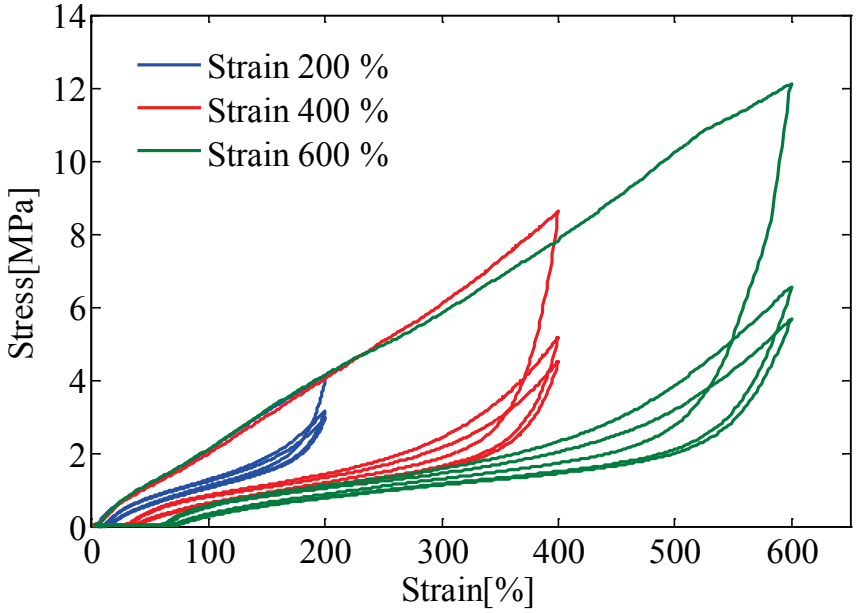

Fig 2.9 S-S curves of CB filled NR when the maximum strains of 200 %, 400 % and 600 % are applied three times with deformation speed of 2.0 mm/s

2.5.3 The effect of frictional heat

In order to confirm the effect of frictional heat, the temperature variation due to ElCE was observed. Before the experiment, the strain of 400 % was applied to the sample ten times in order to remove the Mullins effect and then the sample was fixed again to remove the residual strain. In the experiment, the strain of 400 % was applied to the sample with the maximum speed of the experimental device and kept for 100 s. After that, the strain was returned to zero. Fig 2.10 shows the temperature of the sample (blue solid line) and the applied strain (gray dot line) during the experiment. As a result, it was found that the temperature increases 5.0 °C by extension and it decreases 4.4 °C by contraction. There is no large difference between the increasing temperature and the decreasing temperature. Thus, it was confirmed that the frictional heat does not occur in the experiment.

Since the experiment has been conducted in an adiabatic process and the frictional heat does not occur, it was concluded that the experimental device can apply deformation with a proper deformation speed. The device can evaluate the ElCE properly.

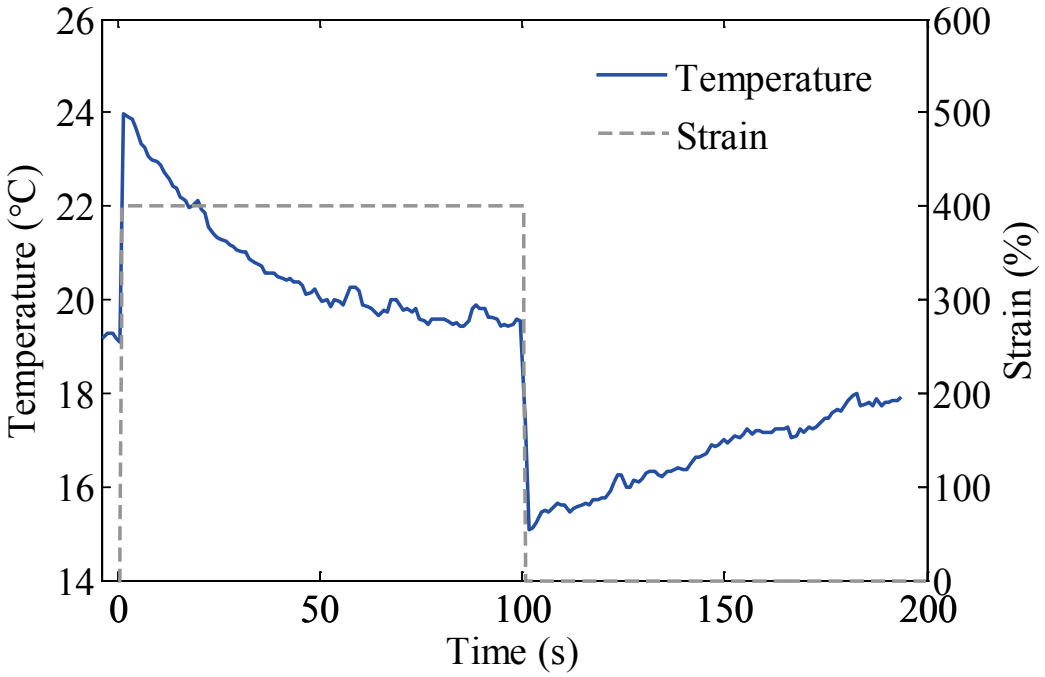

Fig 2.10 Temperature of sample and the applied strain as a function of time

2.5.4 Heat dissipation

In heat dissipation, the heat dissipation by radiation depends on material whereas the heat dissipation by convection depends on flow of ambient environment. In order to calculate the amount of total heat dissipation, it is needed to measure the heat transfer coefficient h in advance. The experimental result of section 2.5.3 is used to obtain h. Fig 2.11 shows the experimental result (blue solid line) and the temperature variations calculated with the heat dissipations.

The red curve represents the temperature variation if the radiation heat transfer is the single transfer taken into account and calculated with the help of the equation 2.4. By deducting successively the calculated value from the maximum and the minimum temperature of the experimental result, the temperature variation is calculated. A discrepancy is observed between the experimental result and this one, due to the fact that the convection heat transfer cannot be neglected. As shown in the equation 2.3, the convection heat transfer can be calculated with the experimental result and the radiation heat transfer. By calculating the equation 2.3 and 2.4, the h value of 3.0 W/m^2 °C is obtained. The best fit between the experimental result and the modeled one (equation 2.4 and 2.5) including the convection transfer (green curve) has been observed for the h value.

For the following, the effect of the heat dissipation will be calculated with the value.

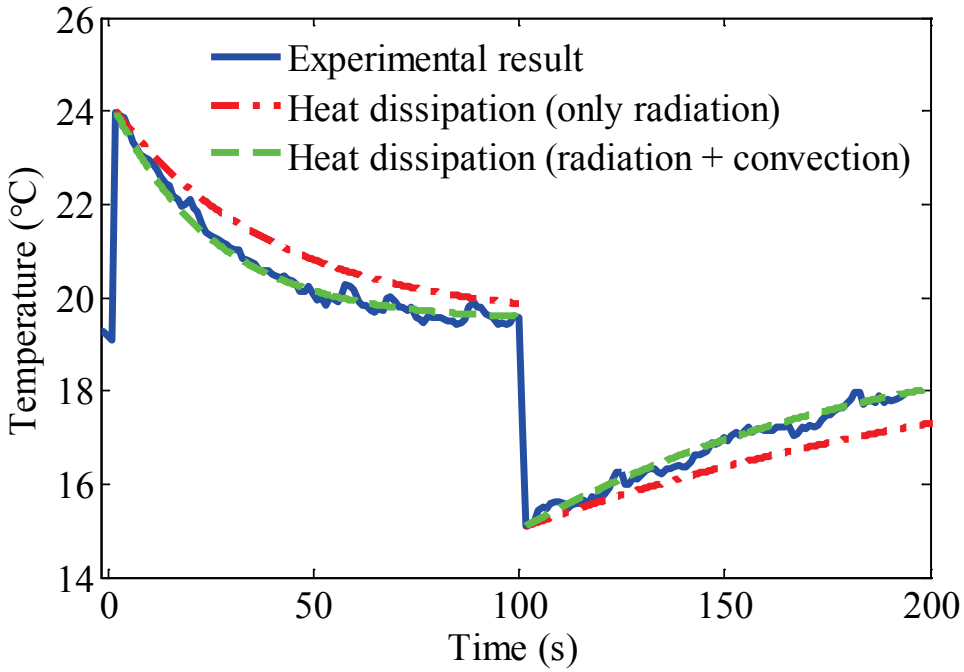

Fig 2.11 Temperature variation caused by heat dissipation as a function of time

2.6 Conclusions

This chapter presented the fabrication method of natural rubber (NR) filled with carbon black (CB) and the experimental benches used in this thesis work.

By using these experimental benches, the foundation of mechanical properties and all the necessary thermal properties to evaluate the elastocaloric effect have been measured as well as the heat transfer coefficient by convection between the sample and the surroundings.

A specific bench has been developed during this Ph D work, to allow the proper measurement of the elastocaloric effect. This bench warrants an accurate measurement of the sample temperature and that the strain cycle is fast enough to work in an adiabatic regime.

Chapter 3

Elastocaloric effect of natural rubber

3.1 Introduction

Natural rubber (NR) exhibits a large temperature variation (> 5 °C) with a small stress (< 1.5 MPa) due to its excellent elastocaloric effect (ElCE) [106]. Moreover, it is non-toxic, environmentally friendly and low cost. Thus, NR is an excellent candidate material for ElCE as mentioned in Chapter 1. Researches about ElCE of NR have, however, just activated in recent years. It is much more difficult to find these works than ones of Shape Memory Alloys (SMAs).

In ElCE, the material exhibits the temperature variation based on the entropy variation due to extension and contraction. When elastomers, such as NR, are stretched, both Mullins effect and strain-induced crystallization (SIC) affect the mechanical property of elastomers. These phenomena are already explained in details in Chapter 1 and 2. Many researchers have devoted but in fact, it is still difficult to clearly relate these two with mechanical properties then with ElCE.

The relationship between the temperature variation and the applied stress has been often used for evaluating ElCE in the researches with SMAs. The relationship between the temperature variation and the applied strain has been also used with NR. NR is, however, a non-linear elastic material, so that it can generate different stresses even when the same level of strain is applied. The opposite case is also true, i.e., the different levels of strain can generate the same stress value. It depends strongly on their morphology. The charge historical information becomes quite important. The discussion of Mullins effect is, then, necessary. Besides, ElCE and SIC seems also strongly correlated. But strain value where SIC starts to be formed is difficult to define by stress-strain (S-S) curve, as described in Chapter 2. Summarizing above, the conventional evaluation methods which use the relationship between the temperature variation and applied stress or strain must be improper for evaluating ElCE on NR and other non-linear elastic materials.

In this chapter, a new evaluation method of ElCE on non-linear material, such as NR, is proposed. The temperature variation is related to the incoming and the outgoing energies. It will be demonstrated that the temperature variations and these energies show a quite straight linear relation. The coefficient between them becomes a specific value for one material which does not depend on applied in advance maximum strain value neither on S-S charge history on the sample. Besides, using the energies used for the energy balance mentioned above, the efficiency of one material, carbon black (CB) filled NR, will be discussed with the ideas of Mullins effect and SIC.

First of all, brief theoretical information is given. The details of some theories are already written in Chapter 1 and 2 but it is again demonstrated to point up the idea

here. After the section for experimental setup, some spontaneous results from experiments are shown to give an image of experiment. Then, above mentioned two factors will be described in the section of discussion.

3.2 Theory

3.2.1 S-S curve, SIC and Mullin effect of NR

It is said that NR can be stretched to several hundred percent in strain, and then returns to its original shape when applied force is released. NR consists of relatively long molecular chains which have a high degree of flexibility and mobility. That is why NR can be stretched with considerably smaller stress compared to metals and ceramics. In fact, a permanent strain exists when an applied maximum strain/stress is big. It is, however, often negligible in front of the maximum applied strain, such as 0 % when it is stretched up to 100 % and 60 % when it is stretched up to 600 %.

It is well known that the S-S curve of NR is non-linear [7, 9 and 10]. When a large strain is applied to NR, the molecular chains are fully stretched because of finite chain extensibility. Since the fully stretched molecular chains are considered to behave as the crystal, crystallized molecular chains are called SIC. The fully stretched molecular chains lead an increase in stress. As a result, S-S curve of NR depicts non-linear shape as shown in Fig.1.17 [70]. Even though these SIC can be determined by wide-angle X-ray diffraction (WAXD), see Fig 1.17, the occurrence of SIC is hard to be recognized only from S-S curve. However, the strain level where the S-S curve increases for the second time in function of increasing strain is generally recognized as the starting point of SIC forming [73, 107].

Besides, NR exhibits a large difference in its mechanical properties between the first and the second deformation because softening happens by the first deformation. This phenomenon is well known as the Mullins effect [97, 98]. The influence of Mullins effect depends on the largest strain applied to the material given for the first time. Thus, the strain charge history is one of the most important information.

It is considered that elastomers are softened by Mullins effect and hardened by SIC as previously described. Although several researches have devoted to these two effects on ElCE on elastomer, such as NR, the state of the art is insufficient to clarify the phenomena.

3.2.2 Energy balance

As previously described in chapter 1 [63-65], the first law of thermodynamics is expressed as:

$$dU = dQ + dW \quad (1.8)$$

where dU is the variation of the internal energy, dQ is the variation of the heat energy received from the external source and dW is the variation of the mechanical energy applied to the material. It is known that dU of ideal rubber during deformation is null. Putting $dU = 0$ in Eq. (1.8), we obtain

$$dW = -dQ \quad (1.22)$$

As we can see from Eq. (1.22), dW and negative value of dQ are equal when the ideal rubber is deformed. In other words, the ideal rubber can convert completely the mechanical energy into the heat energy. Surely, real rubber does not behave completely same to the ideal rubber. The finite chain extensibility which is not considered for the ideal rubber must be the reason. In any case, the conversion of one to other energies of real rubber must be done with high efficiency until the threshold where such chain extensibility occurs.

3.2.3 Two mechanical energies

In uniaxially deformation, the mechanical energy applied to an elastic material due to deformation is given by

$$W = \int f \, dl \quad (3.1)$$

where f is the applied force and dl is the displacement [108].

When rubber is stretched, the force-displacement curve becomes non-linear as shown in Fig 3.1 (a). The mechanical energy at extension (painted area in Fig 3.1 (b)) and contraction (Fig 3.1 (c)) are integral of the force by the displacement, write as W_1 and W_2, respectively.

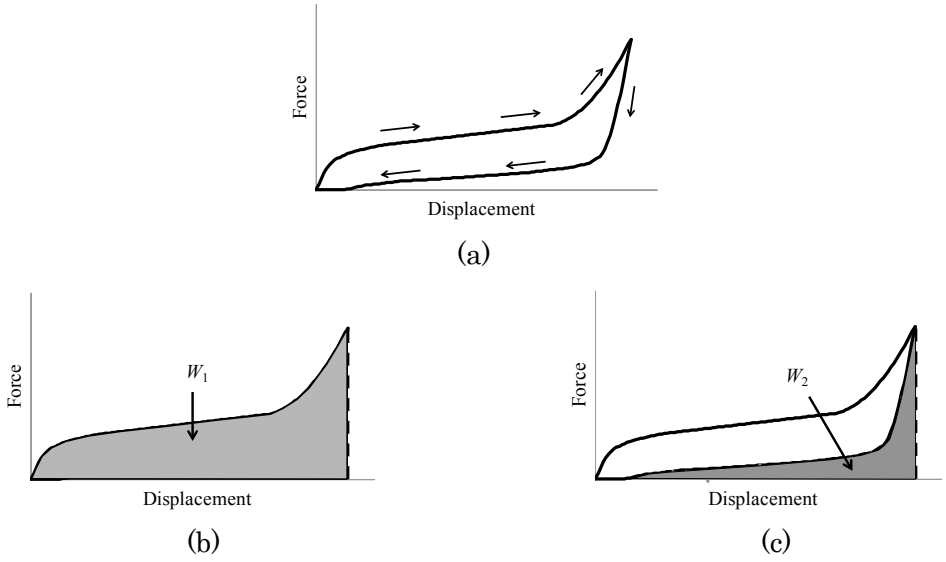

Fig 3.1 Typical force-displacement curve of rubber (a) force-displacement curve, (b) mechanical energy at extension, (c) mechanical energy at contraction

3.2.4 Heat dissipation

In case that the material is out of contact with others, the thermal energy transport between the material and the ambient air depends on the convective heat transfer and the radiative heat transfer, writes

$$\dot{Q}_d = \dot{Q}_c + \dot{Q}_r \qquad (3.2)$$

where $\dot{Q}_d$ is the total of heat dissipation, $\dot{Q}_c$ is the heat dissipation by convection and $\dot{Q}_r$ is the heat dissipation by radiation.

$\dot{Q}_c$ and $\dot{Q}_r$ are expressed as:

$$\dot{Q}_c = A\,h\,(T_s - T_0) \qquad (3.3)$$

$$\dot{Q}_r = A\,e\,\Sigma\,(T_s^4 - T_0^4) \qquad (3.4)$$

where A is the area of surface, h is the heat transfer coefficient, T_s is the surface temperature of the sample (degree in Kelvin), T_0 is the room temperature (degree in Kelvin), e is the emissivity and Σ is the Stefan-Boltzmann constant (5.67×10^{-8} W/m^2 K^4). h depends on the flow of ambient environment. e is the characteristic value of the material [109].

3.3 Material and experimental setup

3.3.1 Material CB filled NR

A) Fabrication

The material used in this chapter is a carbon black (CB) filled natural rubber (NR). Filled NR sheet was purchased from the company (NR 50°, TOHTO RUBBER INDUSTRY CO., LTD., Japan). Compound of the filled NR is prepared by mixing carbon black masterbatch (100 phr (part per hundred rubber by weight)), sulfur (1.00 phr) and Nokusera-CZ (Ouchi Shinko Chemical Industrial Co., Ltd., Japan) (0.75 phr) which is a vulcanization accelerator. Afterward, vulcanized rubber sheet is obtained by hot pressing at 160 °C during 6 min. The thickness of the sheet is around 850 μm.

For measurement of ElCE, space between clamps, i.e. the length of a measured sample surface, was set at 20 mm. The samples which were cut to 20 mm of width and 60 mm of length from the sheet were fixed with the clamps.

As previously described in Chapter 1 and 2, CB introduction must increase the strength. Smaller applied strain generates bigger stress because of CB doping. This is a favorite factor when it is oriented to be used for ElCE, so that CB filled NR was chosen instead of pure NR in the present chapter.

B) Density and specific heat

In order to calculate the volumetric specific heat C_v, the specific heat C_p and the

density ρ of materials were measured as previously mentioned in Chapter 2.

The specific heat was measured by differential scanning calorimetry (DSC) with DSC 131 evo (SETARAM Instrumentation, France) and thermal analysis software CALISTO (SETARAM Instrumentation, France). The heating rate was fixed at 10 °C /min. The crucible made of aluminum was used. Alumina was used as reference material. The specific heat of alumina is 0.80 J/g °C. The weight of sample was 17.0 mg and the temperature range of experiment was from −20 to 60 °C.

The density was measured using a pycnometer, also called specific gravity bottle. As previously described in the second chapter, the density of sample was measured by comparing the weights of distilled water and sample when the volume of sample equal to that of distilled water.

The density ρ and the specific heat capacity C_p were obtained experimentally in this way as 1390 kg/m^3 and 1.212 J/g °C, respectively.

3.3.2 Experimental setup for ElCE measurement

The mechanical property and the ElCE produced by NR were measured using the experimental setup as shown in Fig 2.3. The sample is fixed on testing device by clamping. Single axis robot (RSDG212, MISUMI Corporation, Japan) could uniaxially stretch the sample while generated force is recorded by a force sensor (XFTC300-200N, Measurement Specialities, France). The displacement of the single axis robot is measured by using a vibrometer controller (OFV-5000, Polytec, Germany). The temperature change, generated by entropy change lead by introduction of strain, is measured using a thermal camera (NEC G-120, NEC, Japan). This thermal camera can record thermal images of the sample at 10 Hz. The noise level of the temperature information from this camera is ± 0.1 °C. In order to correct the sample infrared ray (IR) emissivity, the sample was put in a temperature controlled oven then actual surface temperature measured by a thermocouple and the temperature read from the IR camera had been compared. A linear correlation was found and its correction factor was 0.71. A light sensor (BPW 34 B, Osram Opto Semiconductors GmbH, Germany) was put on monitor of the thermal camera to record light signals of monitor. Displacement, force, and information captured by light sensor were recorded by an oscilloscope (DSO 7034A, Agilent, USA). Since light sensor is on when the temperature change occurs, it is possible to check the exact time interval among displacement, force and temperature change.

As it was explained in the section of theory, section 3.2.4, h depends on the flow of ambient environment. h in the test environment was measured as 3.0 W/m^2 K. 0.9 is employed

here as the value of emissivity e of filled NR, according to manual of thermal camera.

3.3.3 Two cross-head speeds for ElCE measurement

The cyclic deformation tests were carried out up to 100 cycles. Four levels of applied maximum strains ε_{max} had been preciously chosen, 100 %, 300 %, 400 % and 600 %. The samples are described as strain 100 % and so on for the sake of convenience in the present chapter.

For the ElCE measurement on extraction and contraction of NR, there are so many factors to be concerned besides the maximum strain value. Because of Mullin effect, it is important that if the material had received already pre-stretch before cyclic loading. For the case with pre-stretch, it is necessary to know if the elimination of permanent strain had been done even if it is quite small, less than 10 % at maximum for NR of the present study. The applied strain wave form changes the temperature variation. Especially when the cross-head speed is low, ElCE cannot be measured in adiabatic condition because of heat dissipation. Moreover, rectangular waveform has to be chosen because NR is a viscoelastic material. Each experimental detail will be shown in the following sections if necessary. Here, test conditions for two factors, cross-head speed and pre-stretch, are mentioned as below.

A) “High-speed” and “low-speed” deformation

Strain was applied until ε_{max} with the fastest speed of this experimental device. Although the maximum speed is indicated as 320 mm/s in the manual, it had been revealed that this device cannot move at such speed when it moves less than 150 mm due to the acceleration (1.13 mm/s^2) and deceleration. Strain 100 % was applied with elongation rate of 2.0 s^{-1} and strains 300 %, 400 % and 600 % were applied with approximately 1.0 s^{-1}.

“Low speed” deformation test was also carried out with elongation rate of 0.05 s^{-1}. Applied ε_{max} in the “low speed” deformation test were limited to two levels, 400 % and 600 %.

B) Pre-stretch

To eliminate the influence of Mullins effect, some samples have pre-stretch before cyclic loading measurement. 10 rapid cycles were applied as pre-stretch. Important is that these pre-stretch has the same ε_{max} to the following cyclic loading. After induction of such pre-stretch, the samples were clamped again in order to remove the influence of residual strain, i.e., permanent strain.

3.4 Results

As it was already described in the precedent section, many factors have to be considered in ElCE measurement of NR; pre-stretch, residual strain, applied wave form, cross-head speed, as well as ε_{max}. To give a basic idea of experimental results, some S-S curves and some temperature variation in function of time will be shown before the deep discussion starts.

3.4.1 Strain-Stress (S-S) curve

A) Cyclic uniaxial deformation with increasing maximum strain tests with rectangular waveform for two cross-head speed

First of all, Fig 3.2 shows S-S curves on cyclic uniaxial deformation tests. Fig 3.2 (a) shows the applied strain wave form in function of time. ε_{max} 100 % is applied for 3 cycles for sample without pre-stretch then increased gradually ε_{max} to 300, 400 and 600 %. Fig 3.2 (b) shows the results of "high-speed" deformation and (c) the "low-speed" deformation. To ensure the time for temperature variation caused by ElCE, each time, 5.0 s keep time at the maximum was taken even if it is not necessary for "low-speed" deformation.

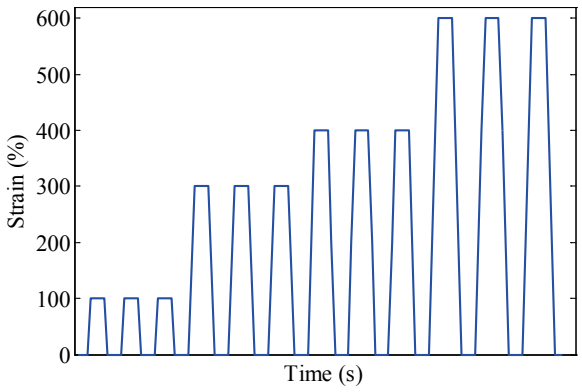

(a)

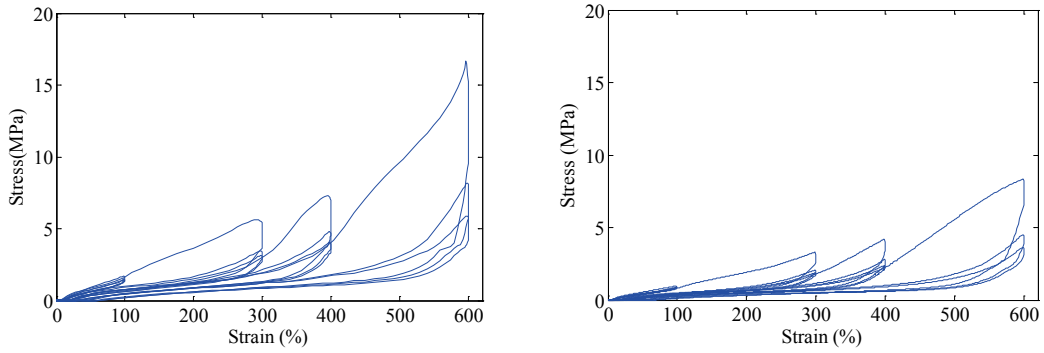

(b) (c)

Fig 3.2 S-S curves on cyclic uniaxial deformation tests (a) applied strain as a function of time (b) S-S of "high-speed" deformation test (c) S-S curve of "low-speed" deformation test

Fig 3.2 (b) clearly shows that the generated stress is quite low when the applied strain is lower than ε_{max} and the stress increases largely when the applied strain exceeds the maximum strain ever applied. This is a typical result of the Mullins effect as previously explained in Chapter 1. Since Fig 3.2 (c) shows the same tendency as Fig 3.2 (b), it was found that the sample is affected by the Mullins effect regardless of the deformation speed. However, amount of the generated stress depends on the deformation speed due to the viscoelasticity of the sample. Besides, the decrease in the stress due to the stress relaxation during 5.0 s of keeping time becomes larger when the deformation speed becomes faster. Due to these facts, the inside area of hysteresis loop in the "high-speed" deformation test is larger than it in the "low-speed" deformation test.

The stress starts to increase not from strain of 0 % after ε_{max} 300 % is applied. This indicates that the residual strain is generated by the deformation. Regardless of the deformation speed, the value of the residual strain is obtained between 5 and 10 % of ε_{max}. As a result, it was found that the residual strain is affected by ε_{max} but the deformation speed does not affect to it.

B) "High-speed" cyclic tests

The cyclic tests up to 100 cycles were carried out with 4 different ε_{max} for the samples without pre-stretch. Strain was applied with rectangular waveform with 5.0 s keep time. Fig 3.2 (a), (b), (c) and (d) shows the S-S curves of only the first, the second, the third and the hundredth cycles for four level of ε_{max}, 100, 300, 400 and 600 %, respectively. For the purpose of clarification, force was obtained by force sensor and the calculated stress values indicated in the figure are just the engineering stress.

First thing that we notice must be a very big inside area of hysteresis loop in the first cycles. Big differences can be observed between the first and the second cycles for 3 maximum strain levels except strain 100 %. As well, the maximum stress considerably decreases from the first to second cycles except strain 100%. Although both of them continue decreasing with an increase of number of cycle, the variations between the second and the hundredth cycle are remarkably smaller than those between the first and the second cycle. The discussion will be continued in the section of discussion.

The open circles in figures show the strain levels where the sign of second derivative change on the second cycle at stretching. There are two for each figure, except strain 100 %. These critical strain values are defined as ε_{c1} (gray circle) and ε_{c2} (black circle) for the lower and the higher, respectively. It should be noted that ε_{c2} is not observed for strain 100 %. Both ε_{c1} and ε_{c2} increase with ε_{max}. The closed circles indicate ε_{c2} on the hundredth cycle. Besides, it was indicated that ε_{c1} does not change with an increase in the number of cycle whereas ε_{c2} increases with an increase in the number of cycle.

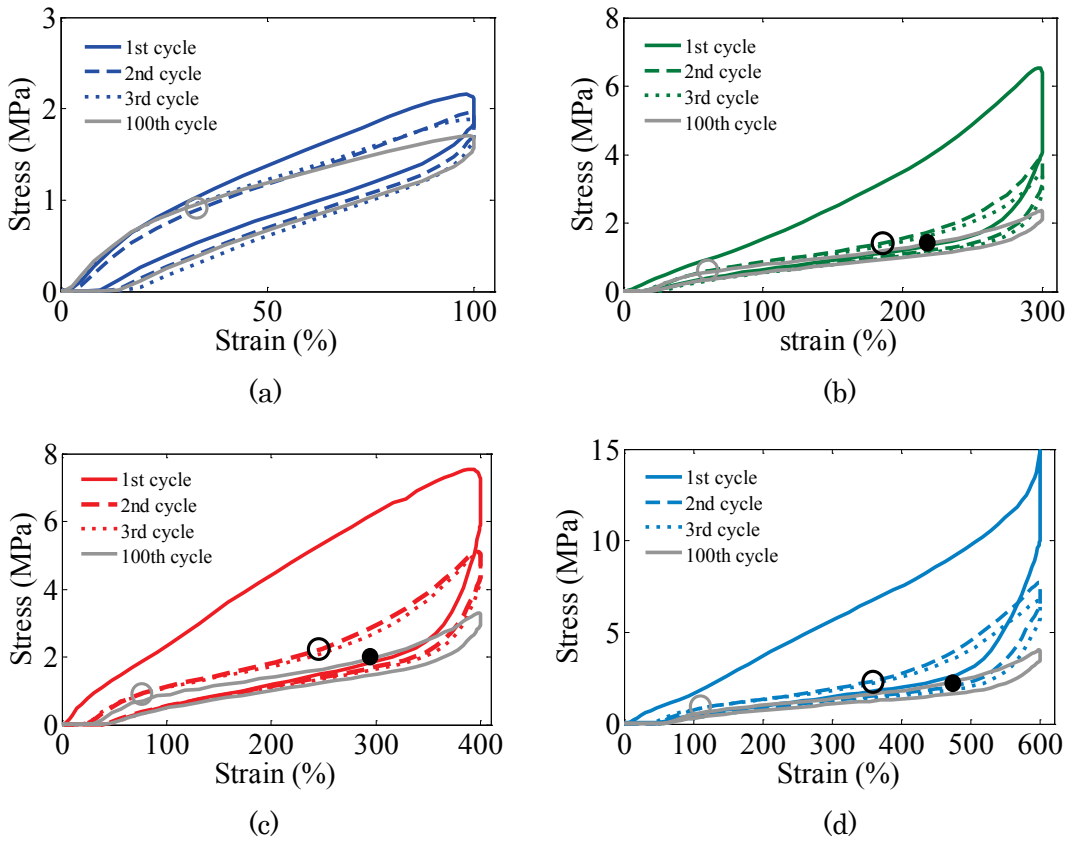

Fig 3.3 Stress-Strain curves of the first, the second, the third and the hundredth cycles in each maximum strain levels; (a) 100 %, (b) 300 %, (c) 400 % and (d) 600 %

It is clearly seen that the shape of the S-S curve depends on ε_{max}. Without ε_{c2} neither big decrease in inside area of hysteresis loop for Strain 100 %, we see here that Mullins effect is difficult to be seen when ε_{max} is quite small such as 100 %.

3.4.2 Temperature variation in function of time

Examples of experimental results of ElCE in function of time are shown in Fig 3.4. Testing condition was rectangular shaped "high-speed" deformation without any pre-stretching. The maximum strain was 400 %. Fig 3.4 (a) shows the first cycles and (b) shows the second. Strain was applied rapidly (elongation rate of 1.0 s^{-1}), kept for 5 s and then released. Its image was depicted by dotted lines. They are the results which ware obtained at the same time to Fig 3.3 (c).

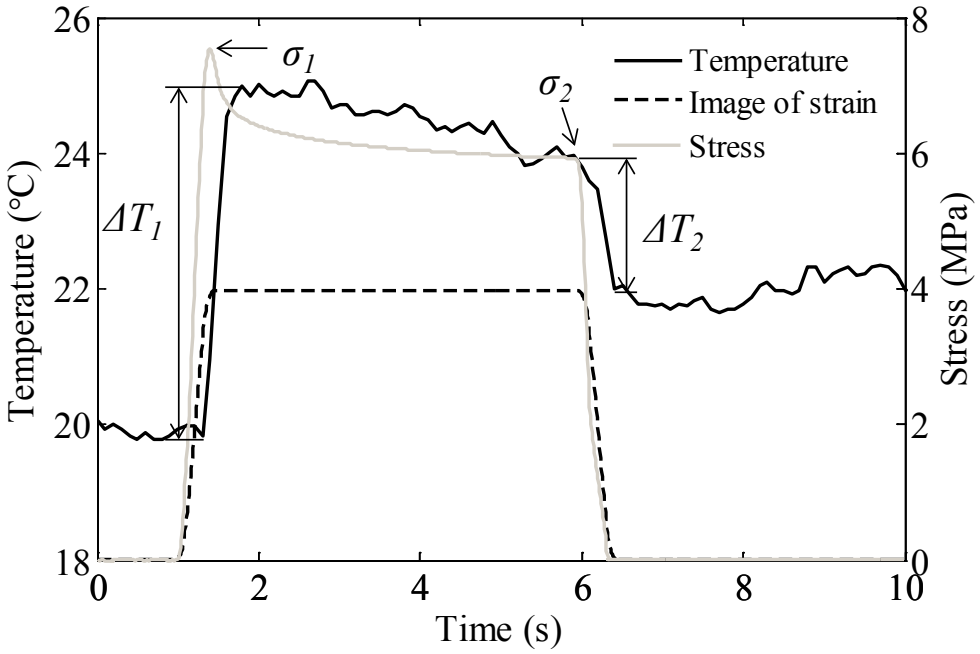

(a)

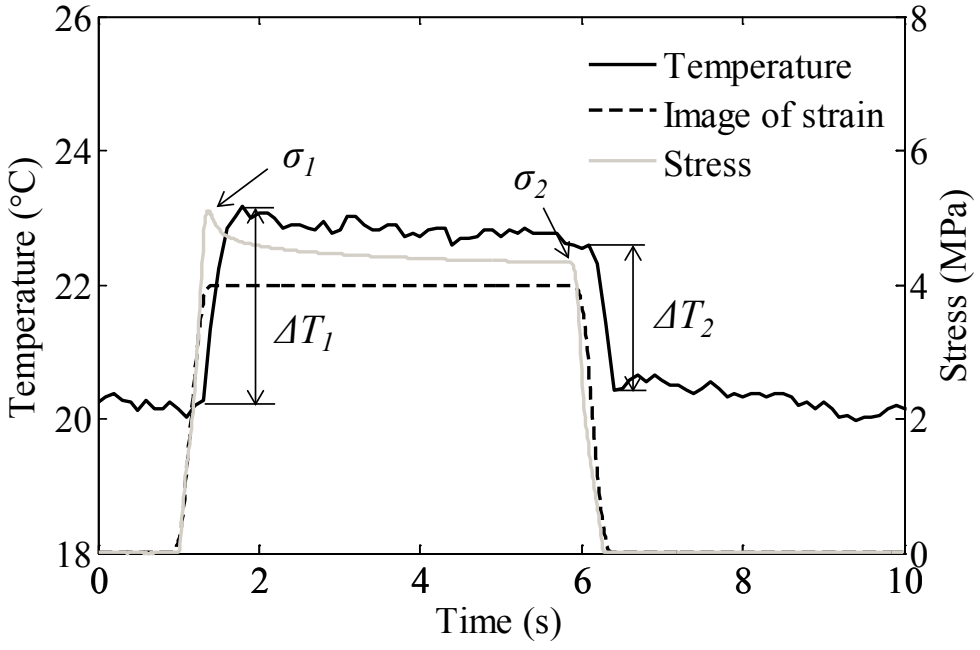

(b)

Fig 3.4 Examples of experimental results of ElCE in cyclic deformation: surface temperature, strain and stress vs. time for strain 400 %; (a) the first cycle and (b) the second cycle

For both cases, stress reaches at a maximum value σ_1 when strain reaches its maximum, and then shows an exponential decrease when the strain is kept. Within 5 s of strain kept time, the saturation is completed to a certain value of σ_2 by stress relaxation. At the same time, temperature of sample surface reaches its maximum with a slight delay to strain application (about 0.5 s). Then, it decreases slightly with the time delay. The difference between room temperature and this maximum temperature is a temperature variation caused by extension, defined as an increase temperature variation, ΔT_1. Since strain reaches its maximum sufficiently earlier than when temperature reaches its maximum, the elongation rate ensures that the sample is still in adiabatic state right after the extension. Thickness of the present sample is large enough, about 850 μm. Less spontaneous heat radiation can be estimated than thinner sample. After 5 s, the strain is returned to zero. Surface temperature decreases drastically due to the contraction. The present temperature variation is called a decrease temperature variation, ΔT_2. It was confirmed that 60 s is large enough to wait that the surface temperature returns to room temperature after contraction. The second cyclic deformation was carried out after when the temperature returned to the room temperature.

In the comparison between (a) and (b), a considerable decrease of ΔT_1 will be already recognized within the first to second cycle as well as the maximum generated strain. This fact is, surely, discussed in the following section.

3.5 Results and discussion

3.5.1 Relationship between stress and temperature change

A) Number of cycle and stress

The stresses which appeared at stretching (σ_1) and the remnant stresses measured just before contracting (σ_2) in cyclic deformation of each maximum strain level are shown in Fig 3.5 (a) and (b), respectively. Time interval between stretching and contracting is 5 s, as already shown in Fig 3.4.

These results show that larger strain always leads larger stress. In cases of strain 300 %, 400 % and 600%, both σ_1 and σ_2 radically decreased after the first cycle. As previously explained, the decreases in σ_1 and σ_2 are estimated having been caused by Mullins effect. In order to confirm it, the reduction rates of σ_1 and σ_2 in each maximum strain are summed up in Table 3.1. These rates of both σ_1 and σ_2 between the first and the second cycles are larger than those between the second and the third cycles. This is true for the three levels of maximum strains, except for its 100 %, of both σ_1 and σ_2. Since the large decreases in σ_1 and σ_2 occur only after the first cycle, it was confirmed

that the decreases in σ_1 and σ_2 due to the Mullins effect occur mainly after the first cycle. This effect can also remain from the second cycles but much smaller. The effect of fatigue should be considered from the second cycle.

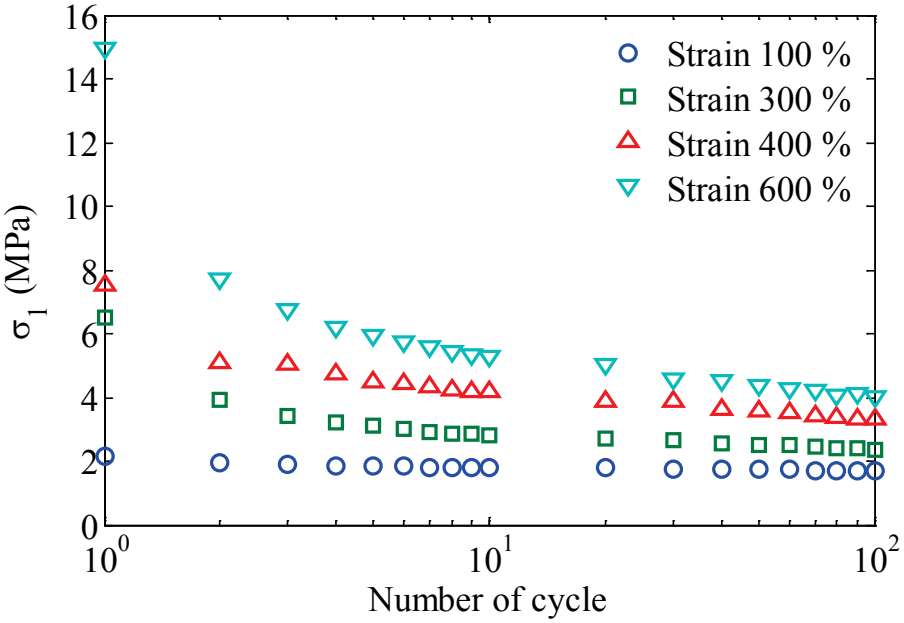

(a)

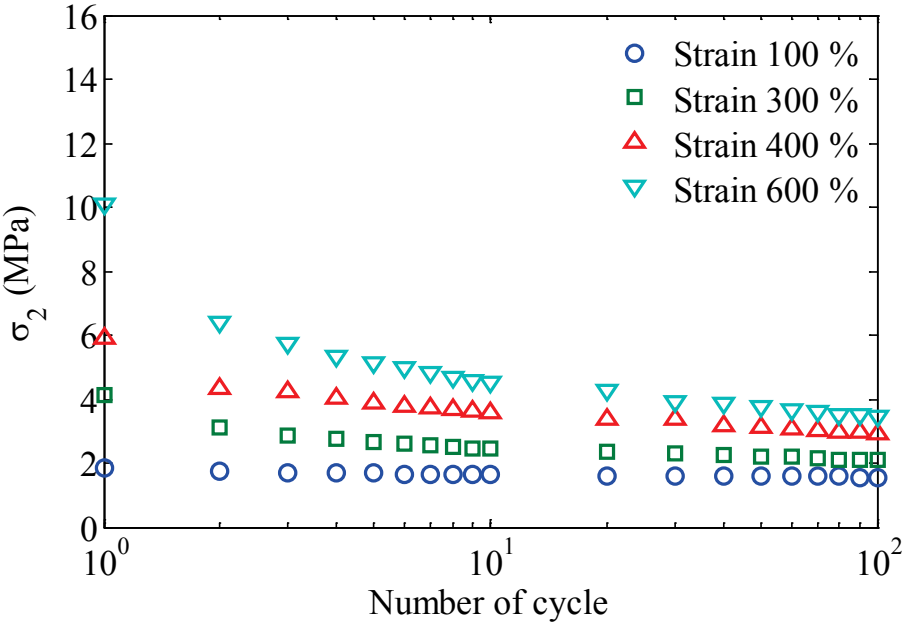

(b)

Fig 3.5 Relationship between the number of cycle and the stress
(a) maximum stress at stretching (σ_1), (b) remnant stress just before contracting (σ_2)

From the second cycle, they decrease gradually then, show the convergence within 100 cycles. The reduction rates between the second and the hundredth cycles were also shown in table 3.1. The rate between the second and the hundredth cycles of strain 300 % are almost equal to it of strain 400 %. In the contrast, it of strain 600 % is much higher than them. This result indicates that the effect of fatigue on strain 600 % is larger than them. It is suggested that the molecular chains of NR are fully stretched until when strain achieved up to 600 %, then it is them who receive all the charge in stress, whereas chains are not fully stretched within the samples of strains 300 % and 400 %.

Table 3.1 Reduction rates of σ_1 and σ_2 in each maximum strain

Strain	Reduction rate of σ_1 (%)			Reduction rate of σ_2 (%)		
(%)	1st → 2nd	2nd→3rd	2nd→100th	1st → 2nd	2nd→3rd	2nd→100th
100	9.2	3.7	12.8	5.0	2.1	9.9
300	47.3	6.02	31.1	23.7	8.6	32.9
400	32.3	1.2	35.2	27.0	2.3	32.4
600	48.4	12.3	47.5	36.2	10.6	45.7

Besides, σ_1 and σ_2 of strain 100 % are relatively stable from the first cycle to the hundredth cycle. This result indicates that there is a threshold to change the tendency of decrease in stress between strain 100 % and 300 %.

From Fig 3.5, one thing is clear that σ_1 and σ_2 are unchanged during cyclic deformation under small strain such as 100 %, as previously described in section 3.4.1 (B).

B) Number of cycle and temperature variation

$|\Delta T_1|$ and $|\Delta T_2|$ in cyclic deformation of each maximum strain level are shown in Fig 3.6 (a) and (b), respectively. $|\Delta T_1|$ of only strain 600 % exponentially decreases in function of number of cycle. It becomes relatively stable from the sixth cycle. $|\Delta T_2|$ of strain 600 % decreases gradually from the first cycle to fifth cycle then becomes stable. In case of strain 300 % and 400 %, $|\Delta T_1|$ in the first cycle is larger than that of other cycles but it becomes stable from the second cycle. On the other hand, their $|\Delta T_2|$ are relatively stable from the first cycle. In case of strain 100 %, both $|\Delta T_1|$ and $|\Delta T_2|$ are stable, as well as the stress, from the first cycle till the hundredth cycle. As $|\Delta T_1|$ and $|\Delta T_2|$ became stable after several cycles for all maximum strain levels, it became clear that the effect of fatigue on the temperature change is quite small. This fact indicates

that the stress and the temperature change have a different relationship with the number of cycles.

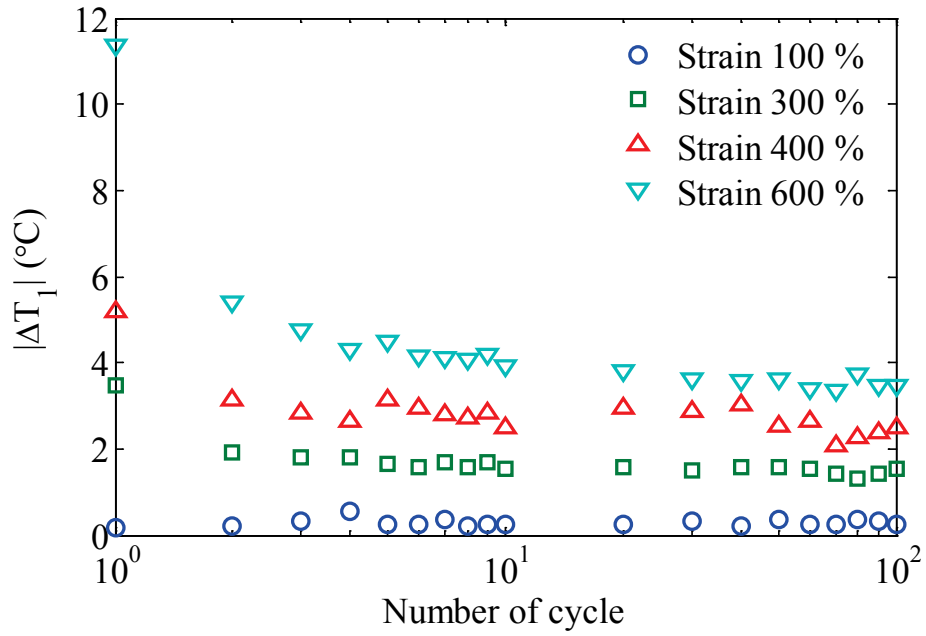

(a)

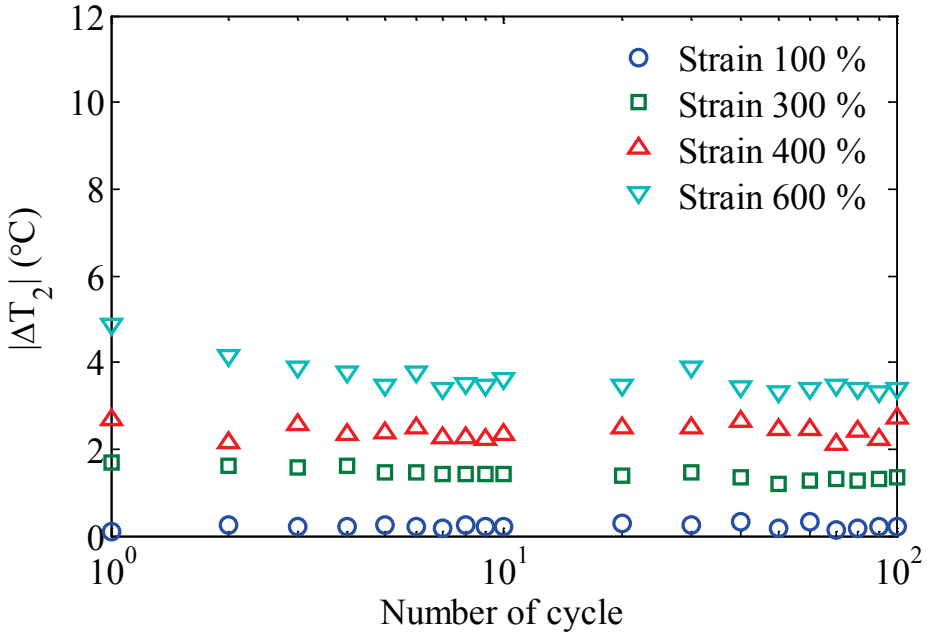

(b)

Fig 3.6 Relationship between the number of cycle and the temperature variation; (a) increasing temperature at stretching ($|\Delta T_1|$) (b) decreasing temperature at contracting ($|\Delta T_2|$)

In the comparison between Fig 3.5 and 3.7, it should be noted that σ_1 of strain 300 % and 400 % decrease radically after the first cycle then gradually by the number of cycle while those $|\Delta T_1|$ decrease radically only between the first and the second cycle then become stable. As shown in Table 3.1, the reduction rates of σ_1 after the first cycle in strain 300 % and 400 % are 47.3 % and 32.3 %, respectively. The rates of $|\Delta T_1|$ in strain 300 % and 400 % are 44.9 % and 39.3 %, respectively. There are no large differences between the rates of σ_1 and those of $|\Delta T_1|$ in strain 300 % and 400 %. The same tendency appears in strain 600 %. The rate of σ_1 is 48.4 % whereas that of $|\Delta T_1|$ is 52.4 % in strain 600 %. Consequently, it was confirmed that $|\Delta T_1|$ is significantly affected by the Mullins effect as well as σ_1. The effects of the fatigue on $|\Delta T_1|$ and $|\Delta T_2|$ might exist but those are quite smaller than the effects of Mullins effect.

C) Stress and temperature variation

In order to evaluate better the correlations between the stresses and the temperature variations at stretching and contracting, the relationships between them are shown in Fig 3.7 (a) and (b), respectively. Many points are depicted for each strain level. The detail information is not indicated in the figures but they correspond to the stress/temperature values of all different number of cycles indicated in precedent figures, Fig 3.5 and 3.7.

The present NR exhibits temperature increase of 4 °C with stress of 5 MPa and temperature decreases of 3.5 ~ 4 °C with 3.5 ~ 6 MPa under room temperature for strain 600 % as shown in Fig 3.7. As described in introduction, some SMAs, studied recently for ElCE, can also exhibit similar level of temperature variation, 4°C, but they require a quite large stress such as 150 MPa [9, 13 and 60]. Instead, the NR can supply the temperature variation with a considerably smaller stress than SMAs.

Fig 3.7 shows that both $|\Delta T_1|$ and $|\Delta T_2|$ have the tendency of increase with σ_1 and σ_2 but they do not have linear relations. It means that different temperature variations are generated by the same stress value if the strain level is different. For example, with 4.0 MPa at stretching, $|\Delta T_1|$ of strain 300 %, 400 % and 600 % are 1.9 °C, 2.7 °C and 3.5 °C, respectively. With 4.0 MPa at contracting, an another example, even an inverse can be seen where $|\Delta T_2|$ of strain 300 %, 400 % and 600 % point out 1.6 °C, 2.3 °C and 3.4 °C, respectively. The present relationship between σ and $|\Delta T|$ is often used as the evaluating method for ElCE. It is clear, however, that it is improper for non-linear elastic material such as NR. It is necessary to improve the evaluating method for the study of ElCE in order to evaluate both linear and non-linear elastic materials.

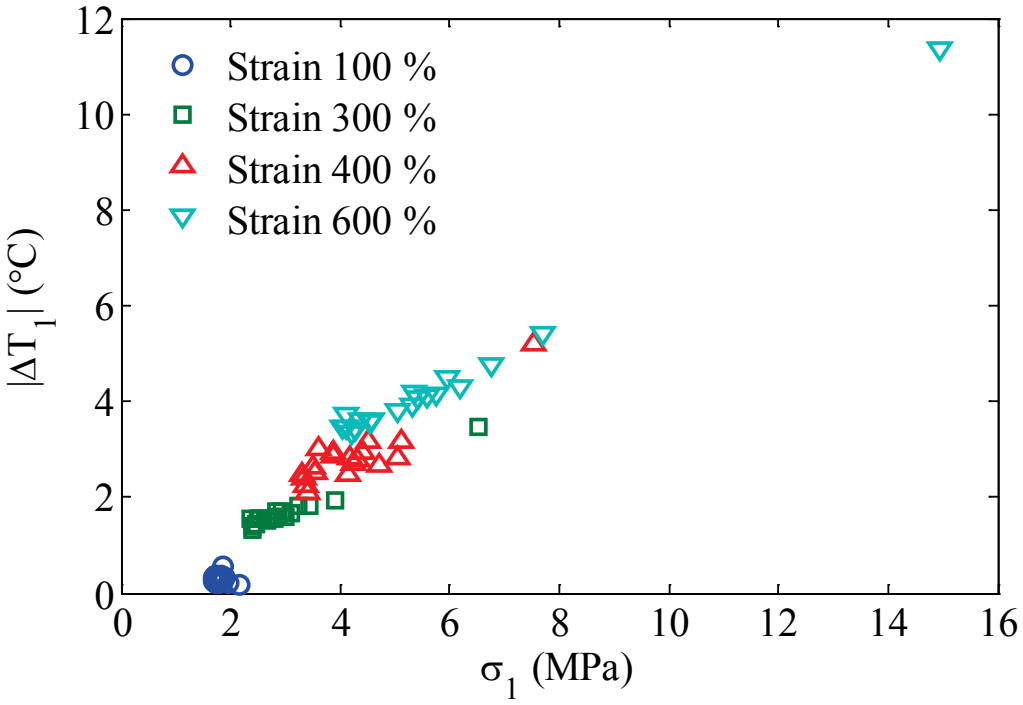

(a)

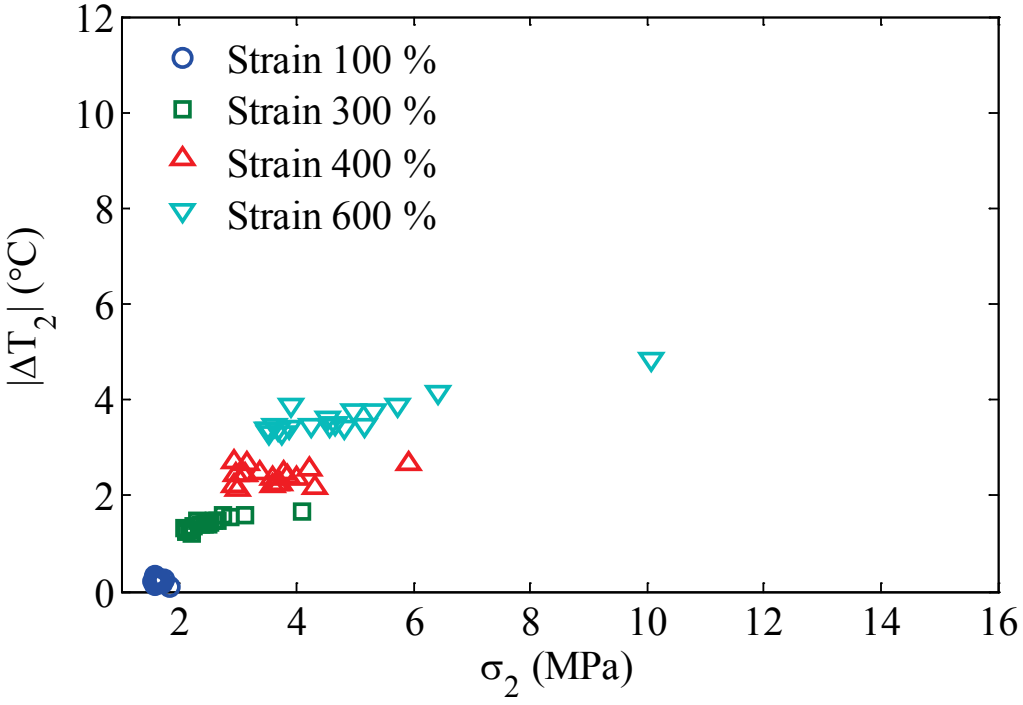

(b)

Fig 3.7 Relationship between the stress and the temperature variation
(a) at stretching (b) at contracting

Generally speaking, the mechanical energy to ideal rubber is equal to the heat energy. Real rubber is different with ideal rubber because the movement of molecular in real rubber is restricted by the crosslink. There is a possibility, however, that real rubber also shows correlation between these energies. I focused on these energies and results and discussions are described in following section, in order to propose a proper evaluating method for the ElCE.

3.5.2 Mechanical energy and temperature variation

As previously described in section 3.2.2, the first law of the thermodynamics indicates that the mechanical energy applied to material is divided into the internal energy stored in material and the heat energy. The present law leads that the elastocaloric effect can be properly evaluated by the mechanical and heat energy. We focused on the mechanical energy expressed by the integral of the displacement with respect to the applied force in order to quantify the mechanical energy, mechanical energy at stretching (W_1) and at contracting (W_2).

The relationships between the mechanical energies and temperature variations are shown in Fig 3.8. It is clearly seen that both $|\Delta T_1|$ and $|\Delta T_2|$ have complete linear relation with mechanical energy for whatever the maximum strain. In the comparison between Fig 3.7 and 3.9, it was revealed that temperature variations have a more accurate correlation with mechanical energy than stress. Even though NR receives the same stress level, as described previously in the section before, the temperature variation depends on strain level. At the same time, the relationships between the stresses and the temperature changes of NR differ depending on strain. Consequently, it was difficult to evaluate ElCE of NR with this conventional method. On the other hands, the relationships between the mechanical energies and the temperature variations show a strong correlation as shown in Fig 3.8. As previously described, Mullins effect and the fatigue affect the applied stress. At the same time, different temperature variations are generated by the same stress value if the strain level is different. Nevertheless, mechanical energy, calculated with applied force and displacement, demonstrates such beautiful linear relation with temperature variation. It means that this evaluation method for ElCE adapts all of strain levels and does not require any historical charge information applied to sample in advance. As a result, I conclude that ElCE of NR which is difficult to be discussed by the conventional method can be exactly evaluated by using the relation between mechanical energy and temperature variation.

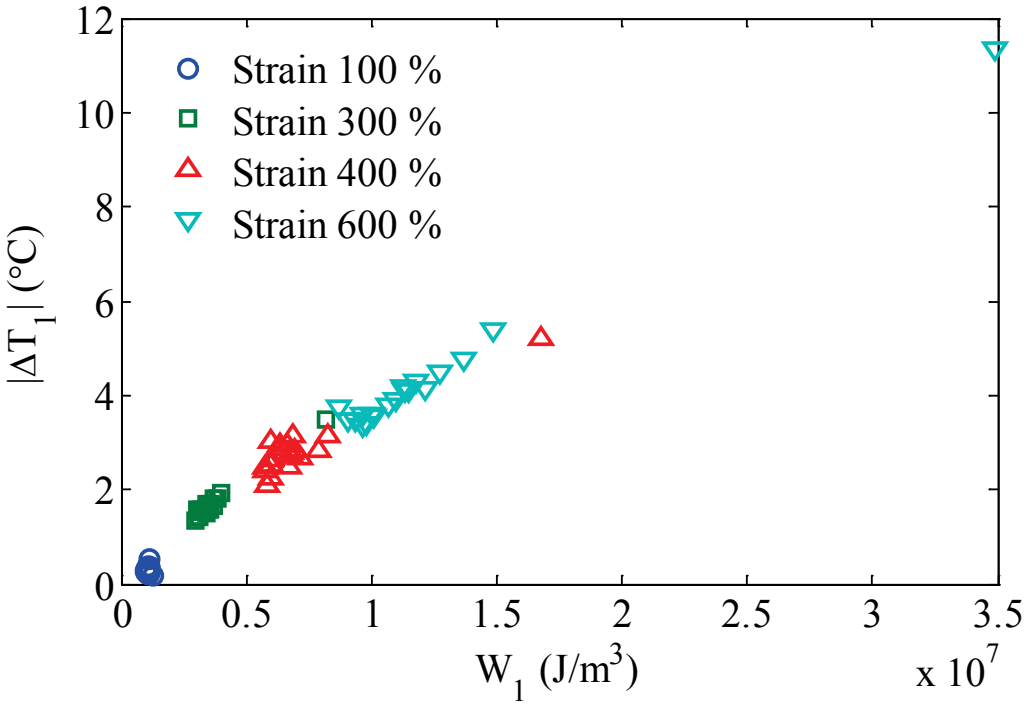

(a)

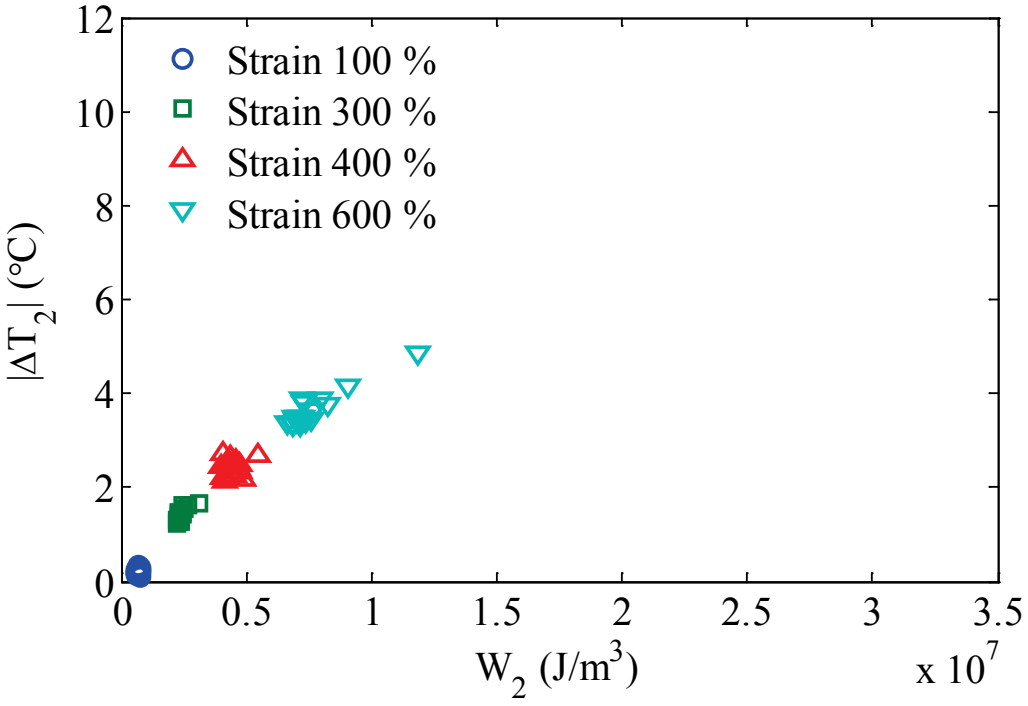

(b)

Fig 3.8 Relationship between the mechanical energy and the temperature variation (a) at stretching (b) at contracting

3.5.3 Conversion efficiency from mechanical energy to heat energy

In order to evaluate ElCE of NR in even more details, the conversion efficiencies from mechanical energy to heat energy are discussed in this section. Heat energy Q with ΔT measured by the thermal camera writes

$$-Q_i = \rho V C_p \Delta T_i \quad (3.5)$$

where ρ is the density, V is the volume of material and C_p is the specific heat capacity. i is replaced by the numbers 1 or 2 where 1 means stretching and 2 contracting.

The conversion efficiency η is the rate between the mechanical energy and the heat energy, which is expressed as:

$$\eta_i = -Q_i / W_i \times 100 \quad (3.6)$$

The conversion efficiencies at stretching (η_1) and at contracting (η_2) in cyclic deformation of each maximum strain level are shown in Fig 3.9 (a) and (b), respectively. It should be noted that the conversion efficiencies of strain 100 % vary a lot because of the difficulty in measuring a small temperature variation (around 0.3 °C). Since the noise level of the thermal camera is ± 0.1 °C, the effect of noise level becomes larger when temperature variation is small. Although the values of the ones of 100 % vary a lot, it seems that the average of the values is about 40 % and it can be recognized that there is no effect of the increase in the number of cycle on the values.

Compared with others (300 %, 400 % and 600 %), η_1 and η_2 of only strain 100 % are clearly smaller (principally below 50 %). In general, it is said that most of applied force to rubber contributes to entropy term under large deformation, and, on the other hand, to internal energy term under small deformation as described in chapter 1 [64, 65]. The difference in the conversion efficiencies indicates that the threshold for changing mechanical energy into heat energy or to internal energy lies between strains 100 % and 300 %. It is estimated that the mechanical energy of strain 100 % is mainly converted to the internal energy. It can be easily estimated that storing the mechanical energy as internal energy leads a reduction in the conversion efficiency. NR is hardly affected by the Mullins effect when a small strain such as 100 % is applied as previously described. Thus, it can be concluded that NR exhibits a characteristic between the energetic elasticity and the entropic elasticity in the strain region where NR is hardly affected by the Mullins effect.

For all strain levels including strain 100 %, the η_1 of the second cycle are approximately 10 % larger than those of the first cycle. The increase in η_1 occurs between the first and the second cycle. This fact suggests that η_1 is increased by the Mullins effect. The reasons are as followings. The internal energy stored in the molecular chains due to stretching is estimated to decrease because of the softening by

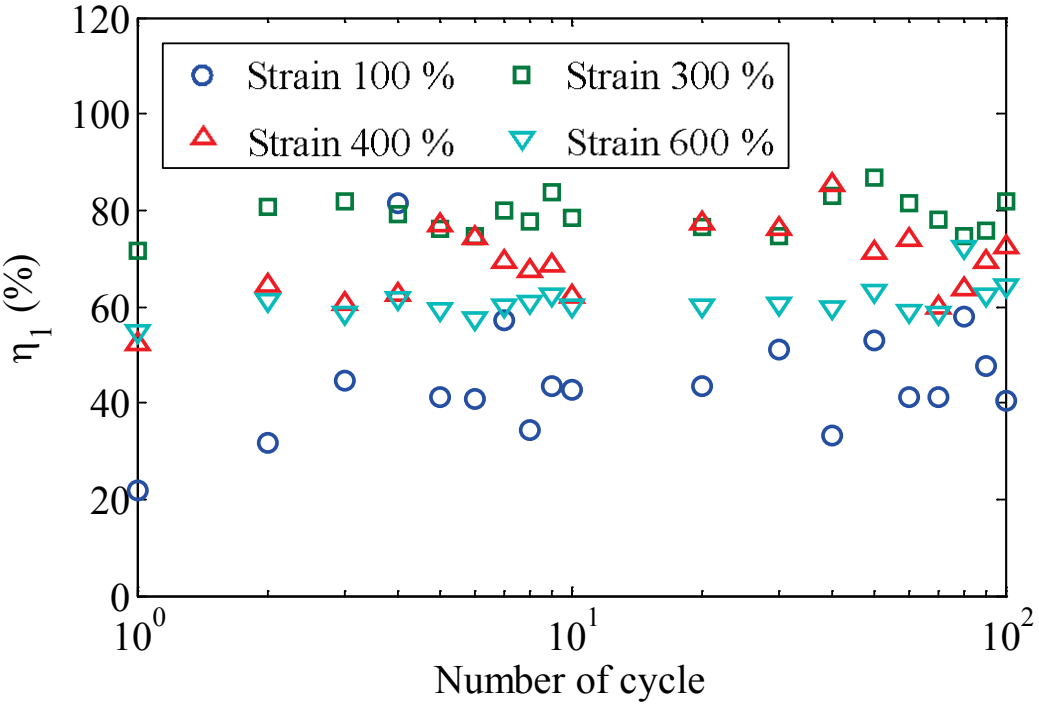

(a)

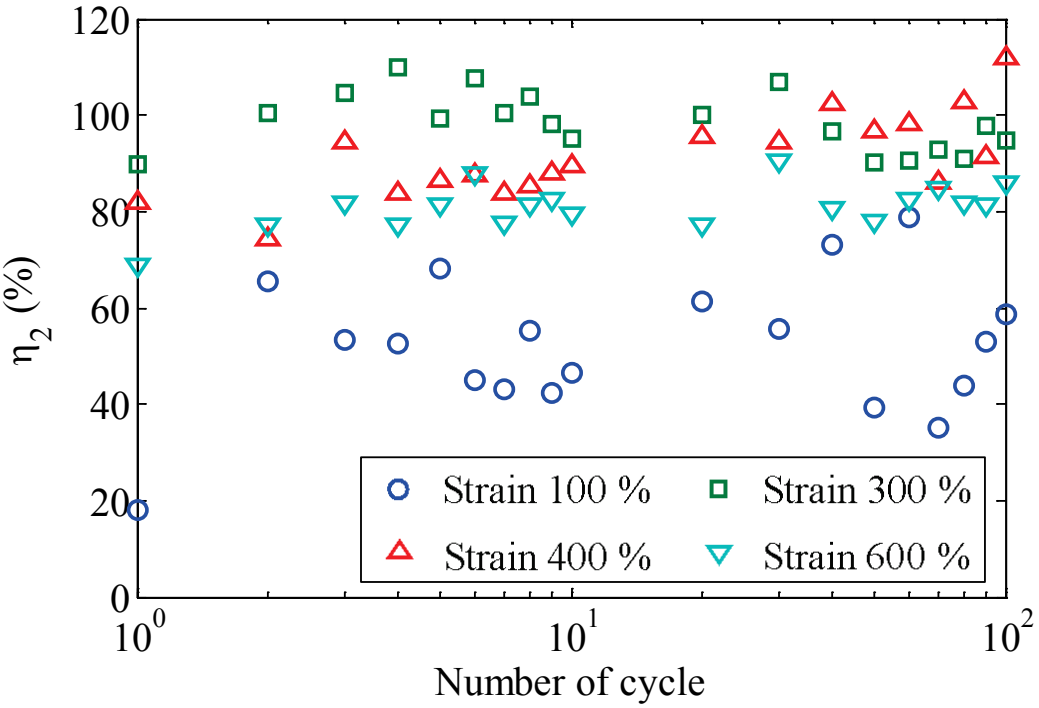

(b)

Fig 3.9 The conversion efficiency from the mechanical energy to the heat energy during cyclic deformation (a) at stretching (η_1) (b) at contracting (η_2)

the Mullins effect. As a result, the molecular chains are stretched smoothly, so that the applied mechanical energy converts to the heat energy effectively. Consequently, η_1 of the sample increases. Although the influence of the Mullins effect on the conversion efficiency was suggested, the detail cannot be clarified only from this result. The further research is needed to conclude the influence.

Fig 3.9 (a) and (b) clearly shows that η_1 and η_2 depend on the strain level. η_1 achieves up to 70 % for both strain 300 % and 400 % whereas its strain 600 % achieves up to 60 %. Compared with them, it is interesting to note that η_1 of 600 % are lower. Besides, it is shown that η_2 of strain 600 % is quite lower than its strain 400 % and little smaller than its strain 300 %. In order to discuss a quite large deformation such as strain 600 %, internal energy must be more discussed. In solid-state material such as metal, it is considered that atomic bonds store the internal energy since the bonding power of atoms is quite strong. Such material has a small freedom degree of arrangement of atoms so that most of the applied load contributes to the internal energy. In case of rubber, the molecular chains are relaxed when strain level is below a threshold. When strain exceeds that critical level, on the other hand, the chains are fully stretched. These fully stretched molecular chains might have similar behavior to atomic bonds of solid-state materials so that they have strong power because the freedom degree of arrangement of molecule becomes smaller, i.e., the fully stretched molecular chains store the internal energy as atomic bonds of solid-state materials. As above mentioned, the conversion efficiencies of strain 600 % are lower than those of strain 300 % and 400 %. The reason for this fact, where the internal energies of strain 300 % and 400 % are smaller than that of strain 600 %, is estimated that only the later one has the fully stretched molecular chains.

In summary, one hypothesis is proposed as followings. The internal energy of NR slightly increases when the applied strain is small, such as 100 %, and then it decreases or becomes constant with increasing strain because most of the force is contributed to the entropy change. It restarts increasing when the deformation overcomes another threshold, between 400 % and 600 % in this case, because there is no more space to relax within molecular chains. Reduction in the conversion efficiency can happen in this case. The discussion will be confirmed in the next section.

3.5.4 Internal energy under “low speed” deformation

A.) Critical strain

In order to validate the present hypothesis, the internal energy was measured with smaller elongation rate, 0.05 s^{-1}, instead of 1.0 s^{-1}. It is difficult to measure the heat per

strain under “high speed” deformation because the temperature variation has delay to strain as previously mentioned in typical results, see Fig 3.3. The effect of heat dissipation is large under quite low speed deformation. In order to eliminate the time difference between temperature variation and applied strain and to reduce the heat dissipation, elongation rate of 0.05 s^{-1} is selected as the proper speed.

The heat dissipation under the “low speed” deformation is considered as following. Since the internal energy is calculated by the difference between the mechanical energy and the heat, the dissipated energy by the heat dissipation is required in order to calculate all of the heat converted by the elastocaloric effect and the internal energy. Not only the heat radiation but also the heat convection has to be considered as the heat dissipation. All of the heat converted by ElCE is calculated by the sum of heat contributed to temperature variation and heat dissipation. Under “low speed” deformation, it is possible to say that. Fig 3.10 shows the mechanical energy, the heat and the internal energy under “low speed” deformation calculated based on such idea when the maximum strain of 400 % is applied.

When the strain is applied, the internal energy increases with strain and suddenly decreases at around strain of 160 %. There is no increase in the heat energy below 160 %.

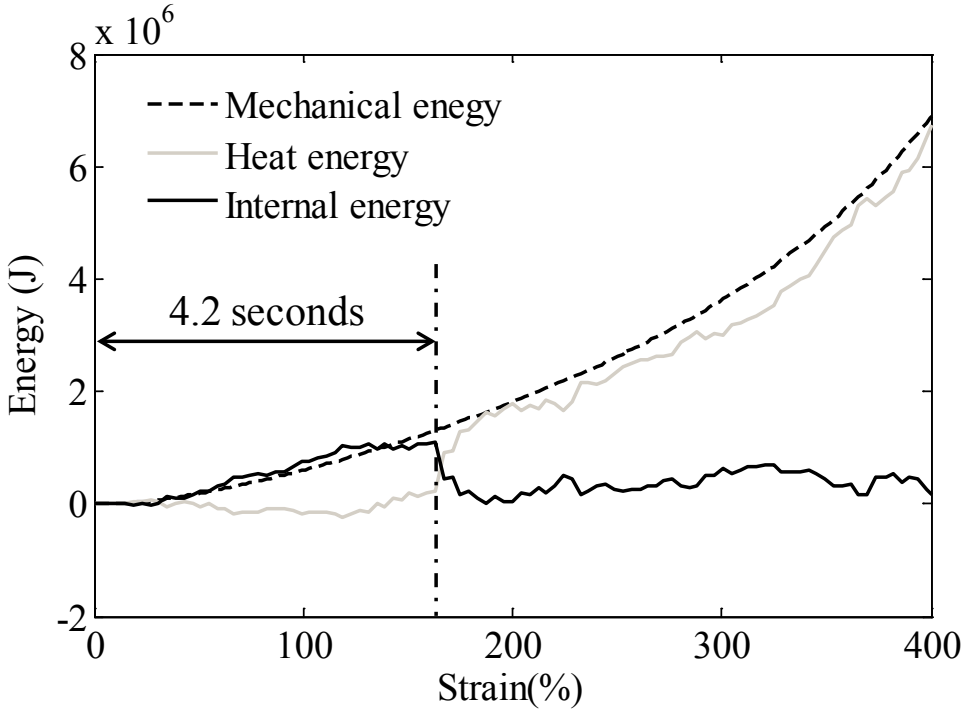

Fig 3.10 The mechanical, the heat and the internal energies during stretching at 0.05 s^{-1} (“low speed”) when the maximum strain of 400 % is applied

This fact indicates that the most of the mechanical energy is converted to the internal energy below this strain level. Then, from this threshold, the heat energy increases in keen slope just as contrasted with the decrease in keen slope of the internal energy. Then, heat energy continues increasing strongly until the end, 400 % of strain. At the same time, the internal energy becomes stable at around 0 J until the end of measurement. It was clearly shown that the most of the mechanical energy is completely converted into the heat energy from 160 % till 400 %. This keen slope regions, strain between about 160 % and 190 %, must correspond to the required time to this radical change. The energetic elasticity drastically changes into the entropic elasticity at the critical strain 160 %. In the present experiment, it took 4.2 s to reach this threshold. In other words, the increase in temperature started after an introduction of deformation with delay about 4.2 s. Storing energy such as the internal energy causes the time interval between the start of deformation and the start of heat energy. In summary, Fig 3.10 shows three steps. First of all, applied energy is totally stocked in material, i.e., totally converted into internal energy. Secondary, a slight time is required to change internal energy to heat energy. Then finally, mechanical energy is no more converted to internal energy and it is converted directly into heat energy.

However, it is difficult to identify the most important factor for the threshold of the energy conversion, a strain or a stretching time. In order to confirm this point, the experiment with slight faster elongation rate, 0.10 s^{-1} ("middle speed"), was carried out. Energetic results are shown in Fig 3.11. It can be seen that the most of the mechanical energy is completely converted into the heat energy from 180 % till 400 %, similar to the result with "low speed" elongation. Until this threshold, it takes 2.2 s which is about double to the one of "low speed". Comparing these results with different elongation rates, it can be concluded that the threshold of the energy conversion depends on a strain, but not a stretching time.

Now, let us discuss "high speed" deformation based on these results. As described previously in typical result (section 3.3), the change of temperature starts after deforming with delay. In the case of "high speed" deformation, it was about 0.5 s, see Fig 3.4. The reason for the time delay will be discussed as followings. Applied energy is firstly converted into internal energy and then into heat energy in not only "low speed" but also "high speed" deformation. Nevertheless, the applied strain is already beyond the threshold when the change of temperature starts in the "high speed" deformation.

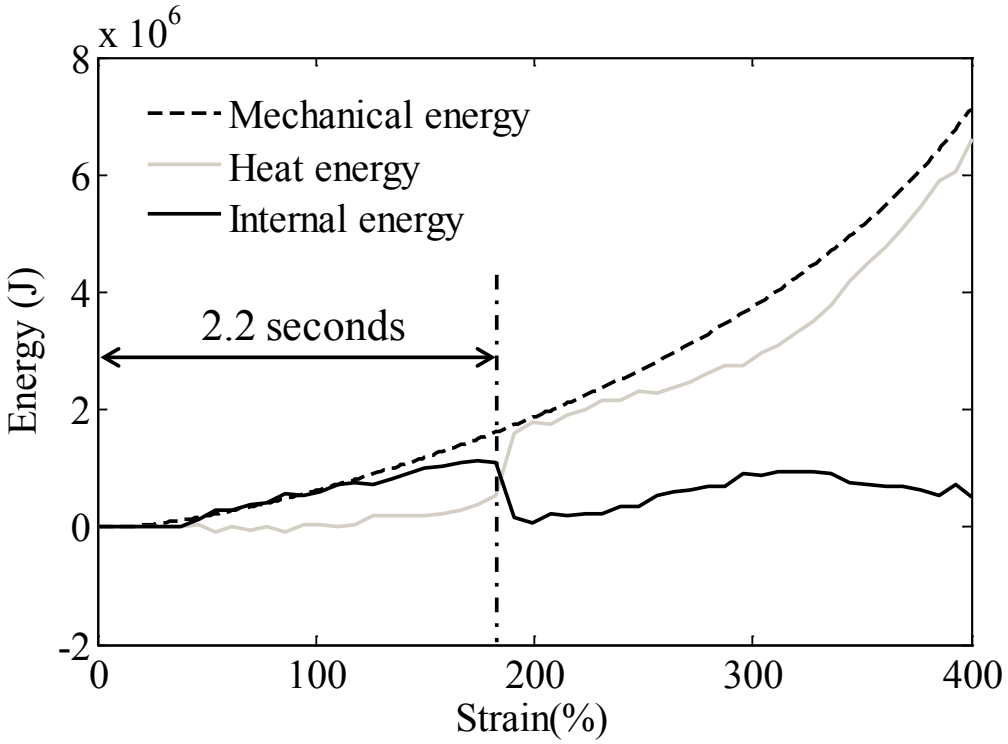

Fig 3.11 The mechanical, the heat and the internal energies during stretching at 0.10 s^{-1} ("middle speed") when the maximum strain of 400 % is applied

Thus, it can be considered that the time delay occurs due to two factors; the threshold and the energy conversion from internal energy into heat energy.

It was suggested in section 3.5.3 that the threshold lies between strains of 100 % and 300 % where mechanical energy changes into heat energy or into internal energy. By the tests with different elongation rate in this section, it was well verified that this threshold depends only on strain level but not a time, and that value is 160 %. A good agreement was obtained; threshold of 160 % exists between 100 % and 300 %. Here, it should be noted that this critical value was obtained with the maximum strain of 400 %. It varies with the maximum strain. Fig 3.12 shows the result when the sample is stretched until strain of 600 %. Below strain of 260 %, an increase of internal energy is seen while heat energy has no increase. At around 260 %, the drastic change occurs. From around 260 %, heat energy increases with mechanical energy and in contrary, internal energy stays at null till around 380 %. The critical strain threshold exists at around 260 % in this case. The internal energy shows different curve with different maximum strain. From the comparison of Fig 3.10 and 3.13, it was shown that a larger maximum strain leads a higher threshold. The stress and the temperature variation change by the maximum strain information that the sample had received in advance.

Here also, special attentions should be paid to the maximum strain in advance because the threshold where heat energy starts to increase is modified by that value.

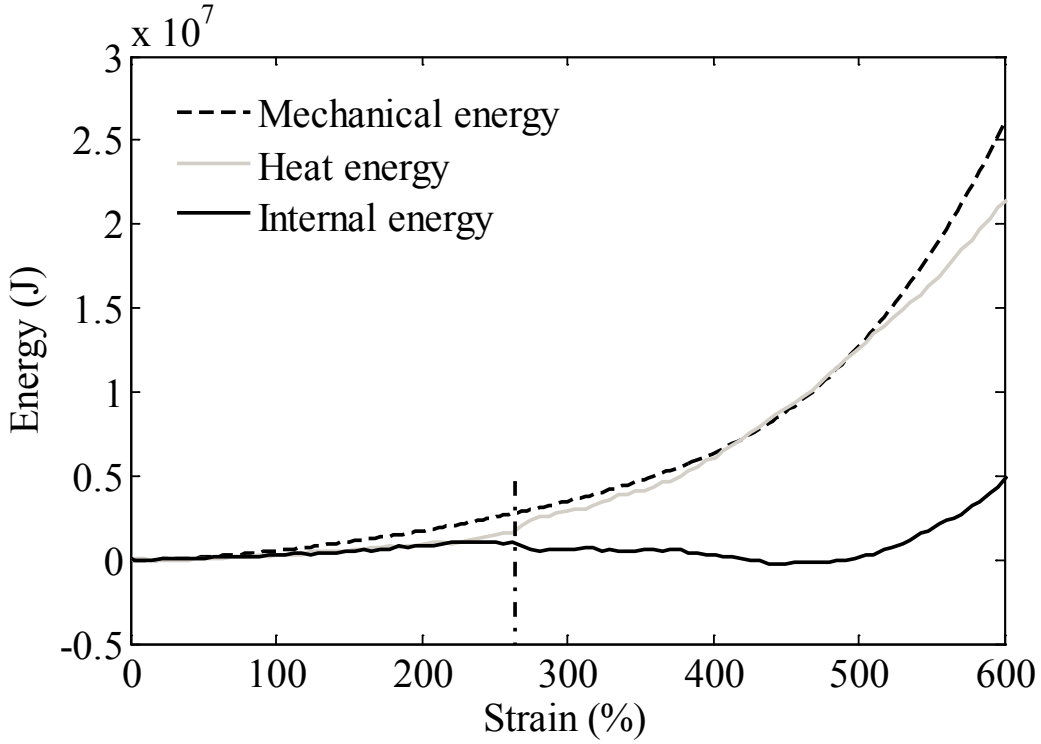

Fig 3.12 The mechanical, the heat and the internal energies during stretching at 0.05 s^{-1} ("low speed") when the maximum strain of 600 % is applied

B.) Second increase in the internal energy

"Low speed" deformation below strain of 400 % was discussed in previous part (3.4.4.A). In this part, "low speed" deformation above 400 % is discussed with the maximum strain of 600 %.

As previously explained, Fig 3.12 shows that the critical strain exists at around 260 %. Internal energy stays then at null till 380 %. It is interesting that it decreases below zero from 380 % then restarts increasing from around 450 % when the sample is stretched until 600 %. It was found that internal energy can rise again after another critical value in strain. This second critical value of strain will be called as the second transition strain for the sake of convenience to make a difference to the first one which will be called as the first transition strain. The second transition strain is discussed here in order to understand morphology change of NR during the extension.

In order to discuss that the molecular chains of NR are fully stretched, the S-S curve under "low speed" deformation with the maximum strain of 600 % is shown in Fig 3.13.

For the purpose of comparison of the results, that with 400 % is also shown in the figure. Note with special emphasis that S-S curve is different by elongation rate, see Fig 3.2. It is shown that the stress starts to increase drastically from around strain of 300 % and linearly strongly from around 450 %. The open circle in the figure marks the strain value where the sign of second derivative of S-S curve changes, corresponding to the open circles in Fig 3.3. The closed square marks strain of 450 %. It is well-known that a stress increases strongly in large deformation area due to fully stretched molecular chains. It can be estimated that SIC starts forming at 300 % (○) then molecular chains are fully stretched from 450 % (□). The strain value 450 % is exactly the same to the second transition strain obtained above. It means that the exponential increase of the internal energy starts at the same time to the exponential increase of the stress. Since there is a good agreement between the strain where the molecular chains are fully stretched and the second transition strain, it was well confirmed that the internal energy starts increasing due to the fully stretched molecular chains. Consequently, it was experimentally confirmed that the fully stretched molecular chains behave as the atomic bonds of solid state material.

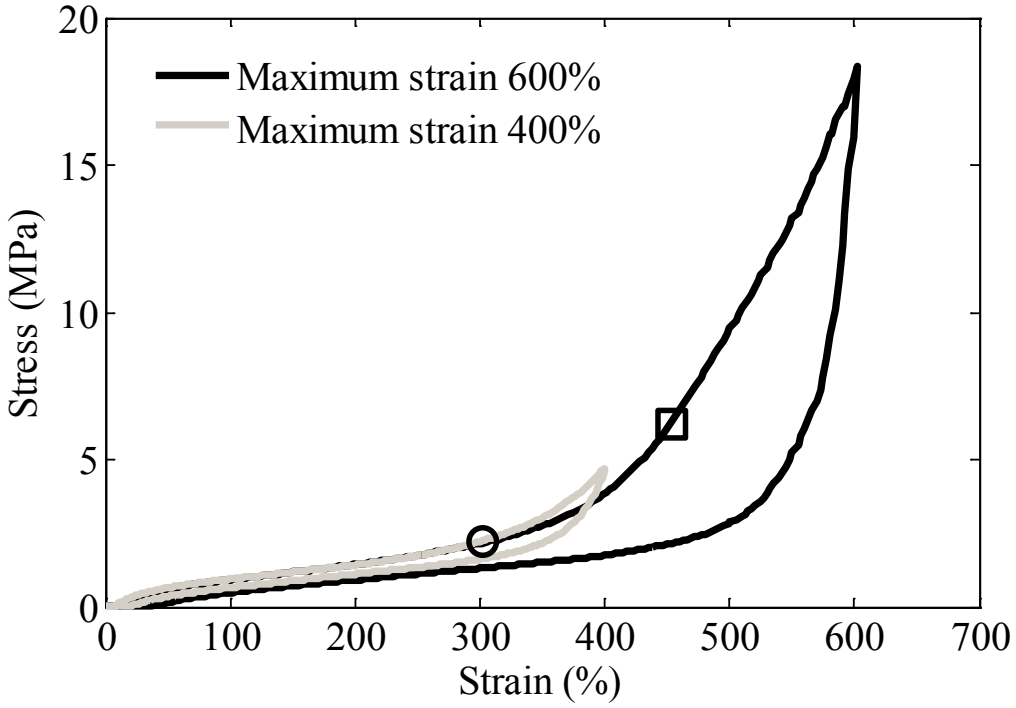

Fig 3.13 The S-S curves during "low speed" deformation (elongation rate of 0.05 s^{-1})

In section 3.4.3, one hypothesis was proposed; the fully stretched molecular chains of NR behave as the atomic bonds of solid-state material. Based on the results in the

previous and the present sections, the hypothesis was experimentally confirmed; the internal energy of NR increases when strain is small, smaller than the first transition strain, and when strain is quite large, larger than the second transition strain.

3.6 Conclusions

Elastocaloric effect (ElCE) of carbon black (CB) filled natural rubber (NR) has been investigated. As a result, it was found that filled NR exhibits a large temperature variation, comparable to some shape memory alloys (SMAs) [9, 13 and 60], with a quite small stress, much smaller than that for SMAs. Moreover, it was experimentally confirmed that not only the applied stress but also the strain are important factors in ElCE of non-linear elastic material such as NR. Since the mechanical energy calculated with the applied force and the displacement shows an extremely strong correlation with the temperature variation caused by ElCE, it was concluded that ElCE of the non-linear elastic material can be evaluated properly with the relationship between the mechanical energy applied to the material and the heat energy released from the material.

The influences of Mullins effect and the strain-induced crystallization (SIC) on ElCE of filled NR were discussed with the relationships between the temperature variation and the applied stress and between the mechanical and the heat energies. It was found that the amount of temperature variation decreases remarkably due to the Mullins effect from the fact that the stress decreases before the strain reaches its maximum and when the strain reaches its maximum. On the other hand, the influence of SIC shows the opposite to the Mullins effect. SIC is a factor for the greatly increase in not only the stress but also the amount of temperature variation. However, the SIC causes the decrease in the conversion efficiency from the mechanical energy to the heat energy because the internal energy stored in the material increases due to the fully stretched molecular chains. One more explication has been tried that the conversion efficiency from the mechanical energy to the heat energy is increased by the Mullins effect. The further verifications are, however, required for this point.

The present study defined the influences of the Mullins effect and the SIC, both of which are the phenomena affecting the mechanical property of elastomer. Although the present evaluation with the energies seems effective, examples are not enough to conclude the detail of the phenomena. The further research such as using other material is needed to validate the evaluation.

Chapter 4

Elastocaloric effect of P(VDF-TrFE-CTFE)

4.1 Introduction

As previously explained, today's modern refrigeration technology is based almost entirely on a compression/expansion cooling cycle. Research on alternative technologies is ongoing through for example the use of caloric materials, such as magnetocaloric [6], electrocaloric [7] and elastocaloric materials [11, 12]. These three effects correspond to the dependence of the entropy on an external quantity (magnetic field, electric field and strain, respectively) in isothermal condition. It is then associated to either an adiabatic temperature variation or a heat exchange with outer medium in isothermal condition.

Elastocaloric effect (ElCE) is a promising solution, especially in shape memory alloys where adiabatic temperature variations up to 20 °C in NiTi wires were reported [57] and some cooling devices optimization were already performed [110]. Apart from shape memory alloys, single crystals [58] or polymers [52] also exhibit elastocaloric coupling. ElCE in natural rubber may be considered as one of the oldest known caloric effect [54], exhibiting a large refrigerant capacity [8]. Some materials exhibit multicaloric properties, such as multiferroics, in which the entropy is a function of electric field, magnetic field, and hydrostatic pressure [15, 16]. It is a fascinating subject of investigation, where the origin of the entropy variations lies usually in a phase transition induced by the external solicitation. On the other hand, relaxor polymers of poly(vinylidene fluoride-trifluoroethylene-chlorofluoroethylene) P(VDF-TrFE-CFE) and poly(vinylidene fluoride-trifluoroethylene-chlorotrifluoroethylene) P(VDF-TrFE-CTFE) are known to exhibit a very large electrocaloric effect, with adiabatic temperature changes up to 5-15 °C demonstrated by several research groups [42, 46 and 47]. Energy density of relaxor polymer may be very high thanks to its very high dielectric strength although the dielectric permittivity is rather low. The crystalline phase of the polymer is believed to be responsible of the dielectric properties and subsequent electrocaloric effect, whereas the amorphous phase appears to be a non-electrocaloric material. However, amorphous polymers are known to be also elastocaloric materials [52, 53] where the elasticity might be entropic origin. As a consequence, the relaxor polymers should be also elastocaloric materials.

This chapter is devoted to the direct characterization of the elastocaloric properties of relaxor polymer P(VDF-TrFE-CTFE), in order to find out its potential to be used as a material for multi-caloric effect.

4.2 Experiment

4.2.1 Terpolymer P(VDF-TrFE-CTFE)

Polyvinylidene-fluoride (PVDF) based polymers are ferroelectrics, and are widely used for sensors and actuators because of their piezoelectricity [48-51, 111, 112]. As explained in chapter 1, materials containing lead (Pb) have been widely used for electrocaloric effect (ECE) but Pb is a poisonous material. Since PVDF based polymers exhibit a temperature variation caused by ECE because of ferroelectrics, PVDF based polymers are expected as Pb-free material for ECE [7].

Neese et al. reported that P(VDF-TrFE) film exhibits a large temperature variation caused by ECE [37]. The temperature variation reported by Neese et al. is 12.6 °C, which is similar to the thin films containing Pd. However, it is required to determine ECE of P(VDF-TrFE) at temperatures above the ferroelectric-paraelectric transition (above 70 °C) in order to obtain a large temperature variation.

Neese et al. and other several research groups reported that relaxor polymers of P(VDF-TrFE-CFE) and P(VDF-TrFE-CTFE) exhibit temperature variation up to 5-15 °C at temperatures between 30-55 °C. These relaxor polymers are formed by the introduction of the third monomer (CFE or CTFE) into the polymer chain of P(VDF-TrFE). Since the third monomer acts like structural defects, the ferroelectric-paraelectric transition temperatures of the relaxor polymers are lower than that of P(VDF-TrFE). On the other hand, the dielectric permittivity decreases due to the introduction of the third monomer. Thanks to their high dielectric strength and ductility, the relaxor polymers exhibit a high energy density although the dielectric permittivity is rather low (see Table 4.1) [50, 113]. As a result, a temperature variation caused by ECE at temperatures between 30-55 °C of the relaxor polymers equal to that at temperatures above 70 °C of P(VDF-TrFE). Since they exhibit a large temperature variation near room temperature, they are also expected as materials for ECE near room temperature.

Table 4.1 Comparison of electromechanical properties of piezoceramics and PVDF based polymers [50, 113]

Materials	Young's modulus Y (GPa)	Maximum strain ε_{max} (%)	Volumetric elastic energy density $Y\varepsilon_{max}^2/2$ (J/cm^3)
Piezoceramics (PZT-5)	61	< 0.1	0.06
P(VDF-TrFE)	3.3	0.2	0.0066
P(VDF-TrFE-CFE)	0.4	5	0.5
P(VDF-TrFE-CTFE)	0.4	4	0.32

4.2.2 Fabrication

Fig 4.1 illustrates the fabrication process for P(VDF-TrFE-CTFE) film. P(VDF-TrFE-CTFE) film was fabricated using a solution-cast method by dissolving polymer powders (purchased from Piezotech SA) in methyl ethyl ketone (MEK) solvent. First of all, P(VDF-TrFE-CTFE) powders were dissolved in MEK at 70 °C for 4 h. This polymer solution was casted onto clean glass plates, and then dried at 70 °C for 2 h in an oven for the evaporation of the solvent. They were peeled off from the plates and then annealed at 110 °C for 2 h on PTFE plate in order to increase the crystallinity and eventually to remove totally the residual solvent. The thickness of the samples was around 40 µm after annealing.

The fabricated terpolymer film exhibits negligible elastocaloric activity. This will be demonstrated in section 4.3.2. The film was then uniaxially stretched 1200 % to its original length, which influences both the crystalline phase properties and align polymer chains of the amorphous matrix [45, 58 and 114]. Moreover, further crystallization upon plastic stretching may act as additional crosslinks, which, combined with pre-alignment of polymers chain, may enhance the entropic elasticity. The thickness of the samples after the stretching was 10 µm. Finally, the films were cut out to 30 mm of length and 20 mm of width.

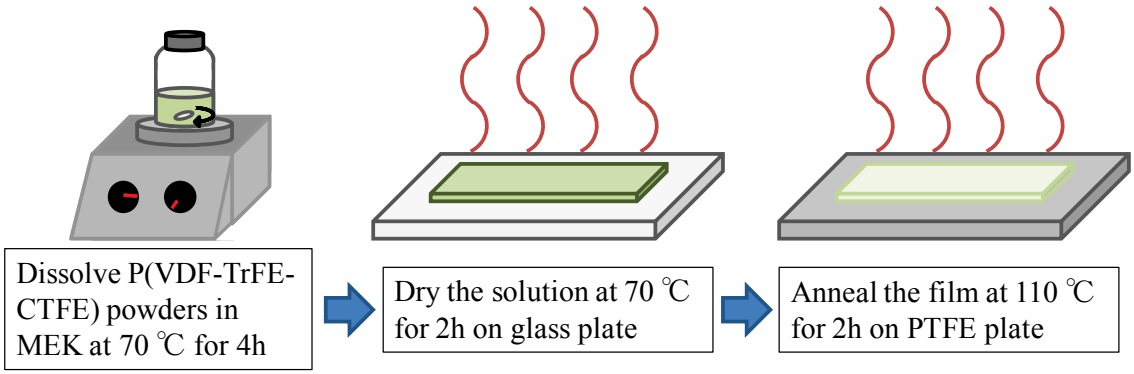

Fig 4.1 Fabrication process for P(VDF-TrFE-CTFE)

4.2.3 Properties characterization

A) Characterization of volumetric specific heat

In order to calculate the volumetric specific heat, the specific heat and the density of materials were measured.

The specific heat was measured by differential scanning calorimetry (DSC) with DSC 131 evo (SETARAM Instrumentation, France) and thermal analysis software CALISTO (SETARAM Instrumentation, France). The heating rate was fixed at 10 °C

/min. The crucible made of aluminum was used. Alumina was used as reference material. The specific heat of alumina is 0.80 J/g °C. The weight of sample was 18.0 mg and the temperature range of experiment was from -30 to 50 °C.

The density was measured using a pycnometer, also called specific gravity bottle. As previously described in the second chapter, the density of sample was measured by comparing the weights of distilled water and sample when the volume of sample equal to that of distilled water.

B) Characterization of static mechanical properties and ElC effect (ElCE) of non-prestretched P(VDF-TrFE-CTFE)

Fig 4.2 illustrates a diagram of the experimental setup for characterizing the mechanical property and the ElCE produced by non-prestretched P(VDF-TrFE-CTFE). The sample was fixed on testing device by clamping. Single axis robot (RSDG212, MISUMI Corporation, Japan) could uniaxially stretch the sample while generated force was recorded by a force sensor (XFTC300-200N, Measurement Specialities, France). The displacement of the single axis robot was measured by using a vibrometer controller (OFV-5000, Polytec, Germany). The temperature change, generated by entropy change causing strain, was measured using a thermal camera (NEC G-120, NEC, Japan). This thermal camera can record thermal images of the sample at 10 Hz. The noise level of the temperature information from this thermal camera is ±0.1 °C. In order to correct the sample IR emissivity, the sample was put in a temperature controlled oven then actual temperature measured by a thermocouple and the temperature reading of the IR camera had been compared. A linear correlation was found and its correction factor was 0.85. A light sensor (BPW 34 B, Osram Opto Semiconductors GmbH, Germany) was put on monitor of the thermal camera to record light signals of monitor. Displacement, force, and data from light sensor were recorded on an oscilloscope (DSO 7034A, Agilent, USA). Since light sensor is on when the temperature change occurs, it is possible to check the exact time interval among displacement, force and temperature change.

For measurement of static mechanical property, space between clamps, i.e. the length of a sample, was set at 10.0 mm and elongation rate was set at 0.0066 s^{-1} (2.0 mm/s). Due to the relation between maximum displacement of this experimental device (200.0 mm) and the fracture strain of the sample, such sample length was chosen for this part.

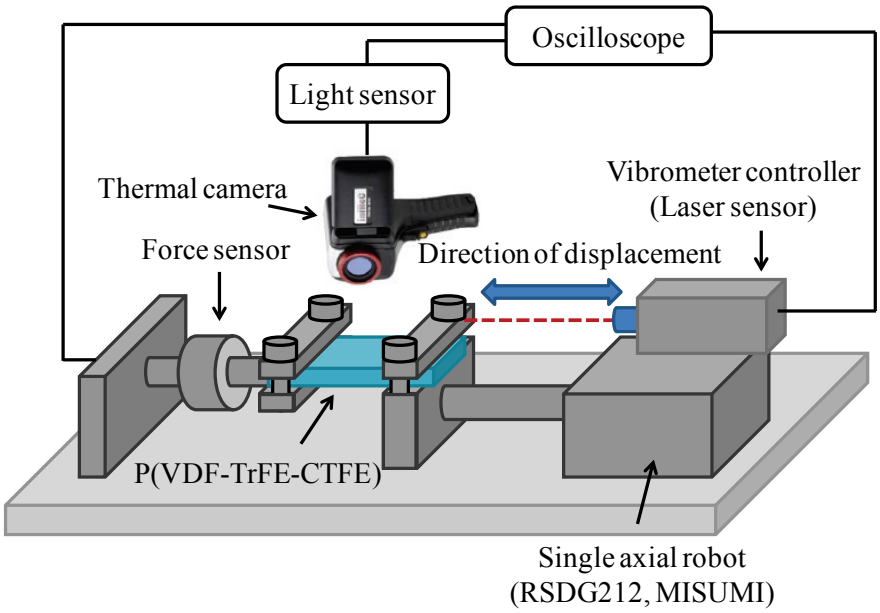

Fig 4.2 Schematic illustration of experimental device with RSDG212

For measurement of ElCE, space between clamps was set at 30.0 mm. Strain from 2 to 20 % were applied with elongation rate of approximately 1.0 s^{-1}. Only for a strain of 400 %, elongation rate of 0.80 s^{-1} was chosen. In order to obtain ElCE, the experiment should be carried out in an adiabatic process. Although the maximum speed is indicated as 320 mm/s in the manual, this experimental device cannot move at the maximum speed when it moves less than 150 mm due to the acceleration (1.13 mm/s^2). The chosen testing speed for measurement of ElCE is thus the fastest one with this device.

C) Characterization of ElCE of prestretched P(VDF-TrFE-CTFE)

Fig 4.3 illustrates a diagram of the experimental setup developed for characterizing the mechanical property and the ElCE produced by stretched P(VDF-TrFE-CTFE). The sample was fixed on testing device by clamping. Different from the set up before, Fig 4.2, Ironless Linear Motor (XMS50, Newport, New York) controlled by function generator (33210A, Agilent, USA) was used to uniaxially stretch while generated force was recorded by a force sensor (ELPF-T2M-250N, Measurement Specialities, Paris), which was fixed to the static side. The generated temperature change of sample surface was measured by the same thermal camera (NEC G-120, NEC, Japan) with a precision of ± 0.1 °C.

The stress that P(VDF-TrFE-CTFE) receives depends on the testing speed because of the viscoelasticity. This will be demonstrated in section 4.3.2. For a large stress application, the acceleration of the experimental device is an important factor,

especially when deformation is small. The present device (RSDG212) requires 0.3 s to move for 0.6 mm whereas that with XMS50 is less than 0.025 s. This cross-head speed is, even though, enough to apply a large stress to P(VDF-TrFE-CTFE) and it can be estimated that all measurements with this speed was carried out in an adiabatic process. This will be confirmed in the section of discussion.

For measurement of ElCE, space between clamps was set at 30.0 mm and elongation rate was set at 20.0 s^{-1} (160 mm/s).

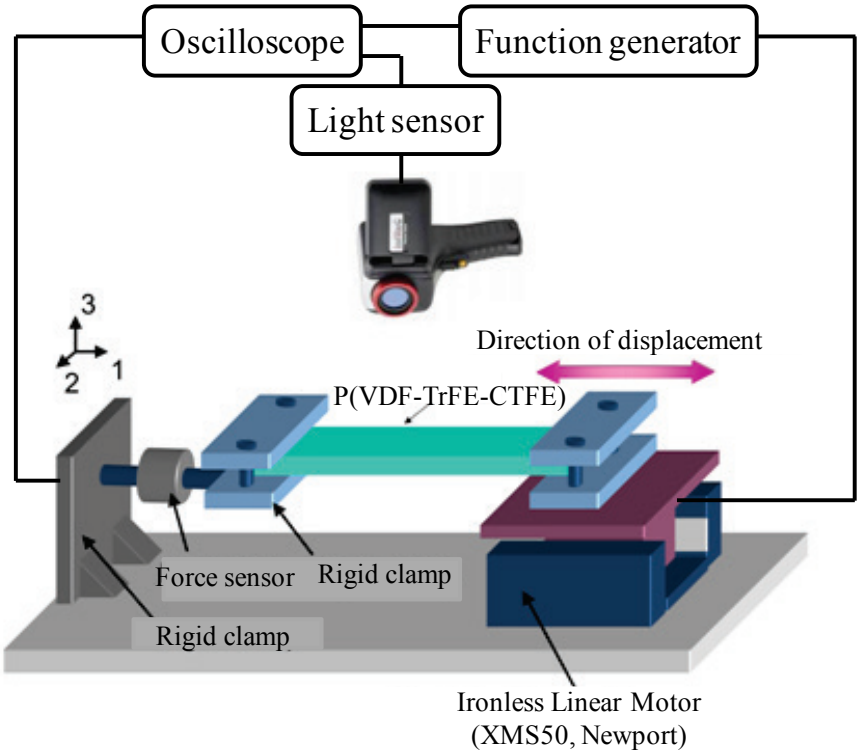

Fig 4.3 Schematic illustration of experimental device with XMS50

4.3 Result and discussions

4.3.1 Mechanical properties of non-prestretched P(VDF-TrFE-CTFE)

The stress-strain (S-S) curve of P(VDF-TrFE-CTFE) with elongation rate of 0.0066 s^{-1} is shown in Fig 4.4. The stress and the strain were calculated with sample size before stretching, so that they are the engineering stress and the engineering strain. The stress increases drastically with an increase in the strain until strain up to 15 % and reaches the yield point at strain of 20 %. After reaching the yield point, the stress is almost constant until strain of 500 %. The stress increases gradually with an increase in the strain when the strain exceeds 500 % and then increases linearly when strain

exceeds 1050 %. After that, the sample ruptures at the strain of 1340 %. As a result, it was found that P(VDF-TrFE-CTFE) shows elastic deformation until strain of 15 % and then plastic deformation from strain of 20 %. Since the stress starts to increase again from strain of 500 %, it is suggested that entanglements of molecular chains are loosed from strain of 20 % and then the molecular chains are fully stretched from shorter chains when the strain exceeds 500%. The entanglements of molecular chains are estimated to be loosed completely at strain of 1050 %. Thus, the S-S curve becomes linear from strain of 1050 %. The second elastic region appears.

The relationship between stress and strain suggests that P(VDF-TrFE-CTFE) shows the energetic elasticity with a strain of less than 20 % and the entropic elasticity with a strain of more than 20 %. Thus, the temperature variation by ElCE must be obtained with a strain above 20 %.

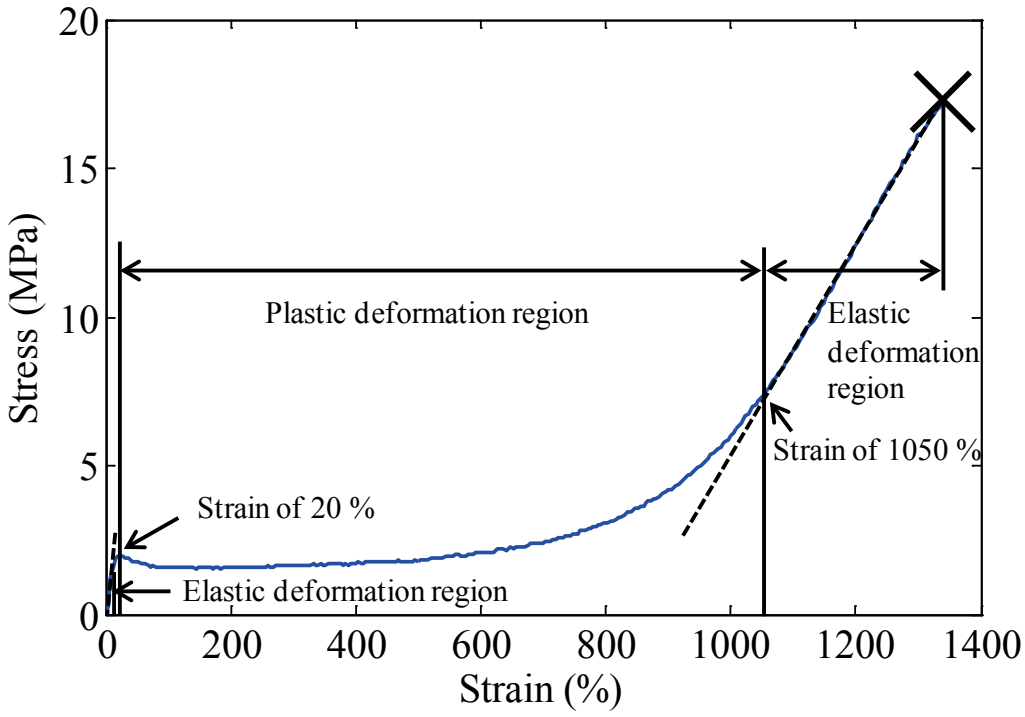

Fig 4.4 S-S curve of P(VDF-TrFE-CTFE) with elongation rate of 0.0066 s^{-1}

4.3.2 Elastocaloric effect of non-prestretched P(VDF-TrFE-CTFE)

ElCE of the non-prestretched P(VDF-TrFE-CTFE) was evaluated in the elastic and the plastic deformation regions. Firstly, ElCE of the P(VDF-TrFE-CTFE) with small strains is described in order to evaluate ElCE in the elastic deformation region. Fig 4.5 depicts testing results when step-by-step strain from 2 to 20 % in increments of 2 % was

applied to the P(VDF-TrFE-CTFE). The strain was applied with elongation rate of 1.25 s^{-1}, kept for 10 s and then released. It is shown that the maximum stress increases with an increase in the strain until strain of 10 % and then the maximum stress became constant even if the strain increased.

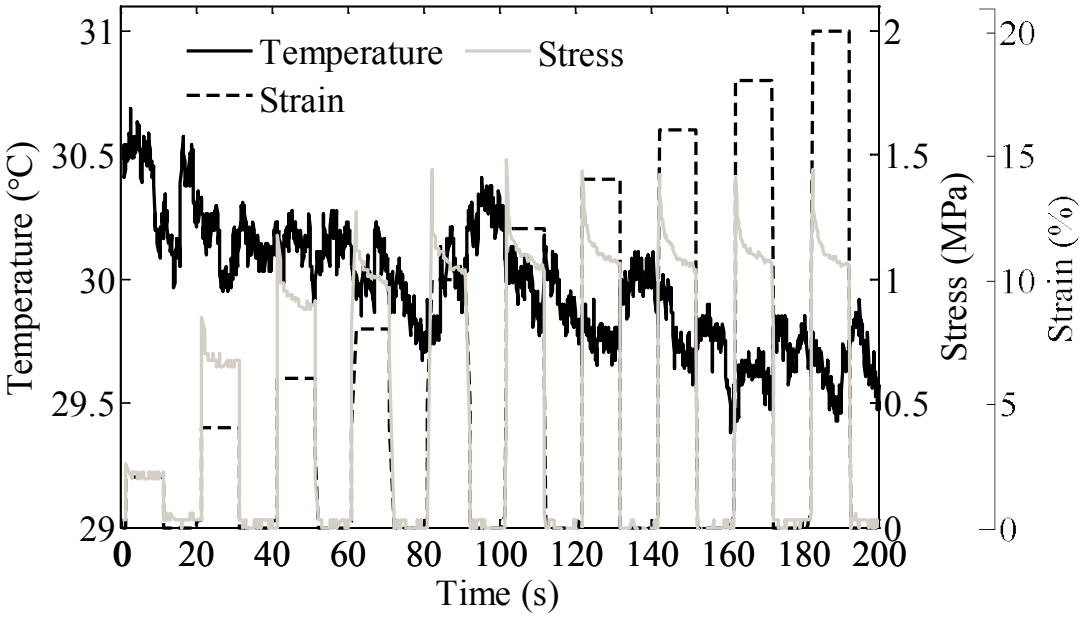

Fig 4.5 Testing results when step-by-step strain from 2 to 20 % in increments of 2 % was applied to the P(VDF-TrFE-CTFE)

It was shown, however, that the yield point of the P(VDF-TrFE-CTFE) is at strain of 20 % in the previous section. The difference of these strain values had been considered then two possible reasons were derived. First one is a deformation behavior. The deformation of P(VDF-TrFE-CTFE) could be in plastic region when maximum strain exceeds 10 % due to the high extension speed. Second possible reason is the viscoelasticity of the material. The experimental device slightly and gradually decelerates before it stops. Since the stress that viscoelastic material receives depends on the elongation rate, such deceleration of the device can lead a decrease in the stress.

In order to confirm the first one, the sample sizes before and after stretching up to 20 % were compared. 20 % was the maximum strain in the operations for Fig 4.5. Results are summed up in Table 4.2. By the comparison, it was found that the P(VDF-TrFE-CTFE) generated, in certain, a permanent strain with the present deformation test but it was quite small, less than 1.3 % in length. From the fact that the permanent strain caused by the present deformation test was quite small, the first

reason was denied. P(VDF-TrFE-CTFE) was stretched entirely in the elastic deformation region. The difference of strain values, 10 % here and 20 % in previous section, is estimated again due to the deceleration and to the viscoelasticity of material.

Table 4.2 Sample sizes before and after stretching up to 20 %

	before stretch	after stretch	permanent strain in percentage
length (mm)	30.0	30.4	1.3 %
width (mm)	20.04	19.90	−0.7 %
thickness (mm)	0.035	0.033	−5.7 %

Although temperature variations can be seen in Fig 4.5, it varies more quickly than a period of applying strain, i.e. regardless of applying strain. This fact leads one conclusion; the P(VDF-TrFE-CTFE) does not exhibit the temperature variation by ElCE in the elastic region.

Fig 4.6 depicts testing results when the strain of 400 % was applied to the non-prestretched P(VDF-TrFE-CTFE). The strain was applied with elongation rate of 0.8 s^{-1}, kept for 10 s and then released. The stress increased drastically at extension

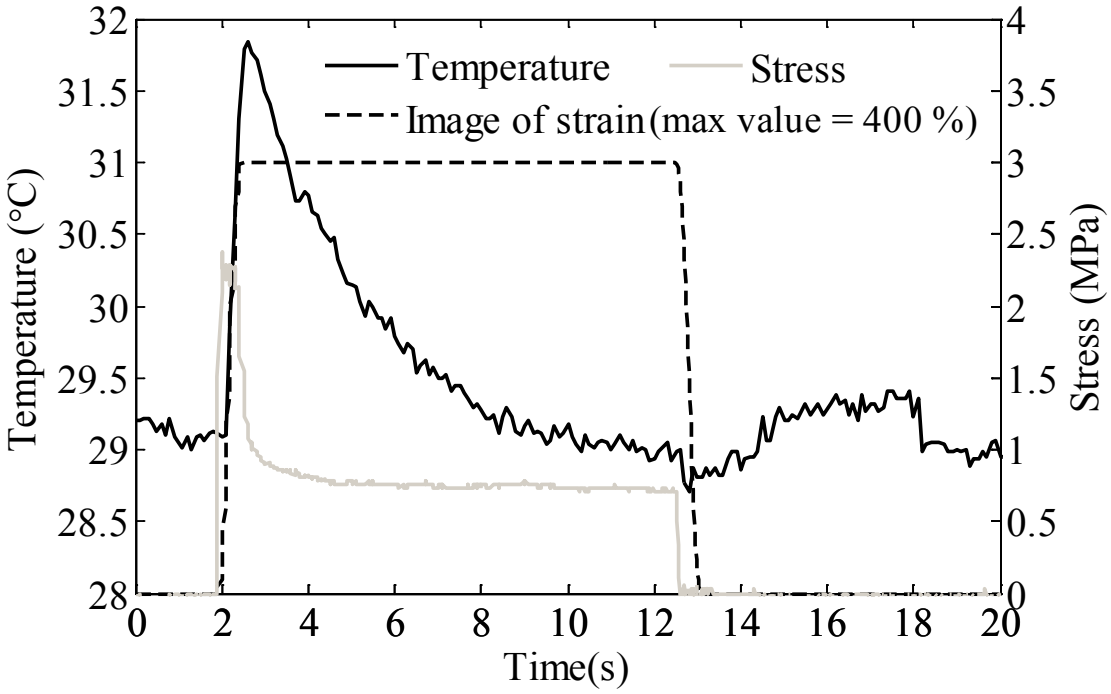

Fig 4.6 Temperature and stress variations as a function of time when 400 % strain was applied to P(VDF-TrFE-CTFE)

and then decreased exponentially. While strain is kept, the stress continues to decrease then becomes constant. In the contraction process, the stress decreases drastically then becomes 0 MPa before the contraction process is finished. This result suggests that the P(VDF-TrFE-CTFE) generated a large permanent strain. The S-S curve when the strain of 400 % was applied to the P(VDF-TrFE-CTFE) is shown in Fig 4.7 and the sample sizes before and after stretching are shown in Table 4.3. The S-S curve shows a quite large hysteresis loop because of a quite large permanent strain. The stress reaches its maximum value (2.4 MPa) at strain of 20 %, decreases little bit then becomes constant (2.2 MPa) at strains between 50 % and 350 %. It is seen that the stress decreases gradually just before the strain reached its maximum strain. This can be explained as followings. The stress that P(VDF-TrFE-CTFE) receives depends strongly on the elongation rate because P(VDF-TrFE-CTFE) is viscoelastic material. Since the speed of the experimental device decreases gradually just before the deformation process is finished, the decrease in the stress occurred just before the strain reached a maximum strain. The stress saturates to 0.70 MPa in the keeping process. It became 0 MPa when applied strain decreased to 380 % in the contraction process. This result indicates that the P(VDF-TrFE-CTFE) generates a quite large permanent strain. By the comparison

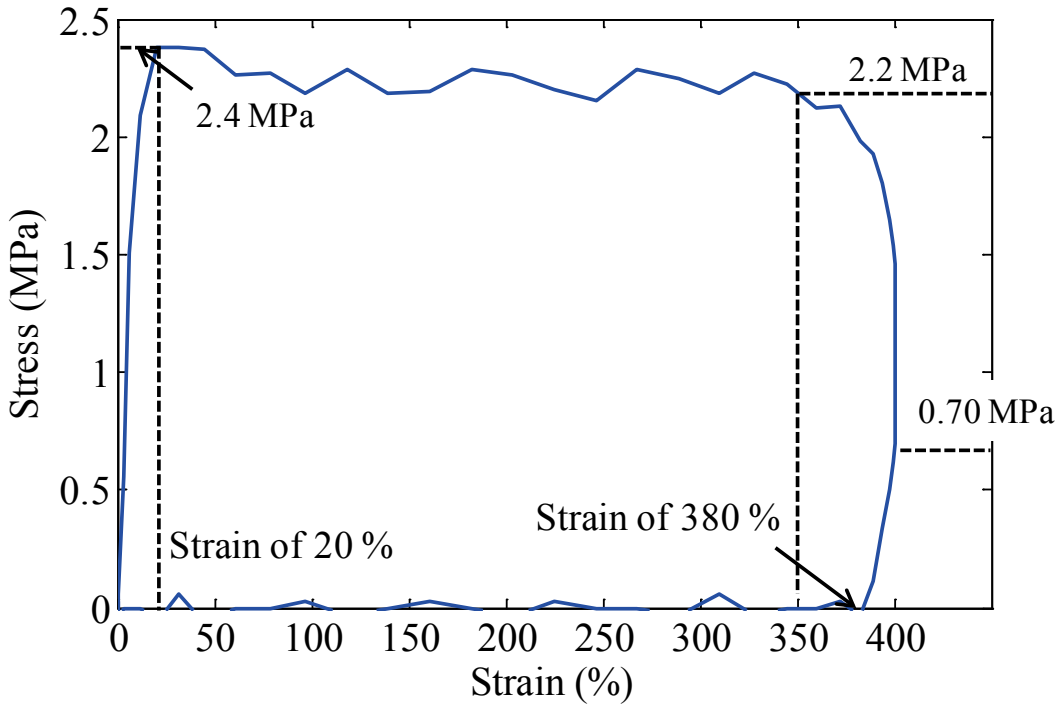

Fig 4.7 S-S curve when strain of 400 % was applied to the P(VDF-TrFE-CTFE) (elongation rate of 0.8 s^{-1}, kept for 10 s at maximum strain)

Table 4.3 Sample sizes before stretching and after stretching up to 400 %

	before stretch	after stretch	permanent strain in percentage
length (mm)	30.0	126.1	320 %
width (mm)	19.90	6.27	−68.5 %
thickness (mm)	0.033	0.023	−30.3 %

between sample sizes between before and after stretching, it was confirmed that the P(VDF-TrFE-CTFE) film generates a permanent strain of 320 % in length due to the extension to strain of 400 %. This value is smaller than the one indicated above, 380 %. Nevertheless, these values were obtained when the stress became 0 MPa.

As we can see in Fig 4.6, temperature of sample surface also increases drastically when the strain is applied. The temperature variation between room temperature and the maximum temperature became 2.7 °C. Within 10 s of keeping process, it decreases exponentially toward room temperature. On the other hand, temperature decreased quite slightly (about −0.2 °C) due to contraction. Compared with the temperature variation caused by extension, that caused by contraction is quite small. Summarizing the above, it was found that P(VDF-TrFE-CTFE) exhibits a temperature variation caused by extension but hardly exhibit it by contraction.

As previously described, the S-S curve of P(VDF-TrFE-CTFE) shows a quite large hysteresis loop because of a quite large permanent strain. When the mechanical energy caused by deformation is quite small, the temperature variation caused by ElCE becomes quite small even if the material completely converts the mechanical energy to the heat energy. Calculating a temperature variation from the mechanical energy without any loss with the result of applying strain of 400 %, temperature variation caused by extension became 2.9 °C and that by contraction became −0.07 °C instead of 2.7 °C and −0.2 °C, respectively, from experimental result shown in Fig 4.6. Since these calculated values are similar values to the experimental results, it was confirmed that P(VDF-TrFE-CTFE) can converts the mechanical energy to the heat energy at a quite high ratio. Certainly, the temperature variation caused by contraction was hardly obtained experimentally due to such quite small mechanical energy during contraction.

Certainly, some mechanical energies were applied during the measurements of which the results are shown in Fig 4.5 and of which the maximum strain is 20 %. It is estimated, however, to be converted into internal energy but not to heat energy, based on what was described in the chapter of rubber, section 3.2.3. As previously described, the S-S curve becomes linear again at, strain of above 1050 %, see Fig 4.4. In this region,

much larger variation of mechanical energy can be applied and, moreover, it can be estimated to be converted more to heat energy. With a strain above 1050 %, much more significant temperature variation can be obtained. This is a work described in the following sections.

4.3.3 Elastocaloric effect of pre-stretched P(VDF-TrFE-CTFE)

A) Temperature and stress variations versus time

As described in the previous section, even though non-prestretched P(VDF-TrFE-CTFE) exhibits only negligible ElCE during contraction, it was estimated that a pre-stretched P(VDF-TrFE-CTFE) can exhibit a large ElCE during contraction. In order to evaluate ElCE of pre-stretched P(VDF-TrFE-CTFE), its film was uniaxially stretched 1200 % to its original length before deformation test. 1050 % is minimum required strain to stay in elastic region based on Fig 4.4, but 1200 % was chosen to be sure. The width and thickness of the sample were 80 mm and 40 µm before the stretching, and 20 mm and 10 µm after the stretching, respectively. Since mechanical properties of the material are strongly affected by deformation speed, it is required to use an experimental device which can move at high speed, do abrupt stop and do abrupt acceleration in order to apply a large mechanical energy to sample. The strain was applied to the pre-stretched sample with XMS50, described previously in section 4.2.3 (C).

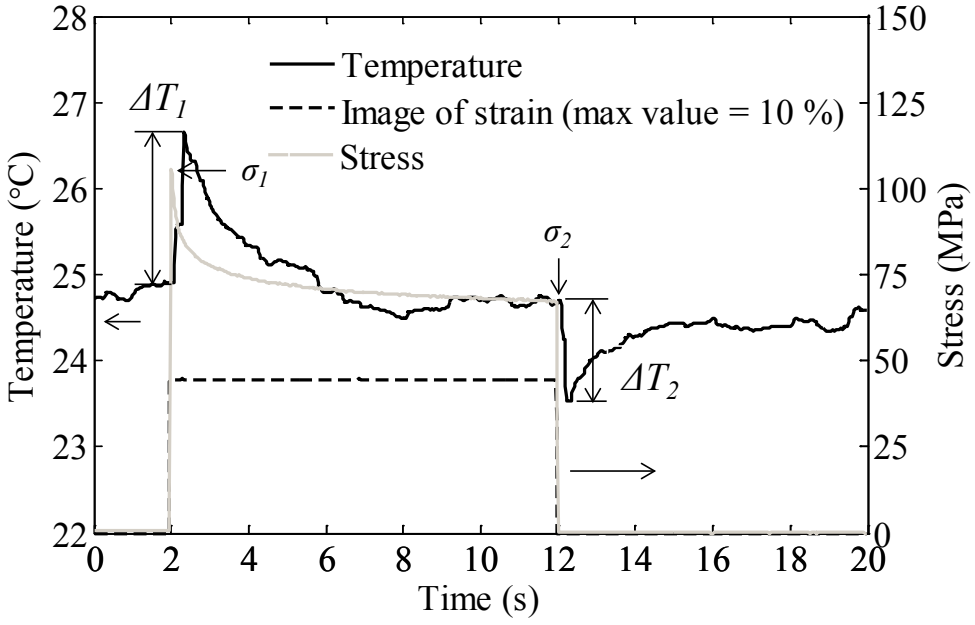

Fig 4.8 Temperature and stress variations as a function of time when 10% strain was applied to pre-stretched P(VDF-TrFE-CTFE)

A typical experimental results as function of time are displayed in Fig 4.8. A step strain is applied rapidly (elongation rate of 20 s^{-1}), kept for 10 s and then released. Fig 4.8 depicts testing results when strain of 10 % was applied to the pre-stretched sample. Stress reaches a maximum value σ_1 when strain reaches its maximum, and then shows an exponential decrease when the strain is kept. Within 10 s of strain kept time, it saturates to a certain value of convergence σ_2 by stress relaxation. At the same time, temperature of sample surface reaches its maximum with a slight delay to strain application (about 0.35 s). Then, it decreases exponentially toward room temperature. The difference between room temperature and this maximum temperature is a temperature variation caused by stretching, defined an increase temperature variation, ΔT_1. Since strain reaches its maximum sufficiently earlier than when temperature reaches its maximum, the high elongation rate ensures that the sample is still in adiabatic state right after the stretching. The thermal time constant of heat exchange with outer medium is estimated around 2 s. These behaviors of temperature variation were observed for all tested strain amplitudes from 3 % to 13 %. The keeping time of 10 s has been chosen to assure both to achieve full stress relaxation and to remove all residual temperature change caused by ElCE. After 10 s, the strain is returned to zero. Different from the case of non-prestretched one, surface temperature decreases drastically below room temperature with slight time delay. It increases then exponentially back to room temperature. The present temperature variation is called a decrease temperature variation, ΔT_2. As can be seen in Fig 4.8, pre-stretched P(VDF-TrFE-CTFE) exhibits significant temperature variations not only at extension but also at contraction. It was confirmed that its ElCE during contraction can be improved by pre-stretching until the second linear region, above 120 %.

B) ElCE versus strain and comparison of elastocaloric coefficient

Maximum stress σ_1 and absolute values of these temperature changes, $|\Delta T_1|$ and $|\Delta T_2|$, versus the maximum applied strain are depicted in Fig 4.9. The maximum stress linearly increases with applied strain up to 13 % strain. This result confirms that the whole experiments were carried out in the elastic deformation region. $|\Delta T_1|$ and $|\Delta T_2|$ also increase with strain but not linear matter. They show more or less parabolic behaviors. The maximum strain level among these experiments was 13 %. After this value, stress-strain behavior becomes nonlinear, hence, for the sake of simplicity, we restricted the study to the linear zone below strain of 12 %.

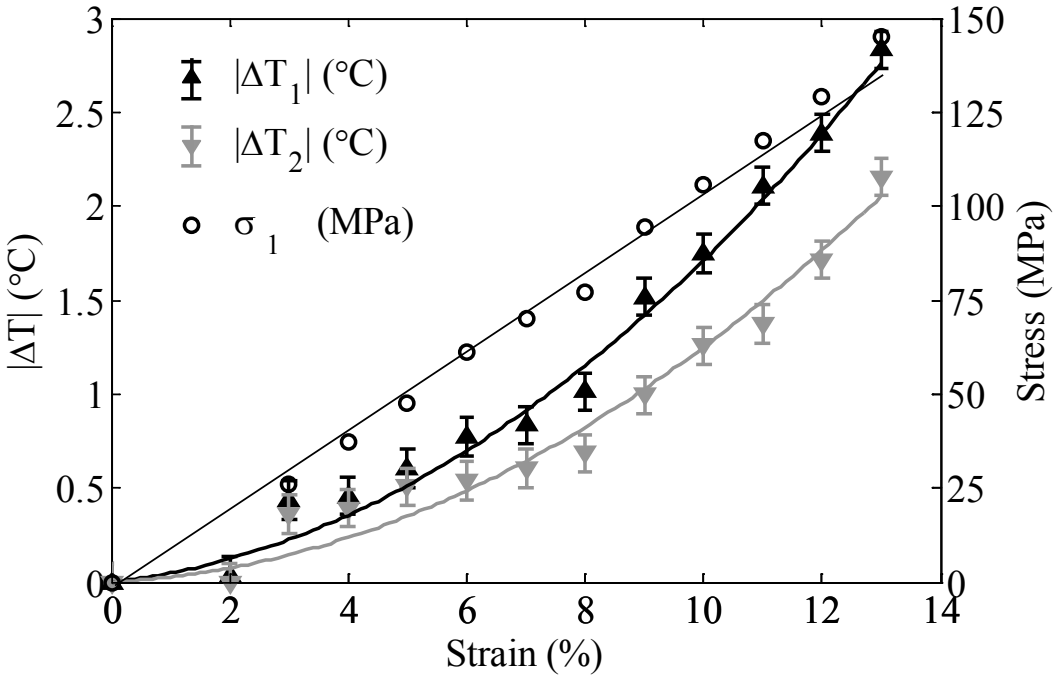

Fig 4.9 Adiabatic temperature variations at stretching $|\Delta T_1|$ and at contracting $|\Delta T_2|$ and stress variations σ_1 as a function of the strain. Solid lines are guides to the eye.

For comparison with other elastocaloric materials, two elastocaloric coefficients (elastocaloric coefficient β and stress elastocaloric coefficient γ) are calculated. β and γ are used to evaluate the elastocaloric conversion effectiveness of elastocaloric materials. β is defined as[107]

$$\beta = \frac{C_v}{T_0} \frac{\partial(\Delta T)}{\partial \lambda} = -\frac{\partial S}{\partial \varepsilon} \qquad (4.1)$$

where C_v, T_0, ΔT, λ, S and ε are volumetric heat capacity, room temperature, elastocaloric adiabatic temperature change, elongation, specific entropy and engineering strain, respectively. It should be noted that deriving with respect to elongation or engineering strain is identical since $\varepsilon = \lambda - 1$.

γ is then defined for the sake of completeness in evaluating elastocaloric performance:

$$\gamma = \frac{\partial S}{\partial \sigma} \qquad (4.2)$$

where σ is the engineering stress.

When it is stretched to 12 % of strain, this material exhibits a large elastocaloric coefficient of β = 179 kJ/m^{3}K. Besides, considering the applied stress, the stress

coefficient is found to be $\gamma = 0.14$ kJ/m^{3}K MPa. In previous chapter, natural rubber (NR) is investigated as an elastocaloric material [106, 107]. Although the ElCE of NR is not linear, the behavior was linearized in order to extract average elastocaloric coefficients. Based on these results, the elastocaloric coefficients of NR were found to reach a $\beta = 8.7$ kJ/m^3 K and $\gamma = 33$ kJ/m^{3}K MPa, for a strain amplitude of 600 %. In case of NiTi wire, shape memory alloy (SMA) known as an excellent elastocaloric material, based on the results from Tusek et al. [12, 57], the elastocaloric coefficients are estimated to be $\beta =$ 2740 kJ/m^{3}K and $\gamma = 0.17$ kJ/m^{3}K MPa after linearization of the properties as for NR. The comparison is summarized in Table 4.4. Typically, the NR requires a large strain and a small stress to induce significant adiabatic temperature variations whereas SMA requires a small strain but a large stress. The case of terpolymer appears to be a trade-off between large strain and large stress. Considering the strain elastocaloric coefficient, terpolymer lies between NR and SMA. On the contrary, the stress elastocaloric coefficient of terpolymer is found to be slightly lower than that of SMA thanks to a strain level similar to that of SMA, but with a much lower Young's modulus, thus showing that the terpolymer may be a high potential material for elastocaloric cooling. Moreover, considering the low density of terpolymer material, the above calculated coefficients expressed per unit of mass instead of volume would make this polymer even more attractive.

Table 4.4 Comparison between different elastocaloric materials at room temperature set at $T_0 = 300$ K except for the case of NiTi where the temperature is $T_0 = 342$ K

Material	Natural rubber [107]	NiTi wire [12, 57]	Stretched P(VDF-TrFE-CTFE)
Applied strain ε (%)	600	5	12
Heat capacity (J/cm^{3}K)	1.8	2.9	3.0
Stress (MPa)	1.6	800	125
Density ρ (kg/m^3)	2.0×10^3	6.5×10^3	2.0×10^3
Adiabatic temperature variation at max strain (°C)	8.7	16	2.15
Isothermal entropy variation (kJ/m^{3}K)	52	156	21.5
Isothermal heat exchange at max strain (J/cm^3)	16	47	6.45
Mechanical energy density at max strain (J/cm^3)	4.9	38	6.26
Elastocaloric coefficient β (kJ/m^{3}K)	8.7	2740	179
Stress elastocaloric coefficient γ (kJ/m^{3}K MPa)	33	0.17	0.14

In case of SMA, the entropy variation upon stretching is proved to be related to a phase transition of which latent heat contributes mainly to the total entropy change (austenite-martensite phase transition)[57]. In case of NR, strain induced crystallization have been extensively experimentally assessed [80], including dynamic cycles up to several tens of Hz [95]. Both elastic entropy and strain-induced crystallization contribute to the entropy variations upon stretching. In order to establish the origin of entropy variation in P(VDF-TrFE-CTFE) terpolymer, mechanical energy and exchanged heat in isothermal condition are calculated and compared. In case of a phase transition occurring upon stretching of the material, the exchanged heat in isothermal condition may exceed the mechanical energy, such as in case of SMA and NR where the origin of the excess heat is the latent heat of transition, and where the internal energy is a function of the strain triggering the phase transition. On the contrary, in pure elastomeric materials, the heat and mechanical energies are identical in absolute value, since the internal energy is a function of the temperature only similarly to a perfect gas, i.e., implying that the mechanical energy is totally converted into heat. For the different tested strain levels, the mechanical energy is calculated both for the application of the strain step, and for the retraction of the sample. The exchanged heat in isothermal condition is estimated from the adiabatic measurement, where $Q|_{\text{isothermal}} = C_V \Delta T|_{\text{adiabatic}}$. It is a rough estimation assuming that the heat capacity is not a function of the strain and that the ElCE is not temperature dependent (at least on the temperature range $T_0 \pm \Delta T$). Fig.4.10 shows the calculated mechanical energy W, isothermal heat exchange Q and internal energy variation $\Delta U = Q + W$ as a function of strain level for an isothermal stretching. Both increasing strain energies and decreasing strain energies are displayed. The difference between increasing and decreasing strain energies is related to irreversibility (such as mechanical losses). Mechanical energy shows a parabolic tendency as a function of strain, as well as heat energy and, on the contrary, internal energy remains almost constant except a slight increase for the highest tested strain level regime. The excellent agreement between heat and mechanical energy both for stretching and retraction proves that the internal energy is not a function of strain, and that the mechanical energy is entirely converted into heat. This behavior is typical to an elastomeric material and shows that the crystalline phase of the terpolymer is not modified by the dynamic stretching of the sample. As mentioned above, ECE of relaxor polymer P(VDF-TrFE-CTFE) is related to the crystalline phase where some structural transitions are induced by the electric field thus for ECE. Since the ElCE is related to the amorphous phase only it can be foreseen that electrocaloric behavior and elastocaloric behavior are totally separate and that

they could be fully cumulative.

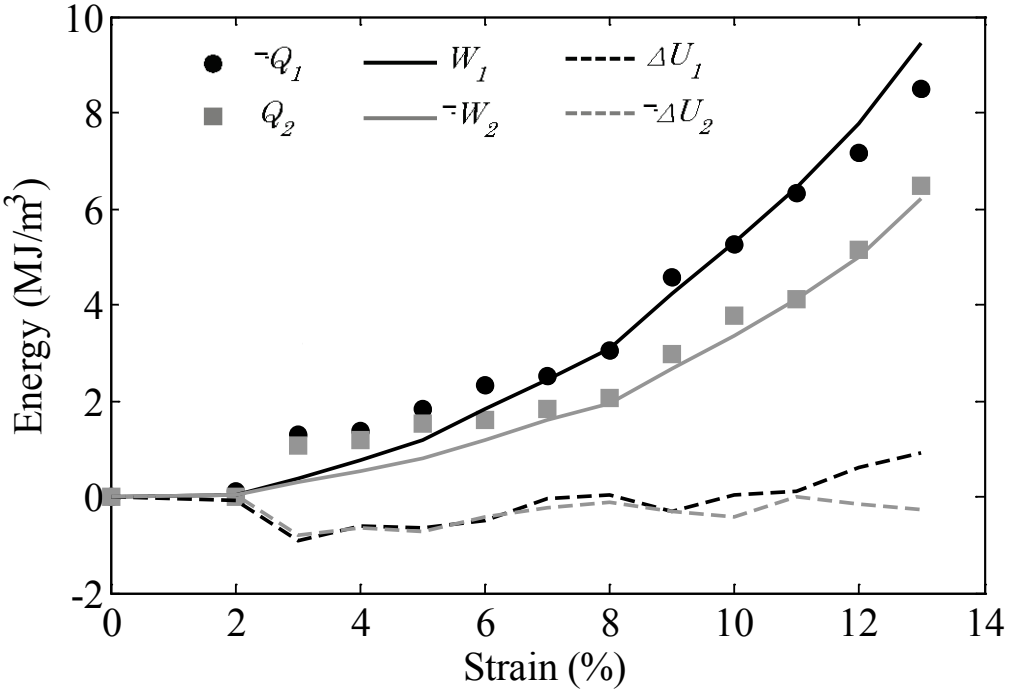

Fig 4.10 Mechanical energy, exchanged heat in isothermal condition and internal energy versus applied strain. Open circles show the heat energy Q values calculated from experimental temperature variation, solid lines show mechanical energy W and dotted lines show internal energy ΔU, both calculated from stress-strain curve at stretching

4.4 Conclusions

Elastocaloric effect (ElCE) of P(VDF-TrFE-CTFE) has been investigated. It was found that it is comparable to that of SMAs and shows quite larger elastocaloric coefficient than rubber. Since P(VDF-TrFE-CTFE) converted most applied mechanical energy into heat energy, it was concluded that P(VDF-TrFE-CTFE) is a very efficient material for ElCE. Previously, it is known that this material exhibits a large temperature variation caused by electrocaloric effect (ECE). In this study it was demonstrated that electrocaloric behavior and elastocaloric behavior are totally separate and that they could be fully cumulative. Thus, P(VDF-TrFE-CTFE) is an excellent candidate for multicaloric effect combining ECE and ElCE.

Considering the application of caloric materials into regenerative systems, a relative motion between active and passive materials is necessary, usually obtained by pumping

heat transfer fluid and requiring an additional energy source [115]. It can be also obtained by translation the active layer between passive plates storing locally the heat to avoid the use of an external regenerator [116]. Using multicaloric P(VDF-TrFE-CTFE), the primary caloric effect may be electrocaloric effect for inducing entropy variations. Then, instead of adding a motion of the polymer between passive plates, one might better use a stretching of the sample, which not only result in the regenerative behavior, but might also contribute to the caloric effect.

Chapter 5

General conclusions and future works

5.1 Conclusions

Elastocaloric effect (ElCE), which is the phenomenon that temperature variation caused by entropy change, is a good candidate for next-generation cooling technology because of non-toxicity, low cost and exhibiting a large variation of heat energy. In the present thesis, ElCE of carbon black (CB) filled natural rubber (NR) and terpolymer, poly(vinylidene fluoride - trifluoroethylene - chlorotrifluoroethylene) (P(VDF-TrFE-CTFE)), was investigated.

In chapter 1, that theory is well described in comparison with other caloric effects and with other cooling technology. Fundamental experiments such as differential scanning calorimetry (DSC) and mechanical property tests are put in chapter 2.

ElCE of CB filled NR was investigated in cyclic deformation with different strain levels in chapter 3. It was found that the material exhibits temperature increase of 4.0 °C with stress of 5.0 MPa at extension and temperature decrease of 3.5 ~ 4.0 °C with stress of 3.5 ~ 6.0 MPa at contraction under room temperature. Such experimental results indicate that the present material can supply reasonable enough temperature variations with a considerably smaller stress than SMAs which are the materials often studied for ElCE.

The relation between stress/strain versus temperature variation is generally used to evaluate ElCE. The experimental results show different amount of temperature variations with the same stress value were, however, found if the strain level is different. Due to the effect of the fatigue, besides, the temperature variations are not constant when the same strain, especially large strain, is applied repeatedly. It was experimentally confirmed that not only the applied stress but also the strain is important factor in ElCE of non-linear elastic material such as NR. After the unsuitability of such evaluation method for non-linear elastic material such as NR was demonstrated, the new evaluation method for ElCE which uses energy balance was proposed in order to solve this problem. A linear relation between the temperature variation caused by ElCE and the applied mechanical energy by deformation was experimentally found. This fact verifies the suitability of the proposed method.

Secondly in chapter 3, the influences of Mullins effect and the strain-induced crystallization (SIC) on ElCE of filled NR were discussed with the relationships between the temperature variation and the applied stress and between the mechanical and the heat energies. The Mullins effect is a factor for the greatly decrease not only in the stress but also in the amount of temperature variation whereas the SIC is a factor for the greatly increase in both of them. Experimentally it was found that the SIC causes the decrease in the conversion efficiency from the mechanical energy to the heat energy.

The reason was estimated that the internal energy stored in the material increases due to the fully stretched molecular chains. Besides, the Mullins effect causes the increase in the conversion efficiency. Honestly to say, the clear distinguish is not possible by the results in the present study. The further verifications are required.

In chapter 4, ElCE of P(VDF-TrFE-CTFE) was investigated in order to find out the potential of polymer as material for ElCE. It was found that present terpolymer, which is not one of the elastomers, can also exhibit a large temperature variation, 2.1 °C, caused by ElCE if a large pre-stretch such as more than 1050 % is applied in advance. Stress elastocaloric coefficient ($\gamma = (\partial S/\partial \sigma)$) of the stretched sample is comparable to that of SMAs and larger than that of NR. It was also shown that the stretched sample converted most applied mechanical energy into heat energy. These facts verify that P(VDF-TrFE-CTFE) can be a high potential material for ElCE. This material is known as a promising material for electrocaloric effect (ECE). In the present study it was demonstrated that elastocaloric behavior and electrocaloric behavior are totally separate and that they could be fully cumulative. Consequently, it was concluded that P(VDF-TrFE-CTFE) is an excellent candidate for multicaloric effect combining ElCE and ECE.

5.2 Future works

The influences of the Mullins effect and the SIC, the phenomena leading softening and hardening, on ElCE were discussed in the present thesis. The influence of the hardness of elastomer, especially rubber, on ElCE was estimated in the different manner that traditional one with the obtained knowledge in the present work. The hardness of rubber depends on the cross link density and the amount of filler. Since a hard rubber has a high cross link density or contains many fillers, it is recognized that the molecular chains are fully stretched with a small strain. These molecular chains may store quite large energy as the internal energy even if quite large mechanical energy is applied, as shown in chapter 3. As a result, the harder rubber may exhibit a smaller temperature variation even though quite large mechanical energy is applied. A soft rubber shows quite high conversion efficiency from the applied mechanical energy to the heat energy whereas it is difficult for it to receive a large mechanical energy. Thus, the soft rubber may exhibit a small temperature variation. The appropriate hardness for exhibiting a large temperature variation efficiently might exist. In order to confirm this estimation, ElCE of rubber with different hardness should be carried out.

Since ECE and ElCE are completely different phenomena on terpolymer as shown in chapter 4, the multicaloric effect combining them can exhibit the summed up

temperature variations. However, it should be noted that the electrostriction occurs when a polymer, especially electroactive polymers such as P(VDF-TrFE-CTFE), is used. The electrostriction can reduce the strain variation caused by the mechanical deformation. There is a possibility that temperature variation caused by ElCE is also reduced by the electrostriction. To construct the practical application, it is required to consider the cyclic applications of both the electric field and the strain in order to obtain effectively and efficiently the temperature variation.

List of Figures

List of Tables

References

[1] Suxin Qian, Jiazhen Ling, Jan Muehlbauer, and Yunho Hwang, Study on high efficient heat recovery cycle for solid-state cooling, *International Journal of Refrigeration* 55 (2015) 102-119

[2] J. Quarini, A. Prince, Solid state refrigeration : cooling and refrigeration using crystalline phase changes in metal alloys, Proceeding of the Institution of Mechanical Engineers, Part C: *Journal of Mechanical Engineering Science* 218 (2004) 1175-1179

[3] J. Romero Gómez, R. Ferreiro Garcia, A. De Miguel Catoira, and M. Romero Gómez, Magnetocaloric effect: A review of the thermodynamic cycles in magnetic refrigeration, *Renewable and Sustainable Energy Reviews* 17 (2013) 74-82

[4] I. A. Starkov, A. S. Starkov, On the thermodynamic foundations of solid-state cooler based on multiferroic materials, *International Journal of Refrigeration* 37 (2014) 249-256

[5] B. F. Yu, Q. Gao, B. Zhang, X. Z. Meng, and Z. Chen, Review on research of room temperature magnetic refrigeration, *International Journal of Refrigeration* 26 (2003) 622-636

[6] Bingfeng Yu, Min Liu, Peter W. Egolf, and Andrej Kitanovski, A review of magnetic refrigerator and heat pump prototypes built before the year 2010, *International Journal of Refrigeration* 33 (2010) 1029-1060

[7] Matjaz Valant, Electrocaloric materials for future solid-state refrigeration technologies, *Progress in Materials Science* 57 (2012) 980-1009

[8] Daniel Guyomar, Yang Li, Gaël Sebald, Pierre-Jean Cottinet, Benjamin Ducharne, and Jean-Fabien Capsal, Elastocaloric modeling of natural rubber, *Applied Thermal Engineering* 57 (2013) 33-38

[9] Fei Xiao, Takashi Fukuda, Tomoyuki Kakeshita, and Xuejun Jin, Elastocaloric effect by a weak first-order transformation associated with lattice softening in an Fe-31.2Pd (at.%) alloy, *Acta Materialia* 87 (2015) 8-14

[10] H. Ossmer, F. Lambrecht, M. Gültig, C. Chluba, E. Quandt, and M. Kohl, Evolution of temperature profiles in TiNi films for elastocaloric cooling, *Acta Materialia* 81 (2014) 9-20

[11] M. Schmidt, A. Schütze, and S. Seelecke, Scientific test setup for investigation of shape memory alloy based elastocaloric cooling processes, *International Journal of Refrigeration* 54 (2015) 88-97

[12] J. Tušek, K. Engelbrecht, R. Millán-Solsona, L. Mañosa, E. Vives, L.P. Mikkelsen, and N. Pryds, The Elastocaloric Effect: A Way to Cool Efficiently, *Advanced Energy Materials*, 5 (2015) 13

[13] Binfeng Lu, Pengna Zhang, Yang Xu, Wen Sun, and Jian Liu, Elastocaloric effect in $Ni_{45}Mn_{36.4}In_{13.6}Co_5$ metamagnetic shape memory alloys under mechanical cycling, *Materials Letters*, 148 (2015) 110-113

[14] A. S. Starkov, I. A. Starkov, Multicaloric effect in a solid: New Aspects, *Journal of Experimental and Theoretical Physics*, 119 (2014) 258-263

[15] Aditya Chauhan, Satyanarayan Patel, and Rahul Vaish, Multicaloric effect in $Pb(Mn_{1/3}Nb_{2/3})O_3$-32$PbTiO_3$ single crystals, *Acta Materialia*, 89 (2015) 384-395

[16] Melvin M. Vopson, The multicaloric effect in multiferroic materials, *Solid State Communications*, 152 (2012) 2067-2070

[17] E. Warburg, Magnetische Untersuchungen, *Annalen der Physik*, 249 (1881) 141-164

[18] J. Tušek, S. Zupan, I. Prebil, and A. Poredoš, Magnetic Cooling - Development of Magnetic Refrigerator, *Journal of Mechanical Engineering*, 55 (2009) 5

[19] Vitalij K. Pecharsky, Karl A. Gschneidner Jr., Magnetocaloric effect and magnetic refrigeration, *Journal of Magnetism and Magnetic Materials*, 200 (1999) 44-56

[20] W. F. Giauque, A thermodynamic treatment of certain magnetic effects. A proposed method of producing temperatures considerably below 1° absolute, *Journal of American Chemical Society*, 49 (1927) 1864-1870

[21] G. V. Brown, Magnetic heat pumping near room temperature, *Journal of Applied Physics*, 47 (1976) 3673

[22] X. X. Zhang, J. Tejada, Y. Xin, G. F. Sun, K. W. Wong, and X. Bohigas, Magnetocaloric effect in $La_{0.67}Ca_{0.33}MnO_6$ and $La_{0.60}Y_{0.07}Ca_{0.33}MnO_6$ bulk materials, *Applied Physics Letters*, 69 (1996) 3596

[23] Y. Sun, M. B. Salamon, and S. H. Chun, Magnetocaloric effect and temperature coefficient of resistance of La2/3 (Ca,Pb) 1/3 MnO3, *Journal of Applied Physics*, 92 (2002) 3235

[24] William A. Steyert, Los Alamos, and N. Mex, High temperature refrigerator, *US Patent* No.4107935 (1978)

[25] John A. Barclay, William A. Steyert, Active magnetic regenerator, *US Patent* No.4332135 A (1981)

[26] J. A. Barclay, Use of a ferrofluid as the heat-exchange fluid in magnetic refrigerator, *Journal of Applied Physics*, 53 (1982) 2887

[27] C. Zimm, A. Jastrab, A. Sternberg, V. Pecharsky, K. Gschneidner, Jr., M. Osborne,

and I. Anderson, Description and performance of a near-room temperature magnetic refrigerator, *Advances in Cryogenic Engineering*, 43 (1998) 1759-1766

[28] C. Zimm, A. Boeder, J. Chell, A. Sternberg, A. Fujita, S. Fujieda, and K. Fukamichi, Design and performance of a permanent-magnet rotary refrigerator, *International Journal of Refrigeration*, 29 (2006) 1302-1306

[29] G. C. Lin, X. M. Xiong, J. X. Zhang, and Q. Wei, Latent heat study of phase transition in Ba0.73Sr0.27TiO3 induced by electric field, *Journal of Thermal Analysis and Calorimetry*, 81 (2005) 41-44

[30] M. A. Itskovskii, L. V. Shchedrina, and M. D. Kladkevich, Pyroelectric and electrocaloric effects in the phase transition region of thin ferroelectrics, *Ferroelectrics*, 29 (1980) 167-174

[31] A. S. Mischenko, Q. Zhang, J. F. Scott, R. W. Whatmore, and N. D. Mathur, Giant Electrocaloric Effect in Thin-Film $PbZr_{0.95}Ti_{0.05}O_3$, *Science*, 311 (2006) 1270

[32] V. K. Agarwal, V. K. Srivastava, Thickness dependence of breakdown field in thin films, *Thin Solid Films*, 8 (1971) 377-381

[33] J. F. Verweij, J. H. Klootwijk, Dielectric breakdown I: A review of oxide breakdown, *Microelectronics Journal*, 27 (1996) 611-622

[34] H. K. Kim, F. G. Shi, Thickness dependent dielectric strength of a low-permittivity dielectric film, *IEEE Transactions on Dielectrics and Electrical Insulation*, 8 (2001) 248-252

[35] T. M. Correia, J. S. Young, R. W. Whatmore, J. F. Scott, N. D. Mathur, and Q. Zhang, Investigation of the electrocaloric effect in a PbMg2/3Nb1/3O3-PbTiO3 relaxor thin film, *Applied Physics Letters*, 95 (2009) 182904

[36] R. Zhang, S. Peng, D. Xiao, Y. Wang, B. Yang, J. Zhu, P. Yu, and W. Zhang, Preparation and characterization of $(1-x)Pb(Mg_{1/3}Nb_{2/3})O_3$-$x$ $PbTiO_3$ electrocaloric ceramics, *Crystal Research and Technology*, 33 (1998) 827-832

[37] B. Neese, B. Chu, S.-G. Lu, Y. Wang, E. Furman, and Q. M. Zhang, Large electrocaloric effect in ferroelectric polymers near room temperature, *Science*, 321 (2008) 821

[38] R. Chukka, J. W. Cheah, Z. Chen, P. Yang, S. Shannigrahi, J.L. Wang, and L. Chen, Enhanced cooling capacities of ferroelectric materials at morphotropic phase boundaries, *Applied Physics Letters*, 98 (2011) 242902

[39] J. Parui, S. B. Krupanidhi, Electrocaloric effect in antiferroelectric PbZrO3 thin films, *physica status solidi (RRL)*, 2 (2008) 230-232

[40] Zuyong Feng, Dongqi Shi, and Shixue Dou, Large electrocaloric effect in highly (001)-oriented $0.67PbMg_{1/3}Nb_{2/3}O_3$-$0.33PbTiO_3$ thin films, *Solid State*

Communications, 151 (2011) 123-126

[41] Zuyong Feng, Dongqi Shi, Rong Zeng, and Shixue Dou, Large electrocaloric effect in highly (100)-oriented $0.68PbMg_{1/3}Nb_{2/3}O_3$-$0.32PbTiO_3$ thin films with a $Pb(Zr_{0.3}Ti_{0.7})O_3/PbO_x$ buffer layer, *Thin Solid Films*, 519 (2011) 5433-5436

[42] S. G. Lu, B. Rožič, Q. M. Zhang, Z. Kutnjak, R. Pirc, Minren Lin, Xinyu Li, and Lee Gorny, Comparison of directly and indirectly measured electrocaloric effect in relaxor ferroelectric polymers, *Applied Physics Letters*, 97 (2010) 202901

[43] S. G. Lu, B. Rožič, Q. M. Zhang, Z. Kutnjak, and B. Neese, Enhanced electrocaloric effect in ferroelectric poly(vinylidene-fluoride/trifluoroethylene) 55/45 mol% copolymer at ferroelectric-paraelectric transition, *Applied Physics Letters*, 98 (2011) 122906

[44] P. F. Liu, J. L. Wang, X. J. Meng, J. Yang, B. Dkhil, and J. H. Chu, Huge electrocaloric effect in Langmuir-Blodgett ferroelectric polymer thin films, *New Journal of Physics*, 12 (2010) 023035

[45] Xinyu Li, Xiao-shi Qian, S. G. Lu, Jiping Cheng, Zhao Fang, and Q. M. Zhang, Tunable temperature dependence of electrocaloric effect in ferroelectric relaxor poly(vinylidene fluoride-trifluoroethylene-chlorofluoroethylene terpolymer, *Applied Physics Letters*, 99 (2011) 052907

[46] V. Basso, F. Russo, J.-F. Gerard, and S. Pruvost, Direct measurement of the electrocaloric effect in poly(vinylidene fluoride-trifluoroethylene-chlorotrifluoroethylene) terpolymer films, *Applied Physics Letters*, 103 (2013) 202904

[47] G. Sebald, L. Seveyrat, J.-F. Capsal, P.-J. Cottinet, and D. Guyomar, Differential scanning calorimeter and infrared imaging for electrocaloric characterization of poly(vinylidene fluoride-trifluoroethylene-chlorofluoroethylene) terpolymer, *Applied Physics Letters*, 101 (2012) 022907

[48] F. Bauer, E. Fousson, Q. M. Zhang, L. and M. Lee, Ferroelectric copolymers and terpolymers for electrostrictors: synthesis and properties, *Electrets, 2002. ISE 11. Proceedings. 11th International Symposium on*, (2002) 355-358

[49] F. Bauer, E. Fousson, Q. M. Zhang, and L. M. Lee, Ferroelectric copolymers and terpolymers for electrostrictors: synthesis and properties, *IEEE Transactions on Dielectrics and Electrical Insulation,* 11 (2004) 293-298

[50] F. Bauer, E. Fousson, and Q. M. Zhang, Recent advances in highly electrostrictive P(VDF-TrFE-CFE) terpolymers, *IEEE Transactions on Dielectrics and Electrical Insulation*, 13 (2006) 1149-1154

[51] F. Bauer, Relaxor fluorinated polymers: novel applications and recent developments,

IEEE Transactions on Dielectrics and Electrical Insulation, 17 (2010) 1106-1112

[52] S.L. Dart, R.L. Anthony, and E. Guth, Rise of Temperature on Fast Stretching of Synthetics and Natural Rubbers, *Industrial & Engineering Chemistry*, 34 (1942) 1340-1342

[53] G.A. Holzapfel, J.C. Simo, Entropy elasticity of isotropic rubber-like solids at finite strains, *Computer Methods in Applied Mechanics and Engineering*, 132 (1996) 17-44

[54] X. Moya, S. Kar-Narayan, and N.D. Mathur, Caloric materials near ferroic phase transitions, *Nature Materials*, 13 (2014) 439-450

[55] Nicolas Candau, Laurent Chazeau, Jean-Marc Chenal, Catherine Gauthier, and Etienne Munch, Compared abilities of filled and unfilled natural rubbers to crystalliza in a large strain rate domain, *Composites Science and Technology*, 108 (2015) 9-15

[56] C. Bechtold, C. Chluba, R. Lima de Miranda, and E. Quandt, High cyclic stability of the elastocaloric effect in sputtered TiNiCu shape memory films, *Applied Physics Letters*, 101 (2012) 091903

[57] J. Tušek, K. Engelbrecht, L.P. Mikkelsen, and N. Pryds, Elastocaloric effect of Ni-Ti wire for application in a cooling device, *Journal of Applied Physics*, 117 (2015) 124901

[58] Erell Bonnot, Ricardo Romero, Lluís Mañosa, Eduard Vives, and Antoni Planes, Elastocaloric effect associated with the martensitic transition in shape-memory alloys, *Physical Review Letters*, 100 (2008) 125901

[59] Jun Cui, Yiming Wu, Jan Muehlbauer, Yunho Hwang, Reinhard Radermacher, Sean Fackler, Manfred Wuttig, and Ichiro Takeuchi, Demonstration of high efficiency elastocaloric cooling with large ΔT using wires, *Applied Physics Letters*, 101 (2012) 073904

[60] Fei Xiao, Takashi Fukuda, Tomoyuki Kakeshita, Significant elastocaloric effect in a Fe-31.2Pd(at. %) single crystal, *Applied Physics Letters*, 102 (2013) 161914

[61] Garrett J. Pataky, Elif Ertekin, Huseyin Sehitoglu, Elastocaloric cooling potential of NiTi, Ni_2FeGa, and CoNiAl, *Acta Materialia*, 96 (2015) 420-427

[62] Y. J. Huang, Q. D. Hu, N. M. Bruno, Jing-Han Chen, I. Karaman, Joseph H. Ross, Jr., J. G. Li, Giant elastocaloric effect in directionally solidified Ni-Mn-In magnetic shape memory alloy, *Scripta Materialia*, 105 (2015) 42-45

[63] L. R. G. Treloar, The elasticity and related properties of rubbers, *Reports on Progress in Physics*, 36 (1973) 755-826

[64] L. R. G. Treloar, The Physics of Rubber Elasticity, *Oxford University Press*, 1975

[65] R. L. Anthony, R. H. Caston, and Eugene Guth, Equations of state for natural and synthetic rubber-like materials. I. Unaccelerated natural soft rubber, *The Journal of Physical Chemistry*, 46 (1942) 826-840

[66] Robert A. Shanks, Ing Kong, General Purpose Elastomers: Structure, Chemistry, Physics and Performance, *Advances in Elastomers I*, 11 (2013) 11-45

[67] Jiri George Drobny, Handbook of Thermoplastic Elastomers, *William Andrew Publishing*, (2007), ISBN: 978-0-8155-1549-4

[68] James E. Mark, Burak Erman and Frederick R. Eirich, Science and Technology of Rubber, Third Edition, *Academic Press*, (2005), ISBN: 978-0-12-464786-2

[69] E. G. Kent, F. B. Swinney, Properties and applications of trans-1,4-polyisoprene, *Industrial & Engineering Chemistry Product Research and Development*, 5 (1966) 134-138

[70] Shigeyuki Toki, Igors Sics, Shaofeng Ran, Lizhi Liu, and Benjamin S Hsiao, Molecular orientation and structural development in vulcanized polyisoprene rubbers during uniaxial deformation by in situ synchrotron X-ray diffraction, *Polymer*, 44 (2003) 6003-6011

[71] Yuko Ikeda, Yoritaka Yasuda, Shinya Makino, Shinya Yamamoto, Masatoshi Tosaka, Kazunobu Senoo, and Shinzo Kohjiya, Strain-induced crystallization of peroxide-crosslinked natural rubber, *Polymer*, 48 (2007) 1171-1175

[72] J. R. Brown, E. A. Hauser, Chemical structure of VULCANIZED RUBBER, *Industrial & Engineering Chemistry*, 30 (1938) 1291-1295

[73] Yoshihide Fukahori, "Mechanism of the self-reinforcement of cross-linked NR generated through the strain-induced crystallization", *Polymer*, 51 (2010) 1621-1631

[74] Fei Zhao, Weina Bi, Shugao Zhao, Influence of crosslink density on mechanical properties of natural rubber vulcanizates, *Journal of Macromolecular Science, Part B: Physics*, 50 (2011) 1460-1469

[75] Maya Shankar Singh, Advanced Organic Chemistry: Reactions And Mechanisms, *Pearson Education*, (2008),ISBN:9788131711071

[76] S. A. Tobias, F. Koenigsberger, Advances in Machine Tool Design and Research 1969, Proceedings of the 10th International M.T.D.R. Conference, *University of Manchester Institute of Science and Technology*, (1970), ISBN: 978-0-08-015661-3

[77] Bryan Ellis, Ray Smith, Polymers: A Property Database, Second Edition, *CRC Press*, (2008), ISBN: 9780849339400

[78] J. W. ten Brinke, S. C. Debnath, L. A. E. M. Reuvekamp, and J. W. M. Noordermeer, Mechanistic aspects of the role of coupling agents in silica-rubber composites,

Composites Science and Technology, 63 (2003) 1165-1174

[79] Yoshihide Fukahori, New progress in the theory and model of carbon black reinforcement of elastomers, *Journal of Applied Polymer Science*, 95 (2005) 60-67

[80] S. Toki, T. Fujimaki, M. Okuyama, Strain-induced crystallization of natural rubber as detected real-time by wide-angle X-ray diffraction technique, *Polymer*, 41 (2000) 5423-5429

[81] Masatoshi Tosaka, Syozo Murakami, Sirilux Poompradub, Shinzo Kohjiya, and Yuko Ikeda, Orientation and crystallization of natural rubber network as revealed by WAXD using synchrotron radiation, *Macromolecules*, 37 (2004) 3299-3309

[82] Shigeyuki Toki, Igors Sics, Chris Burger, Dufei Fang, Lizhi Liu, Benjamin S. Hsiao, Sudhin Datta, and Andy H. Tsou, Structure evolution during cyclic deformation of an elastic propylene-based ethylene-propylene copolymer, *Macromolecules*, 39 (2006) 3588-3597

[83] Masatoshi Tosaka, Shinzo Kohjiya, Yuko Ikeda, Shigeyuki Toki, and Benjamin S. Hsiao, Molecular orientation and stress relaxation during strain-induced crystallization of vulcanized natural rubber, *Polymer Journal*, 42 (2010) 474-481

[84] Yuko Ikeda, Yoritaka Yasuda, Kensuke Hijikata, Masatoshi Tosaka, and Shinzo Kohjiya, Comparative study on strain-induced crystallization behavior of peroxide cross-linked and sulfur cross-linked natural rubber, *Macromolecules*, 41 (2008) 5876-5884

[85] Yoshihisa Miyamoto, Hiromi Yamao, and Ken Sekimoto, Crystallization and melting of polyisoprene rubber under uniaxial deformation, *Macromolecules*, 36 (2003) 6462-6471

[86] Masatoshi Tosaka, Daisuke Kawakami, Kazunobu Senoo, and Shinzo Kohjiya, Crystallization and stress relaxation in highly stretched samples of natural rubber and its synthetic analogue, *Macromolecules*, 39 (2006) 5100-5105

[87] Masatoshi Tosaka, Kazunobu Senoo, Shinzo Kohjiya, and Yuko Ikeda, Crystallization of stretched network chains in cross-linked natural rubber, *Journal of Applied Physics*, 101 (2007) 084909

[88] Nicolas Candau, Rabia Laghmach, Laurent Chazeau, and Jean-Marc Chenal, Catherine Gauthier, Thierry Biben, Etienne Munch, Influence of strain rate and temperature on the onset of strain induced crystallization in natural rubber, *European Polymer Journal*, 64 (2015) 244-252

[89] Shigeyuki Toki, Igors Sics, Shaofeng Ran, Lizhi Liu, and Benjamin S. Hsiao, Molecular orientation and structural development in vulcanized polyisoprene rubbers during uniaxial deformation by in situ synchrotron X-ray diffraction,

Polymer, 44 (2003) 6003-6011

[90] Takeshi Karino, Yuko Ikeda, Yoritaka Yasuda, Shinzo Kohjiya, and Mitsuhiro Shibayama, Nonuniformity in natural rubber as revealed by small-angle neutron scattering, small-angle X-ray scattering, and atomic force microscopy, *Biomacromolecules*, 8 (2007) 693-699

[91] S. Beurrot-Borgarino, B. Huneau, E. Verron, and P. Rublon, Strain-induced crystallization of carbon black-filled natural rubber during fatigue measured by in situ synchrotron X-ray diffraction, *International Journal of Fatigue*, 47 (2013) 1-7

[92] Shigeyuki Toki, Igors Sics, Benjamin S. Hsiao, Syozo Murakami, Masatoshi Tosaka, Sirilux Poompradub, Shinzo Kohjiya, and Yuko Ikeda, Structural developments in synthetic rubbers during uniaxial deformation by in situ synchrotron X-ray diffraction, *Journal of Polymer Science Part B: Polymer Physics*, 42 (2004) 956-964

[93] Nicolas Candau, Rabia Laghmach, Laurent Chazeau, Jean-Marc Chenal, Catherine Gauthier, Thierry Biben, and Etienne Munch, Temperature dependence of strain-induced crystallization in natural rubber: On the presence of different crystallite populations, *Polymer*, 60 (2015) 115-124

[94] Yuko Ikeda, Norihito Higashitani, Kensuke Hijikata, Yota Kokubo, and Yuichi Morita, Vulcanization: New focus on a traditional technology by small-angle neutron scattering, *Macromolecules*, 42 (2009) 2741-2748

[95] N. Candau, L. Chazeau, J.-M. Chenal, C. Gauthier, J. Ferreira, E. Munch, and D. Thiaudière, Strain induced crystallization and melting of natural rubber during dynamic cycles, *Physical Chemistry Chemical Physics*, 17 (2015) 15331-15338

[96] Justin Che, Christian Burger, Shigeyuki Toki, Lixia Rong, and Benjamin S. Hsiao, Crystal and Crystallites Structure of Natural Rubber and Synthetic cis-1,4-Polyisoprene by a New Two Dimensional Wide Angle X-ray, *Macromolecules*, 46 (2013) 4520-4528

[97] L. Mullins, Softening of rubber by deformation, *Rubber Chemistry and Technology*, 42 (1969) 339-362

[98] Julie Diani, Bruno Fayolle, and Pierre Gilormini, A review on the Mullins effect, *European Polymer Journal*, 45 (2009) 601-612

[99] J. Niemczura, K. Ravi-Chandar, On the response of rubbers at high strain rates-Ⅲ. Effect of hysteresis, *Journal of the Mechanics and Physics of Solids*, 59 (2011) 457-472

[100] L. Mullins, Effect of Stretching on the Properties of Rubber, *Rubber Chemistry and Technology*, 21 (1948) 281-300

[101] A. F. Blanchard, D. Parkinson, Breakage of carbon-rubber networks by applied

stress, *Industrial & Engineering Chemistry*, 44 (1952) 799-812

[102] R. Houwink, Slipping of molecules during the deformation of reinforced rubber, *Rubber Chemistry and Technology*, 29 (1956) 888-893

[103] G. Kraus, C. W. Childers, and K. W. Rollmann, Stress softening in carbon black-reinforced vulcanizates. Strain rate and temperature effects, *Journal of Applied Polymer Science*, 10 (1966) 229-244

[104] David E. Hanson, Marilyn Hawley, Robert Houlton, Kiran Chitanvis, Philip Rae, E. Bruce Orler, and Debra A. Wrobleski, Stress softening experiments in silica-filled polydimethylsiloxane provide insight into a mechanism for the Mullins effect, *Polymer*, 46 (2005) 10989-10995

[105] Yoshihide Fukahori, New progress in the theory and model of carbon black reinforcement of elastomers, *Journal of Applied Polymer Science*, 95 (2005) 60-67

[106] Z. Xie, G. Sebald, and D. Guyomar, Comparison of direct and indirect measurement of the elastocaloric effect in natural rubber, *Applied Physics Letters*, 108 (2016) 041901

[107] Z. Xie, G. Sebald, and D. Guyomar, Elastocaloric effect dependence on pre-elongation in natural rubber, *Applied Physics Letters*, 107 (2015) 081905

[108] B. C. Punmia, Ashok Kr. Jain, and Arun Kr. Jain, Mechanics of Materials, *Firewall Media*, (2002), ISBN: 8170082153

[109] Anthony F. Mills, Heat transfer, *CRC Press*, (1992), ISBN: 0256076421

[110] S. Qian, A. Alabdulkarem, J. Ling, J. Muehlbauer, Y. Hwang, R. Radermacher, and I. Takeuchi, Performance enhancement of a compressive thermoelastic cooling system using multi-objective optimization and novel designs, *International Journal of Refrigeration*, 57 (2015) 62-76

[111] Heiji Kawai, The piezoelectricity of poly(vinylidene Fluoride), *Japanese Journal of Applied Physics*, 8 (1969) 975

[112] Andrew J. Lovinger, Ferroelectric polymers, *Science*, 220 (1983) 1115-1121

[113] F. Xia, Z.-Y. Cheng, H.S. Xu, H.F. Li, Q.M. Zhang, G.J. Kavarnos, R.Y. Ting, G. Abdel-Sadek, and K.D. Belfield, High Electromechanical Responses in a Poly(vinylidene fluoride–trifluoroethylene–chlorofluoroethylene) Terpolymer, *Advanced materials*, 14 (2002) 1574-1577

[114] V. Bobnar, X. Li, G. Casar, A. Erste, S. Glinsek, X. Qian, and Q.M. Zhang, Tailoring electrically induced properties by stretching relaxor polymer films, *Journal of Applied Physics*, 111 (2012) 083515

[115] U. Plaznik, A. Kitanovski, B. Rozic, B. Malic, H. Ursic, S. Drnovsek, J. Cilensek, M. Vrabelj, A. Poredos, and Z. Kutnjak, Bulk relaxor ferroelectric ceramics as a

working body for an electrocaloric cooling device, *Applied Physics Letters*, 106 (2015) 043903

[116] H. Gu, X.-S. Qian, H.-J. Ye, and Q.M. Zhang, An electrocaloric refrigerator without external regenerator, *Applied Physics Letters*, 105 (2014) 162905

Résumé Français Thèse Yukihiro YOSHIDA

Chapitre 1 : Introduction Générale

1.1 Contexte de l'étude

La génération de froid est indispensable pour le stockage de la nourriture, la climatisation des locaux, la production et le stockage de gaz liquides, etc. Les systèmes conventionnels sont basés sur des cycles de compression/détente et utilisent des gaz pouvant augmenter l'effet de serre et contribuer au réchauffement climatique.

Au cours de ces dernières années, différents effets ont été étudiés pour proposer de nouveaux dispositifs tout solides et très compacts. Ils utilisent le fait que dans certaines classes de matériaux une variation de température peut être obtenue grâce à une variation d'entropie.

Trois types d'effets sont généralement étudiés :

- L'effet magnéto-électrique
- L'effet électro-calorique
- Et l'effet élasto-calorique.

Certaines études envisagent même de les associer pour développer des systèmes dits « multi-caloriques » et augmenter ainsi leurs performances.

Le but de ce chapitre est de décrire ces trois effets, en insistant sur leurs avantages et leurs inconvénients et en listant les familles de matériaux généralement utilisées. Cette analyse permettra également de justifier le choix de travailler sur l'effet élasto-calorique dans le cadre de cette thèse.

1.2 Présentation des trois effets

1.2.1 L'effet magnétocalorique

Cet effet se caractérise par une variation adiabatique et réversible de la température à cause d'une variation entropique induite par le champ magnétique.

Ce phénomène peut être décrit par les équations suivantes :

$S_T(T, H) = S_m(T, H) + S_l(T) + S_e(T)$

Où S_T, S_m, S_l et S_E représentent respectivement l'entropie totale du matériau, l'entropie magnétique, l'entropie de la maille et l'entropie électronique, H, le champ magnétique et T la température.

$$\Delta S_m(T, \Delta H) = \int_{H_0}^{H_1} (\partial M(T,H)/\partial T)_H \, dH$$

Où ΔSm représente la variation de l'entropie magnétique et M la magnétisation

$$\Delta T_{ad}(T, \Delta H) = -\int_{H_0}^{H_1} \frac{T}{C} \left(\frac{\partial M\ (T,H)}{\partial T}\right)_H dH$$

Où ΔT_{ad} représente la variation de température, en supposant qu'elle se fait dans un régime adiabatique et C la capacité thermique.

Ces équations montrent que les variations attendues sont d'autant plus grandes que la magnétisation M varie avec la température d'où l'intérêt de se placer au voisinage de transitions de phase où elles seront les plus importantes.

La figure 1.1 du manuscrit de thèse explicite le principe physique de conversion : soumis à un champ magnétique extérieur, les moments magnétiques, orientés de façon aléatoire en l'absence de champ sont aléatoirement distribués. L'application du champ magnétique les force à s'orienter augmentant la magnétisation et l'ordre dans le matériau. La variation d'entropie sera donc négative entrainant un échauffement du matériau. Lorsque le champ magnétique extérieur est supprimé, les moments magnétiques perdent leur orientation préférentielle, ce qui conduit à l'apparition d'un état désordonné au sein de la matière. Ceci se traduit par une variation d'entropie positive et donc une diminution de la température.
Le principal matériau utilisé pour cette conversion est le Gadolinium ou un de ses composés. Les deux verrous le concernant sont son coût et le fait qu'il s'oxyde facilement. Des essais ont aussi été réalisés avec des oxydes pérovskites à base de manganèse, mais ils n'ont pas montré des performances élevées.

Les figures 1.2, 1.3 et 1.4 du manuscrit de thèse présentent les différentes configurations qui permettent d'exploiter l'effet magnétocalorique dans un système de refroidissement. Il faut en effet contrôler le transfert thermique entre la source chaude et la source froide, au cours d'un cycle incluant une étape de mise en ordre puis un retour à un état désordonné. La performance du système dépend directement de la fréquence à laquelle ces cycles peuvent être effectués et de la variation de température atteinte sur un cycle, les deux devant être les plus élevées possibles.

1.2.2 L'effet électro-calorique

Il peut être décrit en faisant une analogie avec ce qui a été présenté pour l'effet magnéto électrique : le champ électrique (E) jouant le rôle du champ magnétique (H) et la polarisation (P) celui de la magnétisation (M).
Les équations régissant cet effet s'écrivent :

$$\Delta S(T, \Delta E) = \int_{E_1}^{E_2} (\partial P/\partial T)_E dE$$

$\Delta T_{ad}(T, \Delta E) = -\frac{1}{\rho}\int_{E_1}^{E_2} \frac{T}{C_p} (\partial P/\partial T)_E dE$ où ρ représente la masse volumique du matériau.

La figure 1.5 du manuscrit de thèse présente le principe avec le passage d'un état désordonné à un état ordonné des moments dipolaires sous champ électrique appliqué et l'apparition d'une polarisation macroscopique induite puis le retour à un état désordonné lors de la disparition du champ. La variation de l'entropie est d'abord négative puis positive conduisant respectivement à une élévation puis un refroidissement du matériau. Comme pour l'effet magnéto-calorique, l'effet électro-calorique sera accentué au voisinage d'une transition de phase car la variation de la polarisation avec la température y sera plus grande. Un des avantages de l'effet électro-calorique sur l'effet magnétocalorique est qu'il est généralement plus facile d'utiliser un champ électrique qu'un champ magnétique pour piloter la variation d'entropie. Cependant, l'effet Joule associé à des mécanismes de conduction dans le matériau à la mise sous champ électrique et toujours responsable d'un échauffement du matériau peut venir diminuer l'effet électro-calorique. De la même façon, il faudra également veiller à ce qu'il n'y ait pas de claquage diélectrique au sein du matériau. Les mécanismes qui en sont responsables dépendent étroitement de l'épaisseur. Si dans les matériaux les plus massifs, le claquage trouve son origine dans les défauts micrométriques dispersés en volume, c'est une avalanche électronique qui provoque la rupture des films minces. Le premier mécanisme est connu pour arriver aux champs les plus bas alors que le second nécessite des champs électriques plus élevés. Par conséquent, il sera toujours plus facile d'appliquer des champs électriques forts sur des films minces sans provoquer leur destruction et d'obtenir des variations de température plus importantes (facteur 6 observé dans certains cas). Toutefois, il faut garder à l'esprit que la variation de chaleur ($\Delta Q = C_v V \Delta T$) dépend directement du volume V du matériau et par conséquent qu'il sera difficile d'obtenir de grandes variations sur les films minces même si la variation de température est plus élevée.

Une solution alternative est d'utiliser des céramiques massives ou des films épais de polymères sous réserve de se placer au voisinage des températures de transition pour augmenter ΔT.

Parmi les matériaux les mieux adaptés à cette conversion, les céramiques au plomb occupent une place de choix mais des efforts de recherche pour remplacer le plomb ont conduit à travailler sur des céramiques sans plomb ou sur des polymères fluorés. Cette recherche de matériaux performants est actuellement un des axes sur lequel portent les efforts de la communauté scientifiques.

1.2.3 L'effet élastocalorique

Cet effet est celui étudié dans le cadre de cette thèse. Il fera donc l'objet d'une présentation plus détaillée.

Comme les précédents, l'origine physique du phénomène vient de la variation d'entropie induite par la déformation, la force devenant l'équivalent de la magnétisation ou de la polarisation et la déformation celle du champ magnétique ou du champ électrique.
Les deux équations suivantes décrivent le couplage mis en œuvre :

$$\Delta S(T, \Delta l) = -\int_{l_0}^{l_1} (\partial f/\partial T)_l dl$$

$$\Delta T_{ad}(T, \Delta l) = \int_{l_0}^{l_1} \frac{T}{C} (\partial f/\partial T)_l dl$$

La figure 1.6 du manuscrit de thèse explique schématiquement les étapes de la conversion. Sous l'effet de la déformation, les chaînes moléculaires passent d'un état ordonné à un état désordonné induisant une diminution de l'entropie et donc une élévation de température. Lorsque la déformation est annulée, les chaines retrouvent leur état désordonné entraînant une augmentation de l'entropie donc une baisse de la température.

Un des avantages de l'effet élastocalorique par rapport à l'effet magnétocalorique est qu'il utilise des matériaux sans terre rare, généralement moins chers et moins toxiques et par rapport à l'effet électro calorique qu'il autorise l'utilisation de matériau épais ou massifs. Il reste néanmoins quelques verrous à lever dont la dissipation de la chaleur sous déformation, la génération de chaleur à cause du phénomène de friction, l'existence d'une déformation permanente sous cycle et la perte d'élasticité due à des phénomènes de fatigue.
La figure 1.7 du manuscrit de thèse montre l'influence de la vitesse de déformation sur la variation de température en charge et en décharge. On observe que la variation maximale de température diminue pour les vitesses les plus faibles, à cause de l'échange avec l'environnement. Il faudra donc veiller pour rester en régime adiabatique à ce que la vitesse de déformation soit suffisamment élevée.

La figure 1.8 du manuscrit de thèse montre que l'incorporation de particules de carbone dans un caoutchouc naturel permet d'augmenter l'effet élasto-calorique.
Enfin, il convient de signaler que si la vitesse de déformation devient trop importante, un phénomène de friction va prendre naissance au sein du matériau conduisant à une réduction de la variation maximale de température en décharge.

Comme rappelés précédemment, les deux autres effets susceptibles de limiter la performance sont l'existence d'une déformation permanente et d'une réduction de l'élasticité induite par la fatigue.

Les matériaux couramment étudiés sont les alliages à mémoire de forme et les élastomères. Le tableau 1.1 du manuscrit de thèse présente quelques valeurs couramment observées. Des variations de températures d'une vingtaine de degrés, à température ambiante, ont par exemple pu être observées pour NiTi.

1.3 Equations modélisant l'effet élasto-calorique

A partir des équations constitutives de la thermodynamique, il a été possible de modéliser les variations d'entropie et de température :

$$dU = dQ + dW \quad (1.8)$$

$$TdS = dQ \quad (1.9)$$

Où U est l'énergie interne, Q la chaleur reçue des sources extérieures, W *le travail fourni par les sources extérieures,* T la température et S l'entropie. dW peut s'exprimer par:

$$dW = fdl - pdV \quad (1.10)$$

où f est la force, l l'élongation, p la pression et V le volume. En considérant que la variation de volume reste faible, ce qui revient à négliger pdV dans l'équation (1.10).

Eq. (1.8), (1.9) et (1.10) conduisent à:

$$dU = TdS + fdl \quad (1.11)$$

A température constante, la force extérieure f s'écrit :

$$f = (\partial U / \partial l)_T - T(\partial S / \partial l)_T \quad (1.12)$$

Eq. (1.12) montre que la force extérieure se divise en une force qui contribue à la variation d'énergie interne and une qui contribue à la variation d'entropie.

L'énergie libre d'Helmholtz est définie par :

$$F = U - TS \quad (1.13)$$

En différenciant l'équation 1.13, on obtient

$$dF = dU - TdS - SdT \quad (1.14)$$

(1.11) et (1.14) donnent :

$$dF = fdl - SdT \quad (1.15)$$

La relation de Maxwell sur les dérivées croisées conduit à :

$$-(\partial f / \partial T)_l = (\partial S / \partial l)_T \quad (1.16)$$

Finalement, Eq. (1.12) peut être réécrite sous la forme :

$$f = (\partial U / \partial l)_T + T(\partial f / \partial T)_l \quad (1.17)$$

Selon la nature du matériau, la force induite par la déformation peut contribuer à la variation d'énergie interne ou à la variation d'entropie. Le caoutchouc naturel se place dans le deuxième cas comme le montre la figure 1.9 de la thèse.

La variation de température dans le cas du couplage est due à la variation d'entropie.

$$dS = (\partial S / \partial T)_l \, dT + (\partial S / \partial l)_T \, dl \quad (1.18)$$

$$dS = (C / T) \, dT + (\partial S / \partial l)_T \, dl \quad (1.19) \text{ en remarquant que } C = T(\partial S / \partial T)_l$$

Si la déformation se fait de façon adiabatique, il n'y a pas d'échange de chaleur entre le matériau et son environnement ($dQ = 0$ et à partir de Eq. 1.19, $dS = 0$) soit $0 = (C / T)dt + (\partial S / \partial l)_T \, dl$:

$$\Delta T_{ad}(T, \Delta l) = - T / C \int (\partial S / \partial l)_T \, dl \quad (1.20)$$

Eq. (1.16) et (1.20) s'écrivent alors:

$$\Delta T_{ad}(T, \Delta l) = T / C \int (\partial f / \partial T)_l \, dl \quad (1.21)$$

Dans le cas idéal, pour un matériau dont l'élasticité est d'origine entropique, on montre que tout le travail mécanique fourni est transformé en chaleur. $dU = 0$, dans ce cas, ce qui entraîne :

$$dW = -dQ \quad (1.22)$$

1.4 Elastomère

Les élastomères sont des polymères présentant des chaînes moléculaires relativement longues avec un haut degré de mobilité et de flexibilité. Ils ont de faibles modules élastiques et peuvent être largement étirés.

Le caoutchouc naturel est obtenu à partir de la purification du latex issu de Hevea Brasiliensis appelé encore arbre à caoutchouc. Il est constitué de cis polysipropène. Le caoutchouc peut également être synthétisé, par une réaction de polymérisation de l'isoprène. Les deux types de caoutchouc ont la même formule brute mais des configurations structurales différentes, celle du caoutchouc naturel étant constituée à 100% de la forme cis (figure 1.10 du manuscrit de thèse). Ceci facilite les phénomènes de cristallisation sous élongation aux niveaux les plus bas.

En 1839, Charles Goodyear a découvert la vulcanisation du caoutchouc en le faisant réagir avec du sulfure. Cette opération a considérablement amélioré les propriétés du caoutchouc en termes de capacité à s'allonger et à retrouver sa longueur originale lorsqu'il n'est plus soumis à une déformation externe. La vulcanisation crée un réseau tridimensionnel en pontant ensemble les chaines du polymère comme le montre la figure 1.11 du manuscrit de thèse.

L'introduction de nanoparticules de carbone permet également de renforcer le caoutchouc selon un mécanisme proposé par Fukahori et illustré par la figure 1.12 du manuscrit de thèse.

Autour de la particule de carbone, deux zones vont se succéder : une vitreuse et dure

(GH), directement au contact de la particule, très adhérente et donc peu mobile et une (SH) durcissant sous élongation. La première joue affecte peu le renforcement contrairement à la seconde.

Un point important à prendre en compte est que pour ce type de matériau, la courbe contrainte-déformation est très non-linéaire et que l'élasticité dépend fortement de la vitesse d'élongation. Deux effets sont à considérer pour expliquer un tel comportement : la cristallisation sous élongation et l'effet Mullins. Enfin, il est clair que la loi de Hooke ne peut plus s'appliquer pour exprimer la force en fonction de l'élongation

Cristallisation des élastomères.

Celle-ci peut être induite par une baisse de la température (cristallisation sans direction privilégiée) ou par élongation du matériau. C'est ce deuxième mécanisme qui nous intéresse dans le cadre de notre étude. Soumises à une élongation, les plus longues chaînes vont conserver une orientation aléatoire alors que les plus courtes vont s'orienter de façon préférentielle servant de points de nucléation au-delà d'une certaine valeur d'étirement. Cette cristallisation est réversible et disparaît avec l'étirement. La figure 1.13 du manuscrit de thèse décrit le mécanisme de nucléation et de cristallisation.

En utilisant des techniques de diffraction des rayons de type WAXD et SAXD, il est possible de suivre expérimentalement l'orientation des chaînes et l'évolution de la cristallisation comme le montre la figure 1.14 du manuscrit de thèse.

Toki a montré que la distribution des zones cristallisées se faisait pendant le premier cycle de charge-décharge et que le réseau ainsi obtenu restait sable pendant les cycles suivants comme le montre la figure 1.15 du manuscrit de thèse.

L'effet Mullins

Le comportement mécanique de l'élastomère est modifié après un premier allongement. On constate une perte de rigidité sur les cycles et l'apparition d'une déformation rémanente. La figure 1.16 de la thèse présente un exemple de cet effet sur un ruban de styrène-butadiène.

Le matériau peut recouvrer partiellement ses propriétés originelles après plusieurs heures à température ambiante, plus rapidement pour des températures plus élevées. La figure 1.17 de la thèse présente un exemple de retour partiel aux propriétés initiales après un recuit à 80°C sous vide.

Différents mécanismes présentés sur la figure 1.18 du manuscrit ont été proposé pour expliquer l'effet Mullins. Blanchard et Parkinson ont émis l'hypothèse qu'il était dû à des ruptures de chaînes induites par l'élongation, mais ce mécanisme totalement irréversible est

difficilement compatible avec un recouvrement partiel des propriétés.

Houwink a supposé que les chaînes moléculaires dans le cas d'élastomères chargés glissent sur les particules et créent de nouvelles liaisons, pendant le premier cycle d'étirement. Ce modèle n'explique pas le comportement des élastomères non chargés.

Kraus explique l'effet par une rupture des agglomérats de charges introduites dans le matériau. Cette explication présente les mêmes insuffisances que celle de Blanchard et Parkinson, pour la réversibilité et que celle de Houwink pour le cas des matériaux non chargés.

Hanson propose une séparation des chaînes sous l'effet de l'étirement, une nouvelle imbrication pouvant s'expliquer par un processus thermiquement activé.

Fukahori suggère l'existence de deux phases dans le caoutchouc chargé dont une peut former un réseau. La mise en extension provoquerait une relaxation de ce super réseau entraînant un ramollissement de la structure. Ce modèle n'explique pas l'effet observé dans un polymère non chargé.

A cause de l'effet Mullins, la contrainte va diminuer dans le matériau sous extension. Ceci se traduit par une diminution de l'énergie mécanique, donc de la variation d'entropie et de l'effet élasto-calorique.

De façon générale, l'impact de l'effet Mullins et la cristallisation sur le couplage élasto-calorique n'a pas été étudiée en détail, alors qu'ils affectent tous les deux la courbe contrainte-élongation

1.5 Objective de la thèse

Dans le présent chapitre, trois effets caloriques, leurs avantages et leurs inconvénients ont été décrits. Ces effets caloriques et leur maîtrise conditionnent les technologies de refroidissement futures. L'effet élasto-calorique semble être le plus prometteur en raison de son faible coût et des grandes variations de température auxquelles il pourrait donner accès. Dans ce contexte, les matériaux élastomères ont été moins étudiés que les alliages à mémoires de forme et les travaux les concernant sont très récents.

L'objective de cette thèse était de mettre en place les méthodes nécessaires à la mesure de l'effet élasto-calorique dans les élastomères et d'évaluer l'influence de l'effet Mullins et de la recristallisation induite par la déformation sur la conversion mécano-thermique.

Chapitre 2 : Dispositifs expérimentaux pour l'élaboration et la caractérisation des matériaux

2.1 Introduction

La détermination de l'effet élasto-calorique doit se faire à des vitesses de sollicitations suffisamment élevées pour rester en régime adiabatique et pas trop fortes pour limiter les frictions internes. Il faut donc pouvoir disposer d'un dispositif de mesures permettant de contrôler cette vitesse.

De même, Il est nécessaire de déterminer un certain nombre de caractéristiques physiques du matériau.

Ceci fait l'objet de ce chapitre.

2.2 Matériau – propriétés physiques

2.2.1 Caoutchouc naturel

L'ajout de particules de carbone dans le caoutchouc naturel le rend moins sensible à la fatigue et retarde l'apparition d'une élongation résiduelle après cyclage.

Des feuilles de caoutchouc naturel chargé en particules de carbone ont été achetées à Tohto Rubber Industry CO. Ltd au japon.

2.2.2 Capacité thermique volumique

La capacité thermique volumique C_v est nécessaire pour calculer l'énergie thermique à partir de la variation de température. Elle a été mesurée en utilisant la technique DSC (Differential scanning calorimetry) ou calorimétrie différentielle à balayage qui donne accès à la capacité thermique C_p. L'appareil utilisé est le DSC 131 evo de chez Setaram Instrumentation et du logiciel d'analyse thermique CALISTO de la même société.

Si on connait la densité ρ de l'échantillon, on peut en déduire $C_v = \rho\, C_p$.

La vitesse de chauffe a été fixée à 10°C/min, le creuset utilisé est en aluminium et le matériau de référence est l'alumine dont la capacité volumique spécifique vaut 0.80J/g°C.
La masse d'échantillon est de 17 mg et la gamme de température utilisée s'étend de -20°C à 60°C
La capacité thermique massique est donnée par

$C_p = \frac{q_s}{q_r}\ \frac{m_s}{m_r}\ C_p'$ *où C_p est la capacité thermique de l'échantillon, C_p' celle de l'alumine prise comme référence, q_r est le flux de chaleur entre un creuset vide et un creuset contenant le matériau de référence, q_s est le flux de chaleur entre un creuset vide et le creuset contenant l'échantillon. m_r est la masse du matériau de référence et m_s celle de l'échantillon à tester.*

La figure 2.1 du manuscrit de thèse représente le flux de chaleur (mW) en fonction de la

température pour le matériau de référence et l'échantillon à tester.

La densité a été mesurée en utilisant un pycnomètre. Le principe de la méthode est rappelé sur la figure 2.2 du manuscrit de thèse. La densité de l'échantillon (ρ_s) s'obtient par :

$\rho_s = \frac{m_b - m_a}{m_d - m_a - (m_c - m_b)} \rho_w$ *où m_a est la masse du pycnomètre vide, m_b, celle du pycnomètre avec l'échantillon, m_c, celle du pycnomètre avec l'eau distillée et m_d celle du pycnomètre avec l'eau distillée et l'échantillon. ρ_w est la masse volumique de l'eau distillée.*

La densité du caoutchouc naturel a été trouvée égale à 1390 kg/m^3.

2.2.3 Calibration en température

Pour mesurer de façon précise la variation de température due à l'effet élasto-calorique, la calibration de la caméra thermique a été effectuée en utilisant la procédure suivante. Un échantillon de matériau est placé dans une étuve régulée en température dont on a fixé la valeur. Lorsque l'équilibre thermique est atteint, on admet que l'échantillon est à la température de l'étuve. Sa température de surface est alors mesurée avec la caméra thermique. Il est alors possible d'écrire la loi reliant la température donnée par la caméra thermique avec celle réelle de l'échantillon.

2.2.4 Dissipation de la chaleur

Si l'échantillon n'est pas en contact avec un support, l'échange avec son environnement se fait exclusivement par transfert convectif et radiatif : $\dot{Q}_d = \dot{Q}_r + \dot{Q}_c$, le premier terme correspondant à la puissance totale échangée par transfert radiatif (second terme) et par transfert convectif (troisième terme).

Les deux transferts peuvent s'exprimer avec :

$$\dot{Q}_r = A\varepsilon\sigma(T_s^4 - T_0^4)$$

$$\dot{Q}_c = Ah(T_s - T_0)$$

Où A représente la surface qui échange, *ε la permittivité, σ la constante de Stefan Boltzmann, h le coefficient d'échange superficielle par convection, T_s la température de surface et T_0 la température de l'environnement.*

ε a été pris égal à 0.90 pour le caoutchouc naturel, h dépend du flux d'air autour de l'échantillon (convection naturelle ou forcée).

2.3 Dispositif de mesure de l'effet élasto-calorique

La figure 2.3 du manuscrit de thèse représente le banc de mesure développé dans le cadre de cette thèse pour mesurer l'effet élasto-calorique dans les différents matériaux testés.

L'échantillon est fixé à l'aide d'un porte-échantillon adapté qui le maintient sur les bords. La longueur entre les mors est de 20.0 mm. Un actionneur à axe unique (RSDG212, MISUMI Corporation, Japon) déforme l'échantillon pendant que la force générée est mesurée avec un capteur de force (XFTC300-200N, Measurement Specialities, France). Le déplacement de l'actionneur est mesuré à l'aide d'un vibromètre Laser (OFV-5000, Polytec, Allemagne). La variation de température est mesurée à l'aide d'une caméra thermique (NEC G-120, NEC, Japon) en admettant que le régime est adiabatique. La mesure de température est faite à +/- 0.1°C. La fréquence d'acquisition des images est de 10 Hz.

La caméra ne peut pas être directement connectée à un oscilloscope alors que tous les autres capteurs le peuvent. Pour pouvoir synchroniser les mesures de température avec les autres (force, déplacement), un capteur optique est utilisé.

2.4 Résultats

2.4.1 Capacité thermique massique – capacité thermique volumique

La figure 2.4 du manuscrit de thèse représente la variation de la capacité thermique massique C_p en fonction de la température, entre -20°C et 60°C, suivie par DSC. On observe une augmentation rapide de sa valeur jusqu'à -10°C puis une stabilisation autour de 0°C suivie par une lente diminution.

Autour de 20°C, une valeur de 1.212 J/g°C est mesurée ce qui conduit à une valeur de capacité thermique volumique C_v de 1684 KJ/m^3°C, en prenant 1390 kg/m^3 comme densité pour l'échantillon.

2.4.2 Calibration en température

La figure 2.5 du manuscrit de thèse représente la température mesurée à l'aide la caméra thermique (y) en fonction de la température de l'étuve (x). On observe une variation linéaire entre 0 et 50°C selon la loi y=0.72x +17.

2.4.3 Rupture à la traction

La figure2.6 du manuscrit de thèse représente l'évolution de la contrainte avec la déformation, avec une vitesse de déformation de 2.0mm/s. On note que la rupture se produit pour une déformation de 700 % sous une contrainte comprise entre 14 et 16 MPa.

2.5 Résultats et discussion des résultats obtenus avec le banc de caractérisation

2.5.1 vitesse de déformation

La figure 2.7 représente le déplacement en fonction du temps lorsque la vitesse maximale accessible de 320 mm/s inscrite dans la documentation est appliquée.

On constate que pour un déplacement maximum programmé de 80 mm, il faut en fait 0.5 s, soit une vitesse de 160mm/s.

Ceci reste malgré tout suffisant pour obtenir des vitesses de déformation compatible avec un régime adiabatique.

2.5.2 Propriétés mécaniques

Les figures 2.8 et 2.9 du manuscrit de thèse donnent quelques exemples de courbes (contrainte- déformation) pour des caoutchoucs naturels chargés avec des particules de carbone.

Les essais ont été réalisés trois fois à la suite pour des élongations variant entre 100% et 600%, à une vitesse de déformation de 2 mm/s.

Ils ont permis de mettre en évidence l'effet Mullins pour des élongations supérieures à 200% et l'apparition d'une élongation résiduelle dont la valeur est de l'ordre de 10% de l'élongation maximale appliquée pour les plus fortes valeurs d'élongations.

2.5.3 Friction interne

Afin d'éliminer l'effet Mullins, un échantillon a subi dix cycles d'élongation à 400%, à grande vitesse. Cet échantillon a été ensuite replacé dans le porte-échantillon pour éliminer l'élongation résiduelle.

L'échantillon a de nouveau été déformé à 400% à la vitesse maximale accessible par le dispositif, laissé 100 s avant que la déformation appliquée soit ramenée à zéro.
La figure 2.10 du manuscrit de thèse montre l'évolution de la température au cours du temps pour le cycle décrit juste au-dessus.

L'écart maximum de température mesurée est de 5° à la mise sous déformation et de -4.4°C lorsque celle-ci est annulée. Ceci montre bien que l'influence de la friction interne reste négligeable lors de l'essai puisque les deux valeurs mesurées sont proches en valeur absolue.

2.5.4 Dissipation de la chaleur dans l'environnement

La figure 2.11 du manuscrit de thèse montre l'évolution expérimentale de la température en fonction du temps, celle qu'on obtiendrait en ne prenant en compte qu'un échange radiatif et celle qu'on obtiendrait en ne prenant en compte l'échange radiatif et l'échange convectif. Elle montre clairement que l'échange convectif ne peut pas être négligé. L'ajustement des courbes calculées et mesurées montre que une valeur acceptable de h serait de 3 W/m²°C.

2.6 Conclusions

Ce chapitre a présenté le caoutchouc naturel utilisé dans le cadre de cette thèse et l'ensemble des mesures utiles à l'évaluation de l'effet élasto-calorique. Il a ainsi montré comment ont été déterminées l'ensemble des caractéristiques physiques nécessaires.

Il a également décrit le banc expérimental développé dans le cadre de cette thèse et validé le fait que ses performances lui permettaient de travailler en régime adiabatique. Il a également montré comment les différents effets présentés dans l'introduction (effet Mullins, élongation résiduelle, friction interne, dissipation thermique avec l'environnement) pouvaient ou non se manifester en fonction des conditions expérimentales utilisées.

Chapitre 3 : Effet élasto-calorique dans le caoutchouc naturel

3.1 Introduction

Le caoutchouc naturel présente une large variation de température (>5 C°) sous une contrainte réduite (<1.5 MPa). Il est non toxique et de faible coût, ce qui le rend très séduisant pour des applications de génération solide du froid.

Comme cela a été expliqué dans les chapitres précédents, quand le caoutchouc est étiré, il est le siège de l'effet Mullins et d'une cristallisation induite par la déformation.

Ces deux effets ont été largement étudiés mais sans que leur impact ait été analysé sur le couplage élasto-calorique.

Dans le cadre des alliages à mémoire de forme, la relation entre la variation de température et la contrainte appliquée est usuellement utilisée pour décrire l'effet élasto-calorique. Dans le cas du caoutchouc, cette description est rendue délicate à cause de son comportement fortement non linéaire et hystérétique du matériau. Une nouvelle approche basée sur la mise en évidence d'une relation linéaire entre les différentes énergies mises en jeu et la variation de température a été développée. Les performances peuvent alors être décrites par la valeur de la pente qui correspond à une donnée unique donc à un coefficient propre à un matériau testé.

Quelques considérations théoriques sur l'effet Mullins et la recristallisation induite par la déformation sont présentées en début de chapitre, suivies d'une présentation de la démarche expérimentale et d'une synthèse des résultats les plus parlants.

3.2 Théorie

3.2.1 Courbe déformation-contrainte, cristallisation induite, Effet Mullins

Le caoutchouc naturel, contrairement aux métaux et aux céramiques, peut être étiré, avec des contraintes relativement faibles, de plusieurs centaines de pourcents à cause de ces longues chaînes moléculaires. De plus, si l'on compare à l'étirement maximal possible, la déformation résiduelle permanente est petite : 0% pour un étirement à 100% et 60% pour un étirement à 600%, soit un dixième de la valeur.

La courbe déformation contrainte est fortement non linéaire comme le montre la figure 1.17 du manuscrit de thèse. Lorsqu'une grande valeur d'étirement est appliquée, les chaines moléculaires qui atteignent leur élongation maximale se comportent comme des cristaux, d'où le mécanisme de cristallisation induite par la déformation. Cela se traduit également par une augmentation de la contrainte au sein du matériau. Si cette cristallisation peut être facilement reconnue entre diffraction des rayons X, elle est plus difficile à mettre en évidence sur la courbe contrainte déformation, même si certains auteurs considèrent qu'elle

devient effective à la deuxième augmentation de la contrainte en fonction de la déformation. L'effet Mullins se caractérise par une différence entre un premier cycle et un deuxième cycle d'étirement pour des valeurs élevées d'étirement.

De façon schématique, l'effet Mullins rend le caoutchouc plus souple contrairement à la cristallisation.

3.2.2 Bilan d'énergie

Le premier principe de la thermodynamique permet d'écrire :

$$dU = dQ + dW$$

Où dU est la variation d'énergie interne, dQ la variation de chaleur reçue des sources extérieures,

dW la variation d'énergie mécanique appliquée au matériau.

Pour un caoutchouc idéal (élasticité purement d'origine entropique), on a dU=0 soit

$$dW = -dQ$$

Par conséquent, dans le cas d'un caoutchouc idéal, toute l'énergie mécanique peut être transformée en chaleur.

Ceci n'est bien évidemment pas vrai pour un caoutchouc réel, ne serait qu'à cause de l'extension des chaînes moléculaires sous étirement qui ne peut pas être infinie.

3.2.3 Energie mécanique

Dans le cas d'une déformation uniaxiale, l'énergie mécanique injectée dans un matériau élastique sous étirement s'écrit :

$$W = \int f dl$$

Où f est la force appliquée et dl le déplacement.

Les figures 3.1 a, b et c du manuscrit de thèse présente une courbe typique force déplacement pour un caoutchouc à la mise en étirement et au relâchement ainsi que l'énergie mécanique mise en jeu (W_1 à l'étirement et W_2 au relâchement).

3.2.4 Dissipation de chaleur

Si le caoutchouc n'est pas en contact avec un autre corps, les transferts avec l'environnement se fait uniquement pas transferts radiatif et convectifs.

Ils sont décrits par l'équation suivante : $\frac{\partial Q_d}{\partial t} = \frac{\partial Q_c}{\partial t} + \frac{\partial Q_r}{\partial t}$

Où Q_c représente la chaleur échangée par convection et Q_r celle échangée par rayonnement. Les deux flux de chaleurs s'expriment par :

$$\frac{\partial Q_c}{\partial t} = Ah(T_s - T_0)$$

$$\frac{\partial Q_r}{\partial t} = A\varepsilon\sigma({T_s}^4 - {T_0}^4)$$

Où A est la surface d'échange, h le coefficient d'échange superficiel par convection, T_s la température de surface du matériau, To la température de l'environnement, ε l'émissivité et σ la constante de Stefan Boltzmann.

3.3 Elaboration des matériaux et dispositif expérimental

3.3.1 Caoutchouc chargé par du noir de carbone

A) Présentation du matériau

Le matériau utilisé est du caoutchouc naturel chargé par du noir de carbone acheté à la compagnie NR 50°, TOHTO RUBBER, INDUSTRY CO., LTD, au Japon. L'épaisseur de la feuille est de 850 microns environ.

Des échantillons de 20 mm de large et de 60 mm de long sont découpés.

Comme cela a été rappelé précédemment, l'introduction de noir de carbone rend le matériau moins souple, ce qui permet d'obtenir des contraintes plus élevées.

B) Densité et capacité thermique volumique

Ce paragraphe reprend rapidement des éléments du chapitre II.

La capacité thermique C_p du matériau a été mesurée par DSC, avec une vitesse de chauffage de 10°C/min et en utilisant un creuset en alumine comme référente (capacité thermique de l'alumine : 0.80J/g°C)

La densité a été mesurée à l'aide d'un pycnomètre en utilisant l'eau distillée.

La densité et la capacité thermique ont été respectivement mesurées à 1390 kg/m^3 et 1.212 J/g°C, soit une valeur de capacité thermique volumique de 1684 KJ/m^3°C.

3.3.2 Banc de mesure du couplage élasto-calorique

Le banc de mesure est décrit par la figure 2.3 du manuscrit de thèse. Ce paragraphe reprend les points principaux du paragraphe 2.3. Sont à retenir, le facteur de correction (0.71) à appliquer sur la mesure de la température affichée par la caméra, la mesure du coefficient d'échange par convection h=3.0 W/m²K et la valeur de l'émissivité ε=0.9.

3.3.3 Paramètres à prendre en compte pour la mesure de l'effet élasto-calorique

Jusqu'à cent cycles ont été appliqués aux échantillons testés, pour des valeurs maximales de 100, 300, 400 et 600%.

Un cycle comprend une phase de mise en étirement, une phase de maintien à la valeur maximale de l'étirement et une phase de relâchement.

Pour limiter l'effet Mullins, les échantillons ont été préétirés. Après pré-étirement, l'existence d'une déformation résiduelle est systématiquement contrôlée.

La vitesse de déformation conditionne la nature du régime thermique, à des vitesses trop lentes, la mesure ne peut pas se faire en condition adiabatique.

Pour prendre en compte le fait que le caoutchouc étudié est viscoélastique, la déformation appliquée adopte la forme d'un signe temporel carré.

A) Vitesse rapide et vitesse lente

La vitesse de déplacement la plus rapide annoncée dans la documentation du robot mono axe est de 320 mm/s. A cause des valeurs de l'accélération et de la décélération (1.13 mm/s^2), cette vitesse ne peut être atteinte pour un déplacement inférieur à 150 mm.

Par conséquent, les mesures ont été faites avec une vitesse d'élongation de 1.0 s^{-1} pour les élongations maximales de 300, 400 et 600% et de 2.0 s^{-1} pour celle de 100%.

Des mesures ont également été réalisées à faible vitesse (0.05 s^{-1}) pour des élongations maximales de 400 et 600%.

B) Pré-étirement des échantillons

Pour éliminer l'effet Mullins, certains échantillons ont été préétirés en utilisant 10 cycles rapides pour une élongation au moins égale à l'élongation maximale qui sera utilisée par la suite.

Pour éliminer la déformation résiduelle, les échantillons sont démontés puis remontés sur le support.

3.4 Résultats

Les paragraphes qui suivent présentent respectivement quelques courbes typiques déformation –contrainte en fonction du niveau maximal de déformation appliquée, quelques exemples de courbes déformation –contrainte en fonction du niveau de déformation appliquée pour cent cycles et quelques courbes typiques température, contrainte et déformation en fonction du temps pendant un cycle.

3.4.1 Courbe déformation-contrainte

A) Courbe déformation contrainte pour deux vitesses sur un échantillon n'ayant pas subi de pré étirement

La figure 3.2a du manuscrit de thèse présente l'allure de la déformation appliquée à un échantillon en fonction du temps, les courbes 3.2b et 3.2c, la courbe déformation contrainte associée pour deux vitesses d'élongation.

L'échantillon n'a pas été préétiré et est soumis à douze cycles successifs, l'amplitude de la déformation maximale augmentant tous les trois cycles (100%, 300%, 400%, 600%).

On constate que, quelle que soit la vitesse de déformation utilisée, l'effet Mullins est apparent, que l'effet viscoélastique lié à la vitesse de déformation est aussi présent car la contrainte développée pour un même niveau de déformation n'est pas la même et qu'à partir de 300% d'élongation maximale, quelle que soit la vitesse utilisée, une déformation résiduelle permanent apparaît.

B) Cycles sur un échantillon non préétirés à grande vitesse d'élongation

Chaque échantillon est soumis à cent cycles successifs d'élongation relâchement. Quatre valeurs de déformations (100, 300, 400 et 600 %) sont utilisées pour chaque groupe de 100 cycles, ce qui correspond respectivement aux figures 3.3 a, b, c et d du manuscrit de thèse. La courbe déformation contrainte présente une large hystérésis pour le premier cycle. On constate également une diminution de la contrainte mesurée à la déformation maximale en fonction du nombre de cycles. Cette diminution est plus rapide pour les cycles de numéros les plus bas. Cet effet est moins marqué sur les cycles réalisés avec une déformation maximale de 100%.

Pour chaque deuxième cycle, on observe un seul changement de signe pour la dérivée seconde de la fonction décrivant la contrainte en fonction de la déformation lorsque la déformation maximale est de 100% (cercle gris) et deux changements de signe (cercles gris et noir) pour les autres valeurs.

Les deux valeurs correspondent de déformation ε_{c1} et ε_{c2} augmentent avec la déformation maximale ε_{max}. Si ε_{c1} ne dépend pas du nombre de cycle, il est clair que la valeur de ε_{c2} augmente avec le nombre de cycle (disque noir sur la courbe du centième cycle).

3.4.2 Variation de température en fonction du temps

La figure 3.4 du manuscrit de thèse présente la variation de température mesurée à l'aide le caméra thermique pour une déformation maximale de 400%, lors d'un premier cycle et d'un second. L'échantillon testé n'a pas été préétiré et le second cycle est réalisé quand l'échantillon est revenu à température ambiante.

On observe une augmentation rapide de la contrainte à la mise en étirement suivant d'une décroissance exponentielle pendant la phase de maintien et d'un retour à zéro au relâchement.

La valeur de la contrainte maximale σ_1 et celle σ_2 à la fin de la phase de maintien sont plus petites pour le deuxième cycle.

La variation de température ΔT_1 à la mise en étirement est plus grande que la valeur absolue de celle notée ΔT_2 observée au relâchement, quel que soit le cycle. L'écart entre les deux valeurs est moins élevé pour le second cycle que pour le premier. La valeur de ΔT_1 sont est plus élevée au premier cycle qu'au second.

3.5 Résultats et discussion

3.5.1 Relation entre la contrainte et la variation de température

A) Nombre de cycles et contraintes

Les figure 3.5 a et b du manuscrit de thèse représente l'évolution de σ_1 et de σ_2, en fonction du cycle, pour 4 valeurs de déformations maximales (100, 300, 400 et 600%).

Plus la déformation maximale est élevée, plus les deux valeurs de contraintes sont grandes. Pour les trois déformations les plus élevées, on observe une forte diminution de ces contraintes entre le 1er et le 2ème cycle, ce qui s'explique par l'effet Mullins, précédemment présenté.

Le tableau 3.1 du manuscrit donne le taux de réduction en % des valeurs de contrainte entre le premier et le second cycle, le second et le troisième et le second et le centième. Les résultats pour la déformation maximale à 100% confirment la précédente observation.

Pour la contrainte σ_1 et pour les déformations maximales de 300, 400 et 600%, on note un minimum du taux pour la déformation maximale de 300% entre le premier et le second cycle et le second et le troisième cycle, et une augmentation continu de ce taux entre le second cycle et le centième cycle.

Pour la contrainte σ_2 et pour les déformations maximales de 300, 400 et 600%, on note un minimum du taux pour la déformation maximale de 300% entre le second et le troisième cycle, et une augmentation continu de ce taux entre le premier cycle et le second cycle. Les valeurs du taux sont quasiment identiques entre le deuxième et le centième cycle à 300% et 400% alors que la valeur à 600% est plus forte.

Si la contribution de l'effet Mullins à la diminution de la contrainte est prépondérante entre le premier et le second cycle, des effets de fatigue sont à prendre en compte pour expliquer ce qui se passe à partir du second cycle. Ces effets sont clairement plus importants pour un cycle à 600% de déformation maximale.

En bon accord avec ce qui a été présenté au paragraphe 3.4.1, les variations observées sur les deux contraintes sont clairement petites pour une déformation maximale de 100%.

B) Nombre de cycles et variation de température

La variation de température en valeur absolue à la mise sous étirement $|\Delta T_1|$et au relâchement $|\Delta T_2|$ est représentée par la figure 3.6 du manuscrit de thèse, en fonction du nombre de cycles et pour les 4 valeurs de la déformation maximale.

Pour 600% de déformation maximale, on observe une stabilisation de la valeur de $|\Delta T_1|$ après le sixième cycle, celle pour $|\Delta T_2|$ intervenant après le cinquième.

Pour 300% et 400% de déformation maximale, on observe une stabilisation de $|\Delta T_2|$ à partir du premier cycle alors que $|\Delta T_1|$ connait une diminution entre le premier et le second cycle.

Pour 100% de déformation, $|\Delta T_1|$ et $|\Delta T_2|$ restent stables dès le premier cycle.

La stabilisation rapide de $|\Delta T_1|$ et de $|\Delta T_2|$ laisse supposer que la fatigue n'influence pas de façon significative l'effet élasto-calorique.

Le calcul du taux de réduction de la contrainte σ_1 et de celui de $|\Delta T_1|$ entre le premier et le second cycle conduit à des résultats très similaires (47.3% pour 44.9%, 32.3% pour 39.3% et 48.4% pour 52.4%). Ceci montre que l'effet à prendre en compte pour expliquer la décroissance observée est bien l'effet Mullins.

C) Contrainte et variation de température

Les figures 3.7 a et b du manuscrit de thèse représente l'évolution de $|\Delta T_1|$ et de $|\Delta T_2|$, respectivement en fonction des contraintes σ_1 et σ_2, pour les quatre valeurs de déformations maximales.

Pour la déformation maximale de 600%, une augmentation de température $|\Delta T_1|$ de 4°C à 5MPa et une diminution de température, en valeur absolue, $|\Delta T_2|$ de 3.5°C à 4°C à 3.5-6 MPa sont observées. Ceci est à rapprocher de la valeur de 4°C observée pour des alliages à mémoires de forme, mais sous une contrainte de 150 MPa et montre tout l'intérêt de ces caoutchoucs à bas niveau de contrainte.

$|\Delta T_1|$ et $|\Delta T_2|$ présentent une évolution similaire. Il est à noter que des écarts de température différents peuvent être obtenus pour un même niveau de contrainte correspondant à des valeurs différentes de déformations maximales. Par exemple, à 4MPa, $|\Delta T_1|$ prend les valeurs de 1.9°C, 2.7°C et 3.5°C pour des déformations maximales de 300, 400 et 600%. Le même constat peut être fait pour $|\Delta T_2|$ (1.6°C à 300%, 2.3°C à 400% et 3.4°C à 600%). Par conséquent, il n'est pas possible d'utiliser une relation entre $|\Delta T|$ et σ pour caractériser l'effet élasto-calorique dans ces caoutchoucs.

Dans le cas du caoutchouc idéal, l'énergie mécanique mise en jeu est égale à l'énergie

thermique. Il est intéressant de voir s'il est possible de trouver une relation décrivant le couplage élasto-calorique en utilisant les énergies dans le cas des caoutchoucs étudiés dans le cadre de cette thèse, sachant qu'ils peuvent s'écarter du modèle idéal, ne serait-ce qu'à cause d'un mouvement non complètement libre de leurs chaînes moléculaires, sous déformation.

3.5.2 Energie mécanique et variation de température

Comme il l'a été rappelé précédemment, l'énergie mécanique introduite dans un matériau peut contribuer à la variation d'énergie interne ou à la variation de chaleur.

Les figures 3.8 a et b représentent l'évolution de $|\Delta T_1|$ et de $|\Delta T_2|$ en fonction de l'énergie mécanique dans le matériau à l'étirement (W_1) et au relâchement (W_2), calculée en intégrant la force au cours du déplacement.

Une relation linéaire est observée quelle que soit la valeur maximale de la déformation. Ceci permet de caractériser l'effet élasto-calorique développé au sein de l'échantillon sans avoir en prendre en compte son histoire.

3.5.3 Rendement de la conversion élasto-thermique

La chaleur échangée à l'étirement (i=1) et au relâchement (i=2) peut être calculée à partir de la mesure de la variation de température à l'aide de la caméra thermique (ΔT_i) à l'aide de

$$-Q_i = \rho V C_p(\Delta T_i)$$

où ρ est la densité de l'échantillon, V son volume et C_p sa capacité thermique.

Le rendement, en pourcent, peut alors s'exprimer par : $\eta_i = -\frac{Q_i}{W_i} \times 100$

Les figures 3.9 a et 3.9 b du manuscrit de thèse présente les valeurs du rendement à la mise sous étirement et au relâchement en fonction du nombre de cycles pour les quatre valeurs maximales de la déformation.

Pour 100% de déformation maximale, on observe de fortes variations du rendement manifestement liées à la difficulté de mesurer de façon précise de variations de températures autour de 0.3°C alors que l'incertitude de mesure est de +/- 0.1°C.

De façon grossière, le rendement moyen peut être estimé à 40% et semble indépendant du nombre de cycles. Cette valeur est inférieure à celle obtenue pour les autres déformations maximales. Ceci peut s'expliquer par le fait qu'aux plus faibles valeurs de déformation, la contribution de l'énergie mécanique à la variation d'énergie interne n'est pas négligeable (cf. chapitre 1) et qu'un comportement entropique est favorisé par les déformations les plus fortes. Un optimum est observé autour de la valeur de déformation maximale de 300%.

Quelle que soit la valeur de la déformation maximale, on observe une augmentation du rendement à l'étirement (η_1) entre le premier et le second cycle de 10% environ. Il semblerait que l'effet Mullins, en augmentant la mobilité des chaînes moléculaires, favorise la conversion énergétique.

On constate une valeur moyenne du rendement η_1 autour de 70% pour des déformations maximales de 300 et 400% et de 60% pour une déformation maximale de 600%. Cette diminution pourrait s'expliquer par le fait qu'à partir de 600% d'élongation, les chaînes moléculaires ne puissent plus s'étendre et que l'énergie mécanique contribue à nouveau à la variation d'énergie interne comme dans le cas d'un solide.

En conclusion, la faible valeur du rendement pour la déformation maximale la plus faible s'expliquerait par une contribution importante de l'énergie mécanique à la variation d'énergie interne. Cette contribution tendrait à diminuer en faveur d'un comportement entropique pour les déformations maximales intermédiaires et qu'entre 400% et 600%, la mobilité des chaînes moléculaires diminueraient induisant une redistribution de l'énergie mécanique vers l'énergie interne. Ce point particulier fait l'objet du paragraphe suivant.

3.5.4 Energie interne pour une déformation à faible vitesse

A) Déformation critique

L'énergie interne a été évaluée avec une vitesse d'élongation de 0.05 s^{-1} au lieu de 1.0s^{-1} car le retard entre la variation de la température et l'établissement de la contrainte est plus faible.

L'énergie interne est calculée en faisant la différence entre l'énergie mécanique et la chaleur échangée par convection et par rayonnement avec l'environnement.

La figure 3.10 du manuscrit de thèse représente l'énergie interne, l'énergie thermique et l'énergie mécanique au cours d'un cycle à déformation maximale de 400%, en fonction de la déformation.

Jusqu'à une valeur de déformation de 160%, l'énergie interne augmente puis diminue jusqu'à 0.

L'énergie thermique commence à augmenter dès que l'énergie interne diminue et suit la courbe de l'énergie mécanique.

On distingue donc trois zone : en-dessous de 160%, où toute l'énergie mécanique introduite contribue à l'énergie interne, au-dessus de 190%, où toute l'énergie mécanique est dissipée sous forme de chaleur et une zone intermédiaire de transition entre 160% et 190% où l'énergie interne décroît vers 0 pendant que l'énergie thermique croit de 0 jusqu'à rejoindre la courbe de l'énergie mécanique.

Il faut 4.2 s pour atteindre la valeur de 160%, ce qui se traduit par une augmentation de

la température avec un retard de 4.2s sur la déformation.

Pour vérifier si la transition entre une élasticité énergétique et une élasticité entropique dépend de la valeur de la déformation ou du temps d'étirement, l'expérience est réalisée avec une vitesse de $0.10s^{-1}$. Le temps nécessaire pour atteindre la précédente zone de transition sera donc deux fois plus court.

Les résultats obtenus sont présentés sur la figure 3.11 et montre clairement que la transition qui apparaît autour de 180% (contre 160%) est très certainement liée à la valeur de la déformation.

Pour des vitesses d'élongation plus élevées (déformation maximale à 400%, $1.0s^{-1}$ sur la figure 3.4), un retard de 0.5s environ est observé entre la montée en température et la mise sous étirement. Ceci tendrait à confirmer que le mécanisme décrit précédemment s'applique encore dans ce cas.

La figure 3.12 du manuscrit de thèse représente l'énergie interne, l'énergie thermique et l'énergie mécanique au cours d'un cycle à déformation maximale de 600%, en fonction de la déformation, pour une vitesse d'élongation de $0.05s^{-1}$. On observe à nouveau une transition similaire à celle observée pour une déformation maximale de 400% mais à 260% au lieu de 160 %.

B.) Deuxième augmentation de l'énergie interne.

Un examen attentif de la figure 3.13 met en évidence une ré-augmentation de l'énergie interne lorsque la déformation atteint 450%.

La figure 3.13 du manuscrit de thèse présente la contrainte en fonction de la déformation pour une vitesse d'élongation de 0.05s-1 et pour les déformations maximales de 400 et 600%. Il est important de rappeler que les niveaux de contrainte atteints sur ces courbes dépendent de la vitesse d'élongation (cf. figure 3.2).

On constate que la contrainte commence à augmenter autour de 300% et fortement mais de façon linéaire à partir de 450%.

Le cercle sur la figure montre la valeur de la déformation pour laquelle la dérivée seconde de la courbe change de signe, le carré marque la valeur de 450%.
Il est bien connu que la contrainte augmente fortement dans les zones où les chaînes moléculaires sont commencent à être complètement étirées.

Par conséquent, on peut considérer que la cristallisation débute vers 300% et qu'à 450% les chaînes moléculaires sont complétement étirées et donc peu mobiles. Cette valeur correspond d'ailleurs à celle où l'énergie interne commence à ré augmenter.

Le mécanisme peut alors être décrit de la façon suivante : tant que la déformation est en dessous de la première valeur seuil de déformation, l'énergie mécanique contribue fortement

à l'énergie interne. Cette contribution va ensuite se redistribuer vers l'énergie thermique jusqu'à ce que le matériau adopte un comportement d'élasticité entropique. Au-dessus d'une deuxième valeur seuil de déformation marquée par une variation forte mais linéaire de la contrainte avec la déformation, les chaînes moléculaires sont complétement étirées et par conséquent peu mobiles. On assiste alors à une ré augmentation de l'énergie interne au détriment de l'énergie thermique.

3.6 Conclusions

L'effet élasto-calorique a été étudié dans un caoutchouc chargé avec du noir de carbone. Il a été montré que des variations de température similaire à celles mesurées sur des alliages à mémoire de forme pouvaient être obtenues mais à des valeurs de contrainte beaucoup plus basses.

Il a été mis en évidence une relation linéaire entre la variation de température et l'énergie mécanique injectée dans le système pendant un cycle déformation-contrainte, ce qui permet de caractériser les matériaux, indépendamment de leur histoire et du niveau de déformation.

L'influence de l'effet Mullins et de la cristallisation induite par la contrainte a été analysée. Un mécanisme basé sur l'existence de deux valeurs seuil de déformation, facilement identifiables sur la courbe de déformation-contrainte a été proposé pour expliquer la variation du rendement, lors d'une conversion élasto-calorique.

Chapitre 4 : Effet élasto-calorique dans le P(VDF-TrFE-CTFE)

4.1 Introduction

Parmi différentes familles de polymères, le P(VDF-TrFE-CFE) et le P(VDF-TrFE-CTFE) sont connus pour présenter un large effet électro calorique. Il est donc intéressant d'évaluer leurs performances pour le couplage élastocalorique.
Ceci constitue l'objectif de ce chapitre.

4.2 Expérimentations

4.2.1 Cas du terpolymère P(VDF-TrFE-CTFE)

Les polymères à base de PVDF sont connus pour être ferroélectriques et largement utilisés comme matériaux de capteurs ou d'actionneurs. Ils présentent également l'avantage d'être sans plomb.

Il a été reporté dans la littérature que des films de P(VDF-TrFE) peuvent présenter un effet électro calorique fort avec une variation de température de 12.6°C sous réserve de travailler au-dessus de la transition ferroélectrique-para électrique (70°C) . D'autres articles font état de variations de température comprises entre 5 et 15°C, pour des températures comprises entre 30 et 55°C, pour le P(VDF-TrFE-CFE) et le P(VDF-TrFE-CTFE). Ces polymères présentent une température de transition plus basse que le P(VDF-TrFE) à cause de l'introduction d'un troisième monomère. Ils ont également des permittivités diélectriques moins élevées.

Le tableau 4.1 du manuscrit de thèse compare les propriétés mécaniques de ces polymères avec une céramique de type PZT.

4.2.2 Elaboration

La figure 4.1 du manuscrit de thèse présente la méthode de réalisation des films polymères.

Les poudres de polymères, achetées à Piezotech SA, sont mises en solution dans la Méthyléthylcétone à 70°C pendant 4h. La solution est déposée sur une plaque de verre puis séchée dans un étuve à 70°C pendant 2h avant d'évaporer le solvant. Les films ainsi obtenus sont déposés sur une plaque en téflon puis recuit à 110°C pendant 2h afin d'augmenter la cristallinité. Ils ont une épaisseur moyenne de 40 microns.

Comme il le sera dit plus tard, ces films n'ont qu'une activité élasto calorique faible. Pour les rendre plus actifs, il faut les étirer jusqu'à 1200%, ce qui aligne les chaines polymères dans la phase amorphe, modifie les propriétés de la phase cristalline et dans une certaine limite provoque de la cristallisation qui peut créer des ponts

supplémentaires dans le volume du polymère.

L'épaisseur obtenue en moyenne sur des films étirés est de 10 microns. Les échantillons testés présentent une longueur de 30 mm et une largeur de 20 mm.

4.2.3 Mesures des propriétés

A) Capacité thermique volumique

Elle est déterminée à partir de la densité du film mesurée à l'aide d'un pycnomètre et de la capacité thermique obtenue par DSC.

B) Mesures mécaniques en statique et effet élasto calorique pour un film de P(VDF-TrFE-CTFE) non étiré

La figure 4.2 du manuscrit de thèse présente le schéma de principe du banc utilisé pour déterminer l'effet élasto-calorique pour un film de P(VDF-TrFE-CTFE) non étiré. L'actionneur utilisé pour déformer l'échantillon est un système à axe unique (RSDG212, MISUMI).

Pour la mesure des propriétés mécaniques en statique, un échantillon de 10 mm est utilisé avec une vitesse de 2.0 mm/s soit 0.0066 s^{-1}.

Pour la mesure de l'effet élasto calorique, l'échantillon a une longueur de 30 mm. Une déformation de 2% à 20% a été utilisée avec une vitesse d'élongation de 1.0 s^{-1} environ. Pour une déformation de 400%, la vitesse d'élongation a été fixée à 0.80 s^{-1}. Le choix de ces paramètres garantit un régime adiabatique pendant l'expérience.

C) Effet élasto calorique sur un film de P(VDF-TrFE-CTFE) pré étiré

La figure 4.3 du manuscrit de thèse présent le schéma de principe du banc utilisé pour cette mesure. L'actionnement est réalisé à l'aide d'un moteur linéaire (XMS50, Newport), pouvant appliquer de grandes vitesses de déformation avec une accélération et une décélération très rapide.

La contrainte développée dans le matériau dépend de la vitesse d'étirement à cause de la viscoélasticité du polymère.

4.3 Résultats et discussions

4.3.1 Propriétés mécaniques d'un film de P(VDF-TrFE-CTFE) non préétiré

La figure 4.4 du manuscrit de thèse présente la courbe contrainte-déformation d'un film de P(VDF-TrFE-CTFE) non étiré, avec une vitesse d'élongation de 0.0066 s^{-1}. La contrainte et la déformation sont calculées à partir des dimensions de l'échantillon avant étirement. La contrainte augmente très rapidement jusqu'à ce que la déformation

atteigne 20%. Cela correspond à un domaine élastique pour ce polymère. On observe ensuite un plateau jusqu'à une valeur de déformation de 500% environ puis une ré-augmentation de la contrainte avec la déformation jusqu'à une valeur de déformation autour de 1050%. Cette zone correspond au domaine plastique. Au-delà, on observe à nouveau une relation linéaire entre la contrainte et la déformation jusqu'à la rupture donc un domaine élastique.

4.3.2 Effet élasto-calorique pour un film de P(VDF-TrFE-CTFE) non préétiré

La figure 4.5 du manuscrit de thèse présente la variation de température mesurée à l'aide d'une caméra thermique IR, la contrainte et la déformation, lorsqu'on étire un film de P(VDF-TrFE-CTFE) non préétiré en fonction du temps. Un cycle (durée 20s) se caractérise par une valeur maximale de déformation dont la valeur croît avec le nombre de cycles suivi d'un retour à déformation nulle. Le dernier cycle a été réalisé avec une déformation de 20%. La vitesse d'élongation est dans tous les cas de 1.25 s^{-1}.

A partir d'une déformation de 10%, on n'observe plus d'évolution de la contrainte alors que ce phénomène était apparu en statique qu'à partir de 20%. Ceci peut s'expliquer par le fait que le matériau soit passé dans le domaine plastique dès 10% de déformation ou par un effet viscoélastique lié à la variation de l'accélération (et donc de la vitesse instantanée) au cours du cycle.

Si on évalue la déformation permanente avant un étirement de 20% et après un étirement de 20%, on trouve une valeur de 1.3%, ce qui est relativement faible. Par conséquent, la saturation de la contrainte observée dès 10% de déformation est certainement liée à un phénomène viscoélastique.

La variation temporelle de température observée est beaucoup plus rapide que le cycle de contrainte et beaucoup moins régulière. Ceci donne à penser qu'elle n'est pas due à un effet élasto calorique, ce qui permet de conclure que, celui-ci ne se développerait pas dans le premier domaine élastique d'un film de P(VDF-TrFE-CTFE) non préétiré.

La figure 4.6 du manuscrit présente la même expérience mais pour une valeur beaucoup plus élevée de la déformation (400% contre 20%).

Une augmentation rapide de la contrainte est observée à la mise en étirement suivie d'une diminution jusqu'à une valeur plateau pendant presque toute la durée du maintien de la déformation maximale puis d'une diminution brutale jusqu'à 0, juste avant le début du relâchement de l'étirement. Ceci suggère l'apparition d'une grande déformation permanente, ce que confirment la figure 4.7 du manuscrit de thèse où la courbe contrainte-déformation présente un large hystérésis et la valeur de 320%

mesurée pour cette déformation constante. Une élévation de température de 2.7°C est observée à la mise sous étirement contre une diminution de 0.2°C au relâchement.

Lorsque l'énergie mécanique induite par la déformation est petite, la variation de température liée à l'effet élasto-calorique l'est également. Pour ce matériau, une élévation de température de 2.9°C (contre 2.7°C mesurée) et une diminution de 0.07°C (contre 0.2°C mesurée) ont été calculées.

Il conviendra d'exploiter le domaine des fortes déformations (>1050%) où un deuxième comportement élastique est observé et où l'énergie mécanique induite par la déformation sera certainement beaucoup plus grande.

4.3.3 Effet élasto-calorique pour un film de P(VDF-TrFE-CTFE) préétiré

A) Variations de température et de contrainte observées au cours du temps

Le film polymère a été étiré à 1200% avant d'être testé, pour travailler dans le deuxième domaine élastique du matériau (au-dessus de 1050%), où l'énergie mécanique mise en jeu sera grande. Afin d'éviter les effets viscoélastiques liées à une variation trop lente de la vitesse instantanée, un actionneur (XMS50) a été utilisé. La figure 4.8 du manuscrit de thèse présente la variation de température et de contrainte pour un cycle de 20 s avec une déformation maximale de 10%, à une vitesse d'étirement de 20 s^{-1}. On observe une augmentation très rapide de la contrainte à l'étirement puis une décroissance rapide jusqu'à une valeur plateau conservée pendant tout le maintien à la déformation maximale. Le cycle se termine par un retour rapide à zéro de la contrainte lorsque la déformation est ramenée à 0. Une élévation de température est observée, avec un léger retard, à l'établissement de la contrainte, suivi d'un retour à température ambiante pendant le maintien de la déformation. Une diminution de température est ensuite observée à la disparition de la contrainte. Celle-ci est beaucoup plus significative que celle qui avait été observé sur le film non pré étiré.

B) Effet élasto calorique en fonction de la déformation maximale

La figure 4.9 du manuscrit de thèse présente la variation de température, en valeur absolue, pour un régime adiabatique, à la mise en étirement et au relâchement ainsi que la contrainte maximale mesurée en fonction de la déformation maximale pour des valeurs comprises entre 0 et 14 %.

Une variation linéaire de la contrainte est observée jusqu'à 12%. Ceci confirme que les mesures ont bien été effectuées dans un domaine élastique.

La variation de température, en valeur absolue, augmente plus ou moins de façon parabolique. L'écart entre la variation de température à la mise sous étirement et au

relâchement augmente avec la déformation maximale.

Pour comparer les résultats obtenus avec ceux publiés sur d'autres familles de matériaux, deux coefficients caractéristiques de la conversion ont été introduits :

Coefficient élasto calorique liée à la déformation $\beta = \frac{C_v}{T_0}\frac{\partial(\Delta T)}{\partial \lambda} = -\frac{\partial S}{\partial \varepsilon}$

Où C_v, T_o, ΔT, λ, S et ε sont respectivement la capacité thermique volumique, la température ambiante, la variation de température liée à l'effet élasto-calorique, en régime adiabatique, l'élongation, l'entropie et la déformation.

Coefficient élasto calorique liée à la contrainte $\gamma = \frac{\partial S}{\partial \sigma}$

Où σ est la contrainte.

Pour une déformation de 12%, β a été trouvé égal à 179 KJ/m^{3}K et γ a 0.14 KJ/m^{3}K. Ces résultats sont à comparer à ceux trouvés sur le caoutchouc (chapitre III) : β = 8.7 KJ/m^{3}K et γ=33 0.14 KJ/m^{3}K à une déformation de 600% et à ceux de fils de NiTi pour lesquels des valeurs de 2740 0.14 KJ/m^{3}K et 0.17 0.14 KJ/m^{3}K ont été publiés.

Le tableau 4.4 du manuscrit de thèse reprend ces données et propose les valeurs typiques pour la capacité thermique, le module d'Young, la variation de température en régime adiabatique, la variation d'entropie, la chaleur volumique échangée et l'énergie volumique mécanique.

Il est à rappeler qu'un intérêt de ces polymères est également leur légèreté et que ramenés à l'unité de masse, les valeurs obtenues pour les coefficients de conversion les rendent encore plus attractifs.

Dans le cas des alliages à mémoire de forme, la variation d'entropie sous déformation correspond à une transition de phase (austénite-martensite), pour laquelle la contribution principale à cette variation est liée à la chaleur latente. Dans le cas des caoutchoucs, la variation d'entropie a été reliée à des phénomènes de cristallisation sous étirement, en complément de l'élasticité entropique (orientation des chaînes moléculaires induite par la déformation). Dans ces deux cas, la valeur de la chaleur échangée peut dépasser celle de l'énergie mécanique introduite dans le matériau à cause de la chaleur latente associée à cette transition. L'énergie interne est donc une fonction de la déformation qui induit la transition de phase.

Dans le cas d'un polymère dont l'élasticité est purement d'origine entropique (caoutchouc idéal), la variation d'énergie interne ne dépend que de la température, comme c'est le cas pour un gaz parfait. Par conséquent, les valeurs de la chaleur échangée en régime isotherme et de l'énergie mécanique introduite dans le matériau seront les mêmes en valeur absolue.

Afin d'éclairer les mécanismes pouvant expliquer les effets élasto-caloriques observés dans les polymères P(VDF-TrFE-CTFE), l'énergie mécanique introduite dans le matériau (W), la chaleur échangée en régime isotherme ($Q_{isotherme} = C_v \Delta T_{adiabatique}$) et la variation d'énergie interne ($\Delta U = Q + W$) ont été calculées. Ces calculs ont été réalisés à partir de la mesure expérimentale de la température adiabatique pour Q et des courbes expérimentales « déformation-contrainte » pour W, à la mise sous étirement et au relâchement, avec différentes valeurs de déformation maximale. Il a été considéré que la capacité volumique thermique est indépendante de la déformation et que l'effet élasto calorique ne dépend pas de la température.

La figure 4.10 du manuscrit de thèse représente ces trois grandeurs en fonction de la déformation maximale appliquée. La différence observée entre les résultats obtenus à la mise sous étirement et au relâchement s'explique par des phénomènes irréversibles, comme les pertes mécaniques. L'énergie mécanique et la chaleur échangée, en valeur absolue, présentent des valeurs similaires, ce qui conduit à une variation d'énergie interne nulle. Ceci montre que toute l'énergie mécanique introduite dans le système se retrouve sous forme de chaleur. Ce comportement est le comportement classique d'un matériau élastomère (élasticité purement entropique). Par conséquent, l'effet élasto calorique observé ne dépend pas de la phase cristalline mais uniquement de la phase amorphe. Il a été montré que pour ces mêmes matériaux, l'effet électro calorique était par contre lié à la phase cristalline. En conséquent, les deux effets sont découplés et peuvent être cumulatifs.

4.4 Conclusions

L'évaluation de l'effet élasto calorique pour des films de P(VDF-TrFE-CTFE) préétiré montre un coefficient élasto calorique lié à la contrainte proche de celui des alliages à mémoire de forme et un coefficient élasto calorique lié à la déformation plus élevé que celui du caoutchouc naturel.

Il a été montré que l'effet élasto- calorique était lié au comportement mécanique de la phase amorphe et qu'il ne dépendait pas de la phase cristalline, contrairement à ce qui a été observé pour l'effet électro calorique.

Par conséquent, les deux effets pourraient être simultanément exploités pour ce matériau.

Chapitre 5 : Conclusion Générale et Perspectives

5.1 Conclusions

L'effet élasto calorique est basé sur la variation d'entropie induite par la déformation. Son exploitation pourrait être à la base des futurs systèmes de génération du froid tout solide surtout s'il utilise des matériaux non toxiques et de faible coût de production et qu'il donne accès à des grandes variations d'énergie.

Dans cette thèse, l'effet élasto calorique a été évalué sur des caoutchoucs chargés par du noir de carbone et des terpolymères.

Le chapitre 1 a discuté le principe, les avantages et les inconvénients du couplage magnétocalorique, du couplage électro calorique et du couplage élasto calorique. Il a présenté quelques systèmes de génération du froid les utilisant et décrit les matériaux utilisés, en insistant sur les effets susceptibles d'agir sur la conversion qui pourraient s'y développer : effet Mullins, fatigue, déformation permanente, friction interne, cristallisation…

Le chapitre 2 a décrit les techniques d'élaboration des matériaux et les outils d'investigations en présentant particulièrement le banc de caractérisation de l'effet élasto calorique développé au laboratoire dans le cadre de cette thèse. Il a également permis de montrer que les performances de ce banc le rendaient propre à sa destination.

Le chapitre 3 s'est intéressé à la caractérisation du comportement d'un caoutchouc naturel chargé par du noir de carbone. Une variation de température de plusieurs degrés a pu être mesurée. S'il est courant d'utiliser la relation déformation/contrainte en fonction de la variation de température pour évaluer l'effet élasto calorique, les expériences ont montré que cette méthode ne pouvait pas s'appliquer à ce matériau, à cause de lois de comportement mécanique fortement non linéaires, hystérétiques et très évolutives dans le temps. Une nouvelle méthode de caractérisation a donc été proposée, basée sur la mesure de la variation de l'énergie mécanique en fonction de la température. Celle-ci a montré une loi de comportement linéaire. A partir d'un bilan énergétique effectué pendant l'essai, il a été possible de calculer un rendement énergétique et de prendre en compte l'effet Mullins et la cristallisation sous déformation qui existe dans le caoutchouc naturel.

Le chapitre 4 s'est intéressé à la caractérisation du comportement de terpolymères. Il a montré qu'un pré-étirement était nécessaire pour obtenir un effet élasto calorique significatif. La valeur du coefficient de couplage élasto calorique lié à la contrainte est similaire à celui obtenu sur des fils de NiTi et celle du coefficient de couplage élasto calorique lié à la déformation très supérieur à celui du caoutchouc naturel.

En évaluant l'énergie mécanique introduite dans le matériau pendant un cycle d'étirement-relâchement, la chaleur échangée en régime isotherme et la variation d'énergie interne, il a été montré que l'élasticité dans ces matériaux est exclusivement d'origine entropique. L'effet élasto calorique ne serait donc pas lié à des phénomènes de cristallisation, ce qui n'est pas le cas pour l'effet électro calorique qui s'y développe. Il serait donc possible d'exploiter simultanément au sein d'un même matériau les deux effets.

5.2 Travaux futurs

L'effet élasto calorique sur le caoutchouc naturel n'a pas été évalué en fonction du taux de charges. Il pourrait être intéressant de voir comment ce taux et comment l'organisation des particules modifient les performances du couplage élasto calorique.

Concernant les travaux sur les terpolymères, il conviendrait de vérifier que l'effet cumulatif espéré, du fait des mécanismes indépendants pour les deux couplages, l'est complétement dans la mesure où l'électrostriction de ces matériaux peut modifier la courbe déformation-contrainte, et donc l'effet élasto-calorique, quand on y applique le champ électrique nécessaire pour développer l'effet électro-calorique.

Ceci ouvre des perspectives sur la recherche de cycles champ électrique-déformation optimaux pour exploiter au mieux les deux effets.

FOLIO ADMINISTRATIF

THESE DE L'UNIVERSITE DE LYON OPEREE AU SEIN DE L'INSA LYON

NOM : YOSHIDA
(avec précision du nom de jeune fille, le cas échéant)

DATE de SOUTENANCE : 08/07/2016

Prénoms : Yukihiro

TITRE : Effet élastocalorique dans le caoutchouc naturel et le terpolymère : mécanismes responsables de la variation de température et bilan énergétique sous déformation

NATURE : Doctorat

Numéro d'ordre : 2016LYSEI070

Ecole doctorale : ELECTRONIQUE, ELECTROTECHNIQUE, AUTOMATIQUE (EEA)

Spécialité : Génie Electrique

RESUME :

Les effets électrocaloriques, qui se traduisent par une variation de température induite par une variation d'entropie ont été étudiés comme alternative aux systèmes de réfrigération utilisant un cycle de compression/détente. Le travail de thèse se focalise sur l'étude de l'effet élastocalorique dans le caoutchouc naturel et le terpolymère (P(VDF-TrFE-CTFE).

En premier lieu, l'effet élastocalorique dans le caoutchouc naturel qui compte parmi les meilleurs candidats, a été évalué pour des cycles de déformation réalisés avec différentes valeurs d'allongement. Une variation de température de 4 °C a pu être observée. Il est usuel d'utiliser la relation déformation/contrainte en fonction de la variation de température pour évaluer l'effet élastocalorique. Il a été démontré que cette méthode ne peut pas être utilisée dans le cas du caoutchouc naturel et qu'elle doit être remplacée par la mesure de la variation de l'énergie mécanique en fonction de la température. Et dans ce cas, une variation linéaire entre ces deux dernières grandeurs a été observée. En réalisant un bilan d'énergie pendant l'essai, non seulement, le rendement énergétique a pu être évalué mais il a été aussi possible de prendre en compte l'effet Mullins et la cristallisation induite par la déformation pour le caoutchouc naturel.

Dans un second temps, l'effet élastocalorique a été étudié sur le terpolymère (P(VDF-TrFE-CTFE), ce qui a permis de montrer qu'il était possible d'obtenir une variation de température de 2.1 °C sous réserver de pré-déformer le terpolymère à plus de 1050 % avant. Par comparaison avec d'autres matériaux présentant une bonne conversion élastocalorique, le fort potentiel de ce matériau a pu être mis en évidence. Enfin, il a été mis en évidence que la plus grande partie de l'énergie mécanique était bien convertie en énergie thermique.

MOTS-CLÉS : Effet élastocalorique, Caoutchouc naturel, Terpolymère, Effet Mullins, Cristallisation induite par la déformation

Laboratoire (s) de recherche : Laboratoire de Génie Electrique et Ferroélectricité (LGEF) INSA Lyon

Directeur de thèse : Prof. Daniel GUYOMAR

Président de jury : Prof. Joel POUGET, Directeur de Recherche au UNIV. PARIS 6

Composition du jury :
Prof. Bertrand DUBUS, Dr. Abdelowahed HAJJAJI, Dr. Takeshi MORITA, Prof. Joel POUGET, Dr. Kaori YUSE, Prof. Daniel GUYOMAR